UNIVERSITÁ DEGLI STUDI DI PADOVA

Facoltà di Ingegneria

Corso di Laurea Triennale in Ingegneria dell'Informazione

Optical Interferometer For The Fine Control Of The Polarization Status Of A Beam

Tesi di Laurea in

Ingegneria dell'Informazione

Relatore: Prof.ssa Pelizzo Maria Guglielmina

Correlatore: Dott. Corso Alain Jody

Laureando: Bonaldo Stefano

Anno Accademico 2012/2013

Ai miei cari genitori,
a mia sorella Cinzia

"A man must cling to the belief that
the incomprehensible is comprehensible;
otherwise he would not try to fathom it."

[JOHANN WOLFGANG VON GOETHE]

Contents

Abstract

An optical system for the generation of a beam with a variable and controllable polarization status has been designed, realized and tested. The system is based on a interferometric set up, consisting of a split system, a phase delay system and a recombination system. The input beam is split in two beams, which are linearly polarized respectively on two perpendicular directions. The beams propagate along the two lines of the interferometer. The optical path of the lines is linearly and finely controlled by a piezoelectric translator stage. The beams can then be recombined changing the phase delay between the two. By controlling the optical path, it is possible to obtain every polarization status: linear, elliptical and circular. The system can be all reflective, therefore working in a wide spectral band of the electromagnetic spectrum, from the near-infrared down to the extreme ultraviolet, where the use of transmission optical elements is forbidden. The system can be integrated in different optical set ups in order to enhance their versatility, such as in laser devices, optical instrumentations, synchrotron lines or of free electron lasers beam transport system, and in the visible spectral range can represent an alternative solution to the Liquid Crystal Variable Retarder. Different optical scheme has been mathematically modeled and analyzed. Two setups based on the Michelson and Mach-Zehnder interferometric systems respectively have been realized and experimentally tested on the optical bench, proving the feasibility and proper working of the proposed systems.

Introduction

Light sources with controlled polarization states are of great interest for many applications, as in biology, chemistry, physics, and material science [1]. For example, satellite communications use two polarization states to double the transmission capacity [2–6]; laser sources in different polarization states are required in quantum cryptography [2–6]; circularly polarized light is used in chemistry and biology for the study of molecules with circular dichroism [7]; linearly and circularly polarized light finds applications in various types of ophthalmic metrology [8, 9]. However, in most of these applications, the used lasers are linearly polarized TE and TM. Other polarization states can be only obtained by the use of optical components like the conventional waveplates or the liquid crystals, usually included in the standard interferometric schemes [10]. The current commercial Polarization State Generators (PSG) are optical systems based on liquid crystals and they allow to generate any polarization state as long as the input polarization is linear. The technology is well established in the VIS and in the IR, and although innovative proposals and alternatives have recently been reported [11, 12], the issue is still open and of great interest. In the spectral range of EUV and soft x-rays, the polarization control provides an accurate tool for investigation of the properties of the matter at the nanoscale range [13]. Moreover, the rapid development of sources for generating X ray Free Electron Laser (FELs) can generate femtosecond pulses and short wavelengths and allow a temporal and spatial localization of the magnetic properties of the material [13].

This thesis work presents an innovative polarization control system, conceived to actively control the polarization. The system is based on a interferometric setup, in which each single subsystem can be adapted to work at a specific selected wavelength or spectral range. Such optical system can change the polarization to linear, elliptical or circular, independently by the initial polarization status. The system works in a large band of the electromagnetic spectrum potentially without using any optical elements in transmission; therefore, it can be applied also at short wavelengths in the UV where material is opaque. As it is based on an interferometric principle, the system allows to realize a continuous spatial distribution of polarization along a precise direction of the observation plane. This system can be integrated in different optical setup in order to enhance the versatility, such as on laser lines of synchrotron or of free electron lasers, or it can be sold as PSG

or as an alternative solution to the Liquid Crystal Variable Retarder, whenever it is not necessary to change the polarization status in high frequency. The same system can be adopted in the optical schemes already foreseen at FERMI@ELETTRA for implementing the pump-probe experiments [14].

In the following pages, the system is analyzed trough a detailed mathematical model, which takes into account also second order effects. The system has been constructed and tested at the CNR-IFN Laboratory in Padova (see Figure 1), realizing two configurations: one based on the Michelson interferometer setup and one based on the Mach-Zehnder one. As a first approach, a visible laser light has been used as a source due to the simplest operative conditions. The feasibility and the functioning of both systems was tested. The measurements obtained during the test faithfully reproduce the theoretical simulations demonstrating the capability of the system on controlling the polarization status of the output beam. The next step will be testing the system at shorter UV wavelengths (200-400 nm) and then trying to apply it to the VUV spectral range (<200 nm).

Figure 1: A general view of the real system in CNR-INF Laboratory of Padova.

Chapter 1

The Polarized Light

In general there are different notations to describe the propagation of a electromagnetic wave and its polarization. The most used are the Mueller matrix formalism [15, 16] and the Jones matrix formalism [15, 17]. The Mueller calculus is based on the Stokes vectors and it is ideal to describe the unpolarized or partially polarized light. Each optical element is represented with a 4x4 matrix. On the contrary, the Jones matrix formalism describes a fully polarized light, and it should be particularly preferred in presence of coherent light because it works with electric field amplitude rather than intensity.

As the polarization control system deals with only coherent and polarized beams, the entire analysis is based on the Jones matrix formalism. However some of the basic concepts are reported with the Stokes parameter notation for the sake of simplicity.

1.1 Ellipse of Polarized Light

A beam is said to be polarized when the vibration plane of the electric field follows a well-defined law. Fixing a tridimensional cartesian system xyz, the electric field vector of a generic plane wave propagating along the z direction can be decomposed in the two perpendicular components represented by

$$E_x(z,t) = E_{0x}\cos(\omega t - kz + \delta_x) \qquad [Vm^{-1}] \tag{1.1}$$

$$E_y(z,t) = E_{0y}\cos(\omega t - kz + \delta_y) \qquad [Vm^{-1}]. \tag{1.2}$$

The notations x and y refer to the components in the x and y directions, E_{0x} and E_{0y} are the maximum amplitudes, ω is the angular velocity, δ_x and δ_y are the phase constants, while k is defined as $k = \omega/c$. The original electric field is the vectorial sum of the two x and y component

$$\vec{E}(z,t) = \vec{E}_x(z,t) + \vec{E}_y(z,t). \tag{1.3}$$

This vector describes a locus of points in space, and its components (1.1) and (1.2) can be decomposed through the fundamental relations of trigonometry

$$\frac{E_x}{E_{0x}} = \cos\tau\cos\delta_x - \sin\tau\sin\delta_x$$

$$\frac{E_y}{E_{0y}} = \cos\tau\cos\delta_y - \sin\tau\sin\delta_y.$$

where the propagator term τ is defined as $\omega t - kz$. Consequently,

$$\frac{E_x}{E_{0x}}\sin\delta_y - \frac{E_y}{E_{0y}}\sin\delta_x = \cos\tau\sin(\delta_y - \delta_x)$$

$$\frac{E_x}{E_{0x}}\sin\delta_y - \frac{E_y}{E_{0y}}\sin\delta_x = \sin\tau\sin(\delta_y - \delta_x).$$

Squaring and adding the equation of an ellipse is obtained

$$\frac{E_x^2}{E_{0x}^2} + \frac{E_y^2}{E_{0y}^2} - 2\frac{E_x}{E_{0x}}\frac{E_y}{E_{0y}}\cos\delta = \sin\delta^2, \tag{1.4}$$

where

$$\delta = \delta_y - \delta_x.$$

Equation (1.4) shows that at any instant of time the locus of points described by the optical field propagates as an ellipse (Figure 1.1). This phenomenon is called *polarization of the light*.

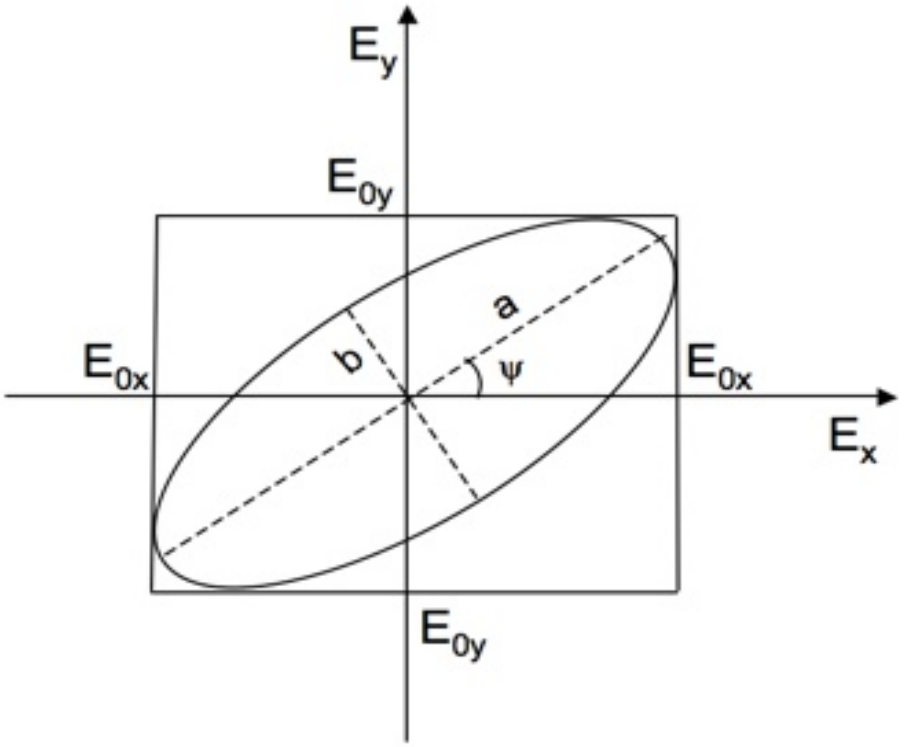

Figure 1.1: The generic polarization ellipse.

From (1.4) it is easy to verify that the polarization ellipse degenerates in special forms for certain values of E_{0x}, E_{0y}, and δ. This main special forms are now analyzed.

1. LINEAR *(horizontally or vertically)*:

   If $E_{0y} = 0$ from (1.1) and (1.2) we obtain

   $$\begin{cases} E_x(z,t) = E_{0x}\cos(\omega t - kz + \delta_x) \\ E_y(z,t) = 0 \end{cases}$$

   With this assumption the electric field lies in the xz plane and the ellipse collapse to a straight line coincident to the x axis. For this reason the light is said to be *linear horizontally polarized*.

   Similarly, the *linear vertically polarized* light is obtain for $E_x(z,t) = 0$ and $E_y(z,t) \neq 0$ (see Figure 1.2).

2. LINEAR *(sloped of ψ angle)*: $\delta = 0$ or $\delta = \pi$.

   Replacing the conditions in the ellipse equation (1.4)

   $$\frac{E_x^2}{E_{0x}^2} + \frac{E_y^2}{E_{0y}^2} \pm 2\frac{E_x}{E_{0x}}\frac{E_y}{E0y}\cos\delta = 0$$

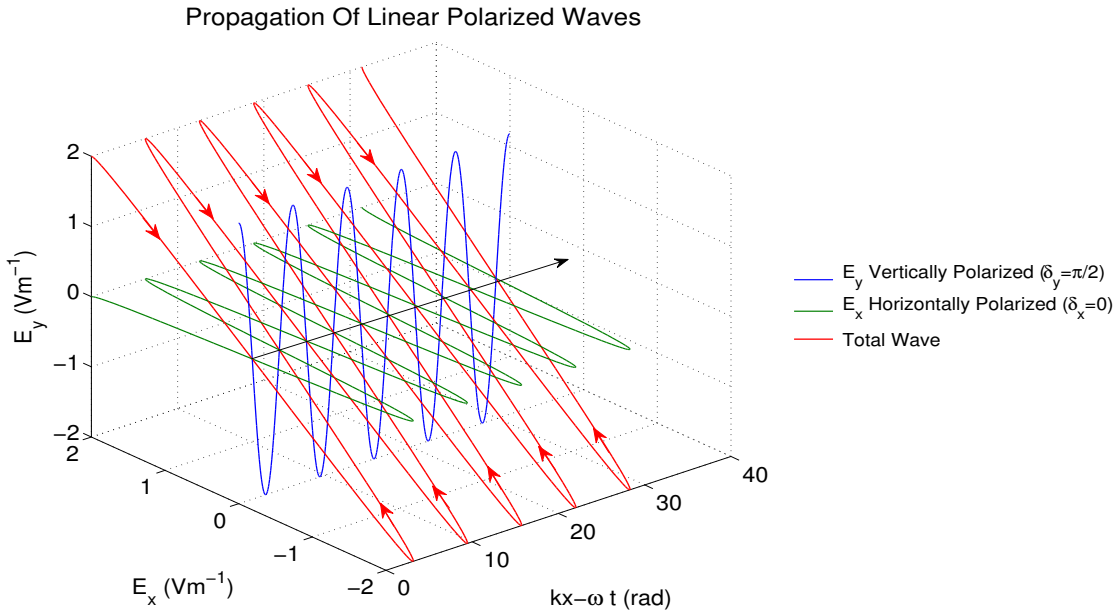

Figure 1.2: Two linear polarized waves are propagating trough the z axis. The blue one is vertically polarized with $E_{0y} = 2$ and $\delta = 0$, while the green one is horizontally polarized with $E_{0x} = 2$ and $\delta = 0$. Their superposition creates a new linear polarized wave, in this case with slope $\psi = 45°$ as the $E_{0x} = E_{0y}$.

that is equivalent to

$$\left(\frac{E_x}{E_{0x}} \pm \frac{E_y}{E_{0y}}\right)^2 = 0$$

$$E_y = \pm\left(\frac{E_{0y}}{E_{0x}}\right) E_x. \tag{1.5}$$

Defining the constant parameter K as

$$K = \frac{E_{0y}}{E_{0x}},$$

the (1.5) can be written as a the equation of a straight line passing through the origin

$$E_y = \pm K E_x$$

where the K is the tangent of the inclination angle ψ of the oscillating plane

$$\psi = \arctan\left(\pm\frac{E_{0y}}{E_{0x}}\right).$$

In this case the light is said to be *linearly polarized with slope* ψ.

In particular if the $E_{0x} = E_{0y}$, then from (1.5)

$$E_x = \pm E_y.$$

This means that light is linearly polarized of $+45°$ if the $\delta = 0$, otherwise linearly polarized of -45° if $\delta = \pi$ (see Figure 1.2).

In general in linear polarized waves the oscillating plane always lies parallel to itself.

3. CIRCULAR: $E_{0x} = E_{0y} = E_0$ and $\delta = \pi/2$ or $\delta = 3\pi/2$.

   From (1.4) the equation ellipse reduces to

$$\frac{E_x^2}{E_0^2} + \frac{E_y^2}{E_0^2} = 1$$

   which is the equation of a circle. Unlike the linear polarization, now the electric filed rotates with a constant angular velocity and the direction of its rotation is fixed by the phase displacement of its component. For clockwise direction δ is $\pi/2$, on the contrary for counterclockwise rotation δ is $3\pi/2$ (see Figure 1.3).

In a general polarized wave the expression of inclination ψ of the ellipse can be derived from algebraic manipulation of the parameters, which ends to the following expression [15]

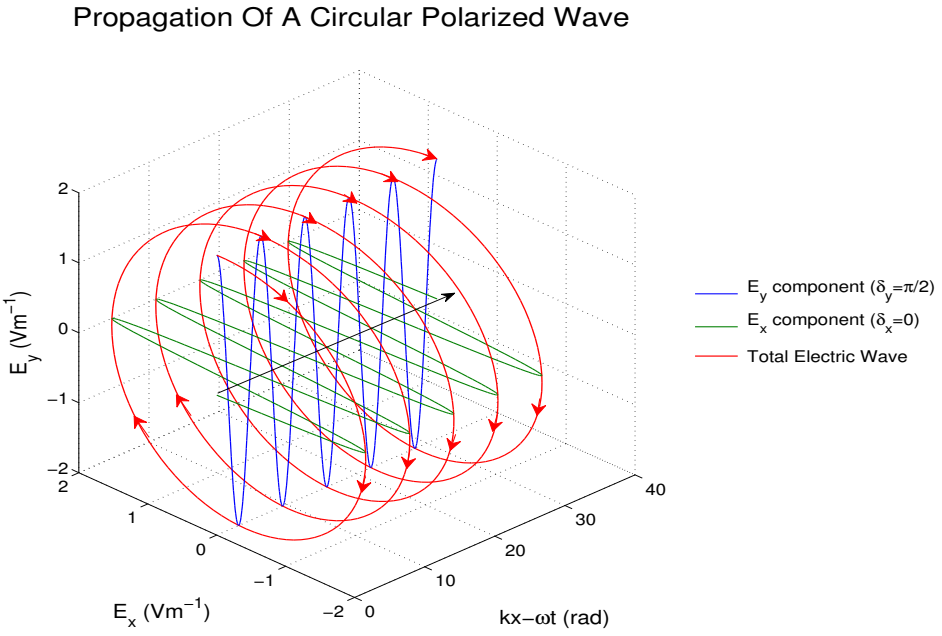

Figure 1.3: A circular polarized wave (red) is propagating trough the z axis with a clockwise rotation and it is decomposed in the two perpendicular components E_x and E_y ($E_{0x} = 2$, $E_{0y} = 2$ and $\delta = \pi/2$).

$$\tan 2\psi = \frac{2E_{0x}E_{0y}}{E_{0x}^2 E_{0y}^2} \cos\delta. \tag{1.6}$$

In order to characterize the polarization ellipse it is useful to introduce an auxiliary angle α, which is defined as

$$\boxed{\tan\alpha = \frac{E_{0y}}{E_{0x}}}, \tag{1.7}$$

$$0 \leq \alpha \leq \frac{\pi}{2}.$$

In this way the relation between the inclination ψ and the parameter α is now evident by (1.6) and (1.7)

$$\tan 2\psi = \frac{2\tan\alpha}{1-\tan^2\alpha}\cos\delta$$

$$\tan 2\psi = (\tan 2\alpha)\cos\delta. \tag{1.8}$$

Another useful parameter is *the angle of ellipticity* χ, which is defined as

$$\boxed{\tan\chi = \left|\frac{b}{a}\right|}, \tag{1.9}$$

$$0 \leq \chi \leq \frac{\pi}{4}.$$

The following relationship with the α angle can be derived

$$\boxed{\sin 2\chi = (\sin 2\alpha)|\sin\delta|}. \tag{1.10}$$

By the trigonometrical properties (1.10) can be rewritten as

$$\sin 2\chi = \frac{2\tan\alpha}{1+\tan^2\alpha}|\sin\delta|. \tag{1.11}$$

The angle of ellipticity χ shows how much the wave is elliptical. Analyzing the extremes of the polarization, $\chi = 0$ indicates a linearly polarized light, as $b = 0$. On the contrary, circular polarized light is characterized by $\chi = \pi/4$, as $a = b$.

The intensity of a generic polarized wave is now analyzed. The *instantaneous intensity* of an electromagnetic wave is defined as

$$I_{ist}(z,t) = \frac{1}{2}cn\varepsilon_0|E(z,t)|^2. \qquad [Watt] \tag{1.12}$$

Usually it is more interesting the *average intensity*, which is defined as the average in time

of the instantaneous intensity

$$\begin{aligned}
\bar{I} &= < I_{ist}(z,t) > \\
&= \frac{1}{2} cn\varepsilon_0 < |\vec{E}(z,t)|^2 > \\
&= \frac{1}{2} cn\varepsilon_0 < |\vec{E}_x + \vec{E}_y|^2 > \\
&= \frac{1}{2} cn\varepsilon_0 < \left(\sqrt{E_{0x}^2 \cos^2(\omega t - kz + \delta_x) + E_{0y}^2 \sin^2(\omega t - kz + \delta_y)} \right)^2 > \\
&= \frac{1}{2} cn\varepsilon_0 < E_{0x}^2 \cos^2(\omega t - kz + \delta_x) + E_{0y}^2 \sin^2(\omega t - kz + \delta_y) > \\
&= \frac{1}{4} cn\varepsilon_0 E_{0x}^2 + \frac{1}{4} cn\varepsilon_0 E_{0y}^2 \\
&= \frac{1}{2} \bar{I}_x + \frac{1}{2} \bar{I}_y. \qquad\qquad [Watt]
\end{aligned}$$

In conclusion

$$\bar{I} = \frac{1}{2} \bar{I}_x + \frac{1}{2} \bar{I}_y,$$

where

$$\bar{I_x} = \frac{1}{2} cn\varepsilon_0 E_{0x}^2$$

$$\bar{I_y} = \frac{1}{2} cn\varepsilon_0 E_{0y}^2.$$

This means that the intensity of a generic polarized wave is the sum of the half average intensity of each perpendicular component. So it is preferable to base the analysis on a normalized intensity I

$$\boxed{I = \frac{\bar{I}}{\frac{1}{4} cn\varepsilon_0} = E_{0x}^2 + E_{0y}^2}. \qquad [\sqrt{Vm^{-1}}] \tag{1.13}$$

1.2 Jones Matrix Formalism

In order to characterize a polarized beam it is necessary to deal with amplitude and phase relations. The two perpendicular components $\vec{E}_x$ and $\vec{E}_y$ are analyzed as different beams and finally superposed to combine the result beam $\vec{E}$. But new problems arise when the beams propagates through several polarizing components. To facilitate the analysis the Jones Matrix calculus is used.

The Jones formalism involves complex quantities contained in 2-dimension vector, called Jones vector, and 2x2 matrices, called Jones matrices. The Jones vector describes the status of polarization of a beam. Preserving the previous notation, a electromagnetic wave $\vec{E}$ propagating along the z direction is represented as

$$\vec{E}(z,t) = \begin{pmatrix} E_x(z,t) \\ E_y(z,t) \end{pmatrix} = \begin{pmatrix} E_{0x}e^{i(\omega t - kz + \delta_x)} \\ E_{0y}e^{i(\omega t - kz + \delta_y)} \end{pmatrix}. \tag{1.14}$$

In the frequency domain the term $\omega t - kz$ can be suppressed, so (1.14) can be written as

$$\boldsymbol{E} = \begin{pmatrix} E_{0x}e^{i\delta_x} \\ E_{0y}e^{i\delta_y} \end{pmatrix} \tag{1.15}$$

which is the formal Jones vector. The maximum amplitudes E_{0x} and E_{0y} are real quantities, but the presence of the exponent with imaginary arguments causes E_x and E_y to be complex quantities. Now the average intensity can be calculated by

$$I = (\boldsymbol{E^*})^{\boldsymbol{T}}\boldsymbol{E} = \begin{pmatrix} E_x^* & E_y^* \end{pmatrix} \begin{pmatrix} E_x \\ E_y \end{pmatrix} = E_xE_x^* + E_yE_y^* = E_{0x}^2 + E_{0y}^2.$$

It is customary to normalize the Jones vector to

$$E_0 = \sqrt{I} = \sqrt{E_{0x}^2 + E_{0y}^2}.$$

So the normalized Jones vector $\boldsymbol{E_{norm}}$ becomes

$$E_{norm} = \begin{pmatrix} \frac{E_{0x}}{E_0}e^{i\delta_x} \\ \frac{E_{0y}}{E_0}e^{i\delta_y} \end{pmatrix}.$$

We now analyze the main type of polarized light trying to find the respective normalized Jones vector.

1. Linear horizontally polarized light: $E_x = 0$, so $E_0^2 = E_{0x}^2$

$$\boldsymbol{E} = \begin{pmatrix} \frac{E_{0x}}{E_0}e^{i0} \\ 0 \end{pmatrix} = \begin{pmatrix} 1 \\ 0 \end{pmatrix}.$$

2. Linear vertically polarized light: $E_y = 0$, so $E_0^2 = E_{0y}^2$

$$\boldsymbol{E} = \begin{pmatrix} 0 \\ 1 \end{pmatrix}.$$

3. Linear +45° polarized light: $E_x = E_y$, so $E_0^2 = 2E_{0x}$

$$\boldsymbol{E} = \frac{1}{\sqrt{2}} \begin{pmatrix} 1 \\ 1 \end{pmatrix}.$$

4. Linear -45° polarized light: $E_x = -E_y$, so $E_0^2 = 2E_{0x}$

$$\boldsymbol{E} = \frac{1}{\sqrt{2}} \begin{pmatrix} 1 \\ -1 \end{pmatrix}.$$

5. Clockwise circular polarized light: $E_{0y} = E_{0x}$ and $\delta_y - \delta_x = \pi/2$, so $E_0^2 = 2E_{0x}$, $\delta_x = 0$ and $\delta_y = \pi/2$

$$\boldsymbol{E} = \frac{1}{\sqrt{2}} \begin{pmatrix} 1 \\ +i \end{pmatrix}.$$

6. Counterclockwise circular polarized light: $E_{0y} = E_{0x}$ and $\delta_y - \delta_x = -\pi/2$, so $E_0^2 = 2E_{0x}$, $\delta_x = \pi/2$ and $\delta_y = 0$

$$\boldsymbol{E} = \frac{1}{\sqrt{2}} \begin{pmatrix} 1 \\ -i \end{pmatrix}.$$

The components of a beam emerging from a polarizing element are linearly [1] related to the components of the input beam. The relations between output and input components can be written as

$$E_x^{out} = j_{xx}E_x + j_{xy}E_y \tag{1.16}$$

$$E_y^{out} = j_{yx}E_x + j_{yy}E_y \tag{1.17}$$

where the E_x^{out} and E_y^{out} are the output components of the emerging beam, E_x and E_y are the components of the incident beam, while the coefficients j_{xx}, j_{xy}, j_{yx}, j_{yy} are the transforming factors. The relations (1.16) and (1.17) can be written in matrix form as

$$\begin{pmatrix} E_x^{out} \\ E_y^{out} \end{pmatrix} = \begin{pmatrix} j_{xx} & j_{xy} \\ j_{yx} & j_{yy} \end{pmatrix} \begin{pmatrix} E_x \\ E_y \end{pmatrix}$$

[1] The linear condition is verified only for isotropic and linear polarizing elements.

$$\boldsymbol{E}^{out} = \boldsymbol{J}\boldsymbol{E}$$

where

$$\boldsymbol{J} = \begin{pmatrix} j_{xx} & j_{xy} \\ j_{yx} & j_{yy} \end{pmatrix}.$$

The 2x2 matrix $\boldsymbol{J}$ is called the Jones matrix. Jones matrix becomes a powerful tool to analyze a beam which impinges N optical elements in series. In this case the output beam can be calculated as the left multiplication of the equivalent matrix Jones to the input Jones vector, so that as

$$\boldsymbol{E}^{out} = \boldsymbol{J}_{eq}\boldsymbol{E} = \boldsymbol{J}_N\boldsymbol{J}_{N-1}.....\boldsymbol{J}_2\boldsymbol{J}_1\ \boldsymbol{E}.$$

1.2.1 Jones Matrix Associated To A Polarizer

Usually a polarizer works in transmission and it linearly polarizes the input wave along its main axis. The behavior of a polarizer follow the Malus law, which can be written in the Jones matrix formalism as

$$\begin{pmatrix} E_x^{out} \\ E_y^{out} \end{pmatrix} = \begin{pmatrix} t_x & 0 \\ 0 & t_y \end{pmatrix} \begin{pmatrix} E_x \\ E_y \end{pmatrix}, \tag{1.18}$$

where t_x and t_y are the transmission coefficient along the x and y direction. However, for a better analysis it is common to consider the main axis of the polarizer parallel to the the x direction and rotate the polarizer system through a rotation transformation. In case of an *ideal horizontal polarizer*, the Jones matrix is

$$\boldsymbol{J}_p = \begin{pmatrix} 1 & 0 \\ 0 & 0 \end{pmatrix}.$$

However, *real polarizers* are not able to fully polarize the input beam. To characterize the quality of an horizontal polarizer, a rejection coefficient P_{ML} is introduced

$$P_{ML} = \frac{t_y}{t_x}.$$

with the corresponding Jones matrix

$$\boxed{\boldsymbol{J} = \begin{pmatrix} t_x & 0 \\ 0 & t_y \end{pmatrix}}.$$

A good horizontal polarizer has a rejection coefficient close to 0, as t_x is close to 1 and t_y to 0. The rotation of the polarizer can be controlled by the $\boldsymbol{J}(\theta)$ matrix through the rotation transformation

$$\boldsymbol{J}_{rotated} = \boldsymbol{J}(-\theta) \begin{pmatrix} t_x & 0 \\ 0 & t_y \end{pmatrix} \boldsymbol{J}(\theta), \tag{1.19}$$

where $\boldsymbol{J}(\theta)$ is defined as

$$\boldsymbol{J}(\theta) = \begin{pmatrix} \cos\theta & \sin\theta \\ -\sin\theta & \cos\theta \end{pmatrix}$$

and θ is the angle between the x direction and the axis of the polarized.

1.2.2 Jones Matrix Associated To A Mirror

A parallel analysis is made for mirror elements. The s direction is fixed coincident to the y axis, while the p direction is fixed coincident to the x axis. When a polarized wave propagating on the z direction impinges on a vertically positioned mirror, the reflected wave changes its polarization status with the respect to the incident one. In fact each incident angles involve different Fresnel reflection coefficients r_p along the x axis and r_s along the y axis, and so different rejection parameter P_M. Also the phase delay between the p and s components usually changes. Only in the case of normal and grazing incidence the reflection doesn't affect the polarization status because $r_p \simeq r_s$. So the Jones matrix $\boldsymbol{A}$ for a mirror is

$$\boxed{\boldsymbol{A} = \begin{pmatrix} r_s e^{j\varphi_s} & 0 \\ 0 & r_p e^{j\varphi_p} \end{pmatrix}}$$

where the φ_s and φ_p are the phase delay introduced by the reflection. Now collecting the term $r_s e^{j\varphi_s}$

$$\boldsymbol{A} = r_s e^{j\varphi_s} \begin{pmatrix} 1 & 0 \\ 0 & P_M e^{j\Delta\varphi} \end{pmatrix}$$

where $P_M = r_p/r_s$ is the rejection parameter for a mirror, while $\Delta\varphi = \varphi_p - \varphi_s$ is the phase delay. As for the polarizer in (1.19), a rotation of the plane of incidence of a θ angle (Figure 1.4), is represented by the following rotation transformation

Jones matrix of a polarizer and of a mirror are similar: both of them have a rejection parameter and a phase delay. For a polarizer the rejection parameter depends on its building quality, and usually it is very close to 0. On the contrary the rejection parameter of a mirror changes on its incident angle θ_i. Moreover, the polarizer works in transmission, so the output phase is unchanged with the respect to the input one. Conversely the mirror works in reflection, so the output have a phase delay depending on the working angle. But

in general both optical element could be described by the following general Jones matrix

$$\boxed{\boldsymbol{J} = \begin{pmatrix} p_x e^{j\varphi_x} & 0 \\ 0 & p_y e^{j\varphi_y} \end{pmatrix}}. \tag{1.20}$$

$$\boldsymbol{A}_{rotated} = \boldsymbol{J}(-\theta)\boldsymbol{A}\boldsymbol{J}(\theta). \tag{1.21}$$

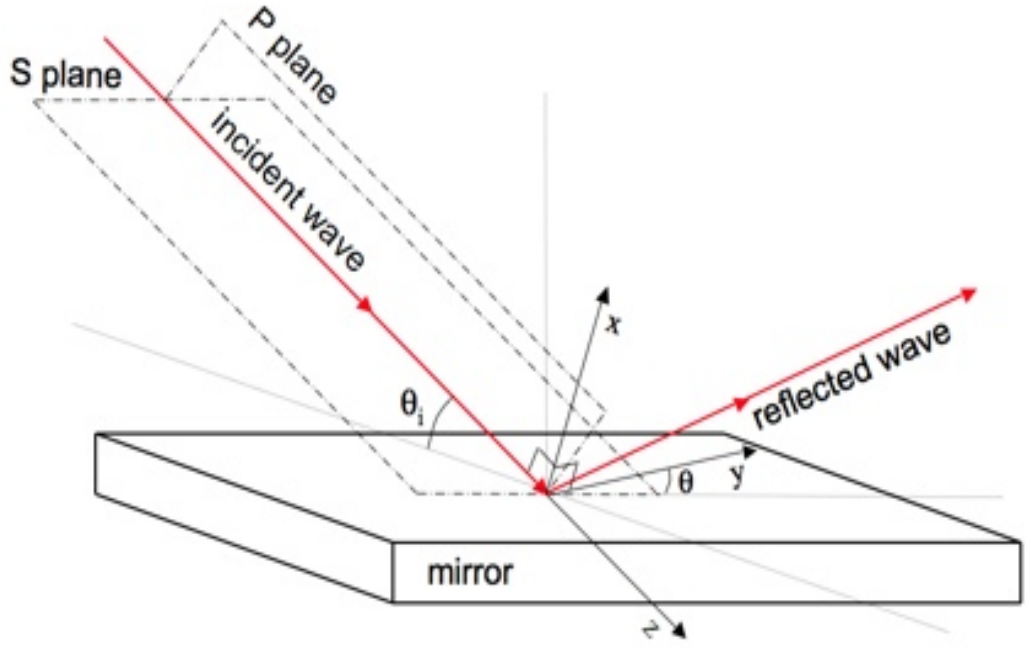

Figure 1.4: A wave is propagating along the z axis and it is reflected on a mirror. The cartesian axis are drawn with black arrows. The dotted lines indicates the S and P oscillating plane. The incident angle θ_i is the angle between the surface of the mirror and the direction of the wave, while the rotating angle θ is the angle between the surface of the mirror and the y direction.

1.3 Brewster Angle

The polarization reflection is a optical phenomenon, which occurs at the interface between two dielectric surfaces. It is useful to polarize light without the use of polarizing plates; it is a fundamental method to obtain a polarized wave in the EUV range, where the materials do not transmit radiation. Suppose to have an unpolarized light, which is incident on a dielectric surface with the incident angle θ_i equal to the Brewster angle. The reflected wave comes linearly polarized on the S plane, while the refracted one is slightly polarized.

This phenomenon is described by the Fresnel equations

$$r_s = \frac{n_1 \cos\theta_i - n_2 \cos\theta_t}{n_1 \cos\theta_i + n_2 \cos\theta_t} \tag{1.22}$$

$$r_p = \frac{n_1 \cos\theta_t - n_2 \cos\theta_i}{n_1 \cos\theta_t + n_2 \cos\theta_i} \tag{1.23}$$

where θ_i is the incidence angle, θ_t is the refracted angle, while n_1 and n_2 are the refractive index. For $n_2 > n_1$ the Snell low imposes that $\theta_t < \theta_i$. The cosine function is in inverse proportion to the amplitude of the angle and so the numerator of (1.22) can't be zero. The same explanation can be applied to the case for $n_2 < n_1$.

On the contrary the r_p expression (1.22) can be zero, when

$$n_1 \cos\theta_t - n_2 \cos\theta_i = 0.$$

Appling the Snell low, the Brewster's conditions are obtained.

$$\frac{n_2}{n_1} = \tan\theta_i.,$$

and so the Brewster angle θ_B

$$\boxed{\theta_B = \theta_i = \arctan\frac{n_2}{n_1}}.$$

In this way the p reflection index is killed (Figure 1.5), and the reflected wave is composed only by the s component, which makes the output wave linearly polarized.

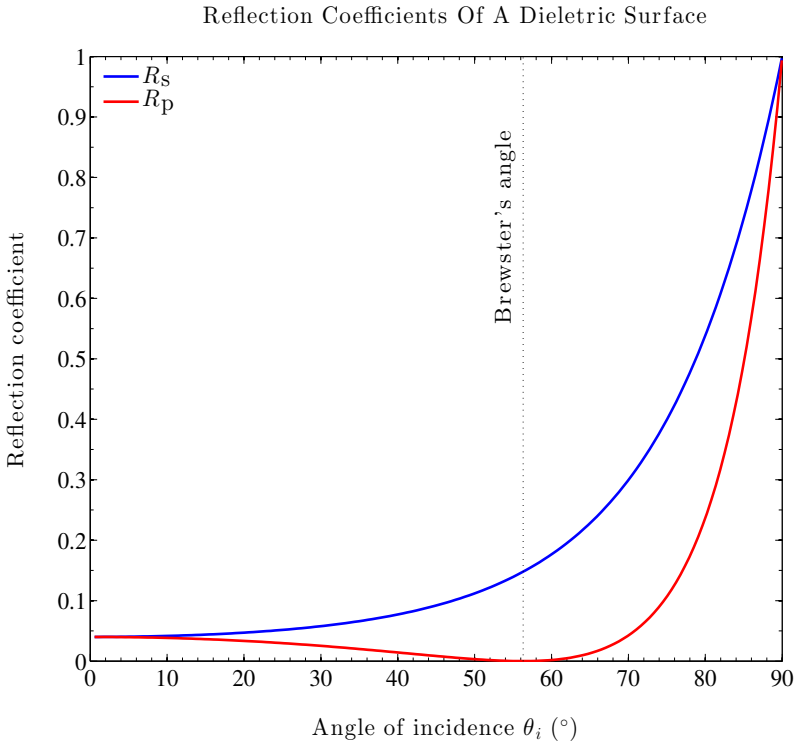

Figure 1.5: This plot is made on the Fresnel equations and it can simulate the real behavior of a dielectric mirror. The refractive index of the dielectric mirror is set to 1.51, which is characteristic of a BK7 mirror working with wavelength of 632.8 nm. It is evident the dependance of the reflective coefficients with the incident angle θ_i. At normal incidence the wave is completely reflected in both s and p direction, while at 56.6° the p component is killed. In this last condition we say that the mirror is working at its Brewster angle. It is curious to see that at normal incidence both reflective coefficients are one and so the entire wave is reflected.

Chapter 2

The Polarization Control System

Before beginning the analysis of the polarization control system, it is important to fix the position of the cartesian axes. As we will work with beams propagating on a optical bench, it is convenient to set the *horizontal plane* zx parallel to the plane table, while the perpendicular one is denoted as the *vertical plane* xy. Moreover, when a wave propagates horizontally lying on the zx plane, the z direction is set along its propagation direction. In this way the y axis became normal to the plane table and vertically directed (see Figure 2.1). Finally, hereafter the x axis is denoted as the p direction, while the y axis as the s direction.

As introduced before, the purpose of the system is to change the polarization state of a incoming beam. To understand the basic principle of the system we suppose to work with two different waves E_1 and E_2 derived from the same source, and so with equal wavelength. The two waves are linearly polarized on the two perpendicular directions s and p

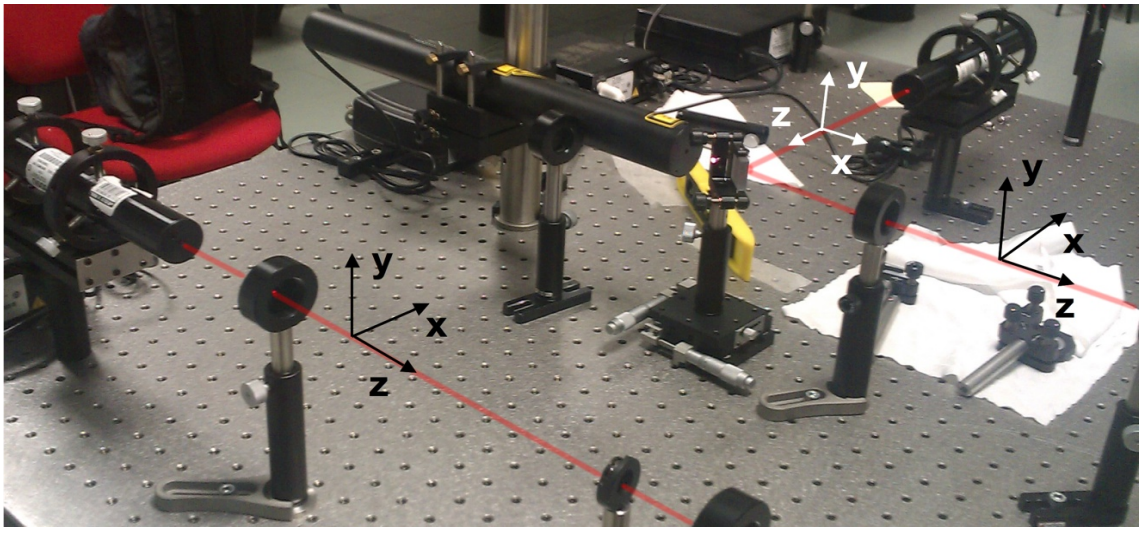

Figure 2.1: The position of the cartesian axes is shown for two different beams. For waves parallel to the plane table zx, the z axis is set along the propagation direction. In this way the y axis, called s direction, is perpendicular to the plane table.

and they are propagating along the same z axis. Both waves have the same maximum amplitude E_0 and their initial phase are respectively φ_1 and φ_2. In Jones notation

$$\begin{cases} \boldsymbol{E}_1 = \begin{pmatrix} E_0 e^{i\varphi_1} \\ 0 \end{pmatrix} \\ \boldsymbol{E}_2 = \begin{pmatrix} 0 \\ E_0 e^{i\varphi_2} \end{pmatrix} \end{cases}$$

Now the phase constant of E_2 vector could be express as

$$\begin{cases} \boldsymbol{E}_1 = \begin{pmatrix} E_0 e^{i\varphi_1} \\ 0 \end{pmatrix} \\ \boldsymbol{E}_2 = \begin{pmatrix} 0 \\ E_0 e^{i(\varphi_1+\Delta\varphi)} \end{pmatrix} \end{cases}$$

where $\Delta\varphi = \varphi_2 - \varphi_1$. If the two waves are now superposed and the phase constant φ_1 is suppressed for convenience, the total wave expression is obtained

$$\boldsymbol{E}_{out} = \boldsymbol{E}_1 + \boldsymbol{E}_2 = \begin{pmatrix} E_0 \\ E_0 e^{i\Delta\varphi} \end{pmatrix} = E_0 \begin{pmatrix} 1 \\ e^{i\Delta\varphi} \end{pmatrix}. \tag{2.1}$$

Controlling the phase delay $\Delta\varphi$, it is possible to control the polarization ellipse of the total wave. For example, a linear polarized wave can be obtained by introducing $\Delta\varphi = 0$. A clockwise circular one is formed by $\Delta\varphi = \pi/2$. In general it is possible to create different forms of elliptical waves controlling the phase delay $\Delta\varphi$.

A conceptual sketch of our polarization control system is illustrated by a blocks diagram in Figure 2.2. The system is composed of a source system, which generates a monochromatic, coherent and well-collimated beam. The in-beam E_{in} is then divided by a split system in two different lines, s and p; the p line and s line have a double function. The first is changing the polarization of each line in a linearly polarize wave, the second is introducing a phase delay. So at the exit of the phase shift system the two beams are linearly polarized on two perpendicular directions with a certain phase delay $\Delta\varphi$ between them. At this point the electric field can be expressed according to equation (2.1). When the two lines are superposed through a recombination system in a unique interferometric beam, a total wave E_{out} is obtained. Depending on the difference of phase delay that is introduced, elliptical, circular or linear polarize beam are created (see Figure 2.3).

As the system is based on the interference of two different lines, coherence and monochromaticity are essential for the success of the experiment. The exiting beams from the phase

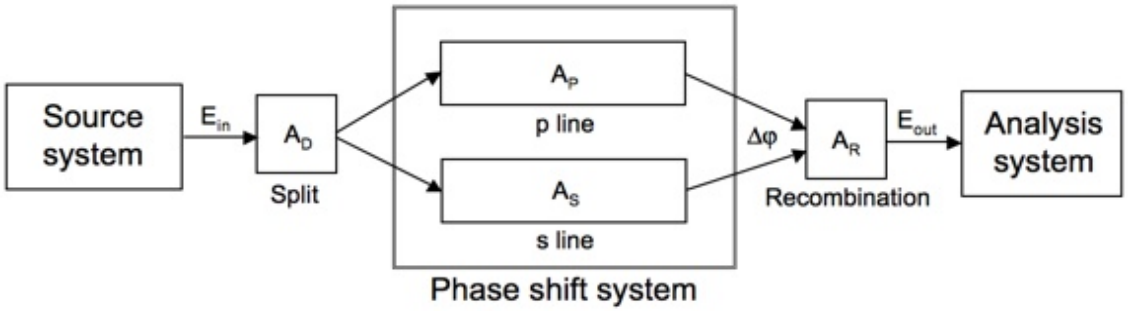

Figure 2.2: The block diagram describes our polarization control system. A source system creates the beam, which is then divided in two different lines by the spilt system. The s line and the p line polarize the beams in two perpendicular directions, introducing a phase shift of $\Delta\varphi$. The two beams are now recombined in unique beam E_{out} and the $\Delta\varphi$ introduced by the phase shift system determines the polarization of the output beam. Finally an analysis system is introduced to characterize the ellipticity of E_{out}.

shifter system should be equalized, which means that the maximum amplitude E_{0x} and E_{0y} of each line should be equal to a unique value E_0. The balance of the two lines is essential to obtain a circular polarized wave, which is reached with $\Delta\varphi = \pi/2$. With balanced lines it is possible to create different state of ellipticity, but all of them have the minor or the mayor axis tilted of $\psi = \pm 45°$ with the respect to the x axis (see Figure 2.3). On the contrary, an unbalanced system leeds to a different ψ angle of inclination, and a circular polarized wave cannot be generated. A simulation of the effects of an unequalized system is shown in Figure 2.4. In this last condition a phase delay of $\pi/2$ leeds to an elliptical polarization, which has the mayor and minor axes coincident to the x and y directions. As the aim is to obtain all degrees of ellipticity, it is important to work with well-balanced systems.

The sub-systems of the system under investigation can be implemented and configured on the base of the wavelength at which it works. This makes it flexible for different applications in a wide band of the electromagnetic spectrum. But it is important to understand that each block of Figure 2.2 consists of a series of optical elements, which can described by an equivalent Jones matrix. In this way any configuration is defined by a matrix $\boldsymbol{A}_{eq}$. The output electric field E_{out} is then written

$$\boldsymbol{E}_{out} = \boldsymbol{A}_{eq}\boldsymbol{E}_{in} = \boldsymbol{A}_R\boldsymbol{A}_P\boldsymbol{A}_S\boldsymbol{E}_{in} \tag{2.2}$$

where $\boldsymbol{A}_S$ is the Jones matrix for the split system, $\boldsymbol{A}_P$ is the one for the phase delay system and $\boldsymbol{A}_R$ is the matrix for the recombination system.

In the next pages i will present the main characteristics of an optimal source system to test the control polarization system are presented.

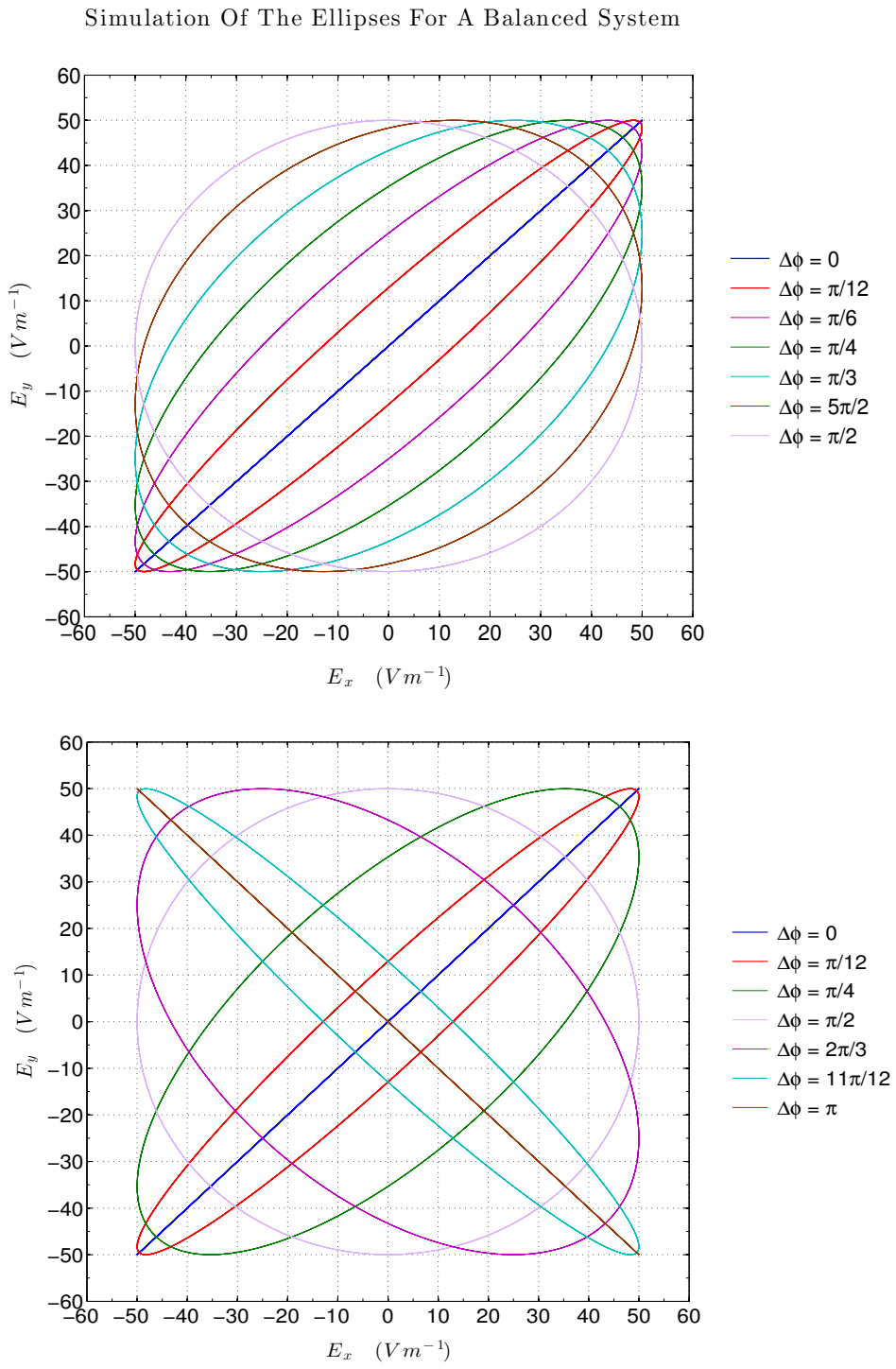

Figure 2.3: The graphic shows some of the possible ellipses created by the superposition of the two perpendicular polarized waves E_x and E_y. The $\Delta\varphi$ indicates the phase displacement between the x and y components. The maximum amplitude of the two components are equalized, so it results that $E_{0x} = E_{0y} = E_0$ which is fixed to 50 Vm^{-1}. In this way it is possible to create a perfectly circular polarized wave for $\Delta\varphi = \pi/2$. Moreover it is evident that for an equalized system all ellipses are rotated of $\psi = \pm 45°$.

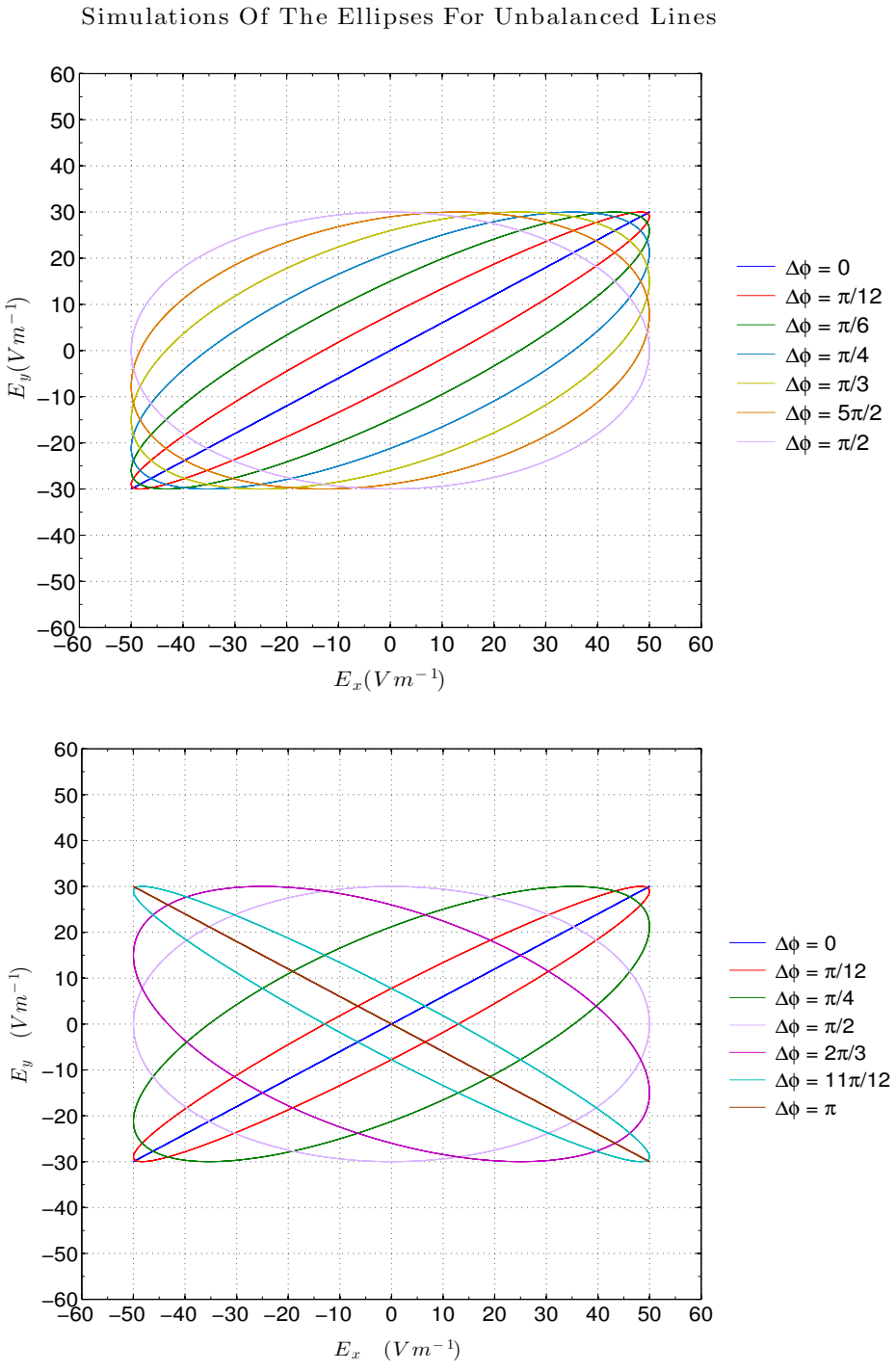

Figure 2.4: The graphic shows some of the possible ellipses created by the superposition of the two perpendicular polarized waves E_x and E_y. The $\Delta\varphi$ indicates the phase displacement between the x and y components. The maximum amplitude of the two components are disequalized, as $E_x = 50\ Vm^{-1}$ and $E_y = 30\ Vm^{-1}$. In this way for $\Delta\varphi = \pi/2$ the ellipse has inclination of $\psi = 0$, while the minor and the maximum axes are respectively equal to E_y and E_x. For $\Delta\varphi = \pi/2$ the unbalanced system creates a linear wave with inclination $\psi = \arctan \frac{E_{0y}}{E_{0x}} \simeq 59°$.

2.1 Source System

As explained above, the control polarization system is based on the interference of two beams. The best way to test the variable polarization system is through a monochromatic, well-collimated and coherent light beam. For this reason a He-Ne laser at the wavelength of 632,8 nm is used as a source. In order to obtain a uniform and parallel beam, the

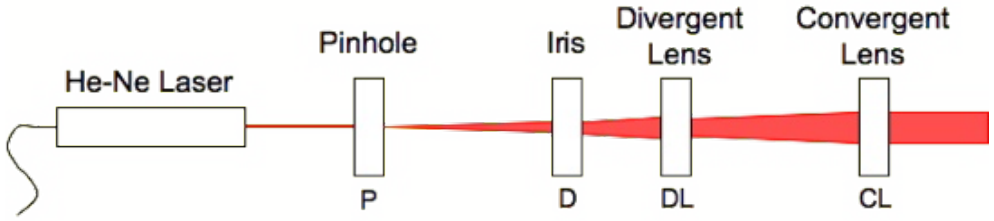

Figure 2.5: A He-Ne device creates the laser beam. A pinhole (P) creates the diffraction image, but only the central peak is selected by the iris (D). Finally the beam is collimated by a diverging lens (DL) followed by a converging one (CL).

high order modes of the laser is spatially filtered using a pinhole. A diffraction image of Frounhofer is created by the pinhole, and the central spot is isolated by an iris. The opening angle θ of the central diffraction spot is defined by the following [18]

$$\frac{\pi D \sin\theta}{\lambda} = 3,8317 \tag{2.3}$$

where D is the diameter of the pinhole and $0 < \theta < \frac{\pi}{2}$ for construction. This means that for a fixed wavelength the exiting beam diverges in relation to the diameter of the pinhole. In order to collimate the beam a diverging lens followed by a converging one is used (see Figure 2.5). The diverging lens is not essential for the collimation. The lens system is dimensioned in order to magnify the beam at a proper size. The diverging lens determines the magnification of the spot, while the converging one makes the beam collimated.

In order to obtain a beam of radius r_2, the pinhole of diameter D, the diverging lens focal f_1 and the converging lens focal f_2 must be obtained. In reference to Figure 2.6 the Gauss equation to the fisrt lens is [18]

$$\frac{1}{s_{i1}} - \frac{1}{s_{o1}} = \frac{1}{f_1} \tag{2.4}$$

where s_{i1} is the distance between the image point and the lens, s_{o1} is the distance between the source point and the lens, while f_1 is the focal length [1]. Since the pinhole has dimension at the micron order, we can approximate the distance d_i to 0.

For construction

$$s_{o1} = -d_1.$$

[1] All analysis are made by the cartesian convention. The light is propagating from left to right. Heights over the optical axis are positive. Distances positioned at right of a reference point are positive.

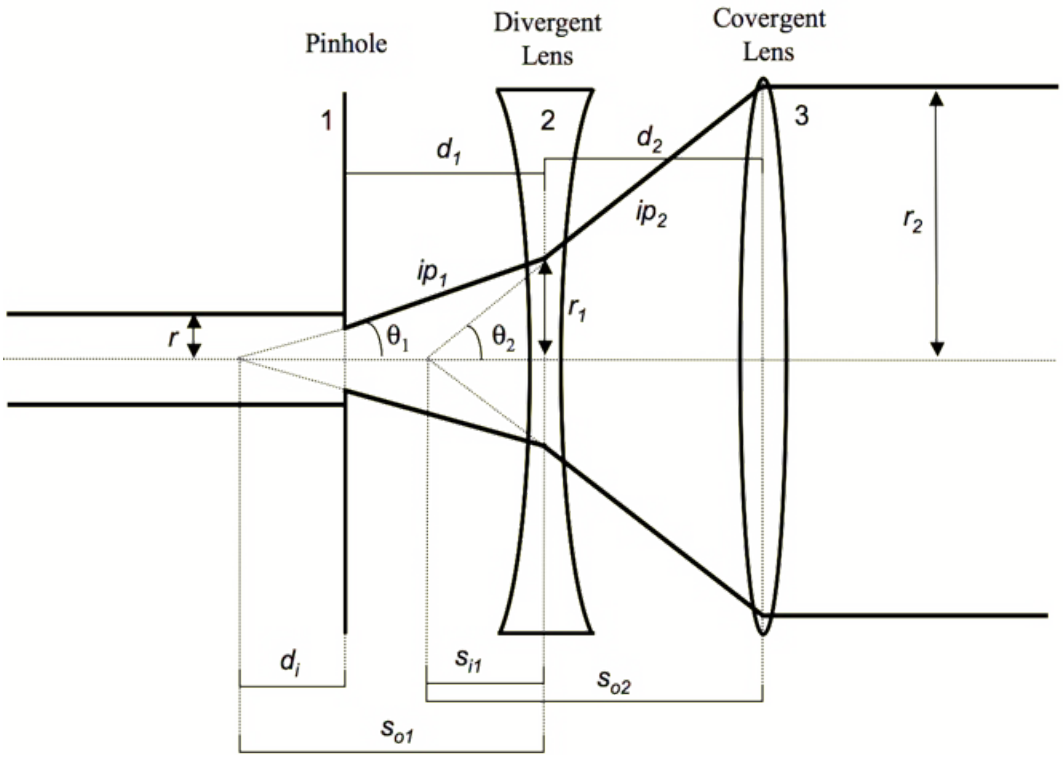

Figure 2.6: A schematic view of the beam in the collimator system.

By the relation (2.4)

$$\frac{1}{s_{i1}} - \frac{1}{s_{o1}} = \frac{1}{f_1}$$

and consequently

$$s_{i1} = \frac{f_1 d_1}{-f_1 + d_1}. \tag{2.5}$$

For construction of the system the image point and the object point are

$$s_{o2} = -(d_2 - s_{i1}) = s_{i1} - d_2 \tag{2.6}$$

and

$$s_{i2} = \infty.$$

Applying the Gauss equation to the convergent lens

$$\frac{1}{s_{i2}} - \frac{1}{s_{o2}} = \frac{1}{f_2}$$

it results that

$$s_{o2} = -f_2. \tag{2.7}$$

Combining the relations (2.5), (2.6) and (2.7), the *collimation condition* of the beam is

obtained

$$d_2 = s_{i1} - s_{o2} = \frac{f_1 d_1}{-f_1 + d_1} + f_2$$

$$\boxed{d_2 = f_2 + \frac{f_1 d_1}{-f_1 + d_1}}. \tag{2.8}$$

Figure 2.6 shows that the radius r_1 and r_2 are defined by the trigonometrical relations as

$$r_1 = d_1 \tan\theta_1 \tag{2.9}$$

and

$$r_2 = -s_{o2} \tan\theta_2. \tag{2.10}$$

By the inverse function of (2.10)

$$\tan\theta_2 = \frac{r_2}{-s_{o2}} = \frac{r_2}{f_2}, \tag{2.11}$$

and the (2.11) can also be calculated as

$$\tan\theta_2 = \frac{r_1}{-s_{i1}} = \frac{r_1(f_2 - d_1)}{f_1 d_1}. \tag{2.12}$$

The *magnification condition* is derived by the relations (2.9), (2.11) and (2.12)

$$\frac{r_1(f_2 - d_1)}{f_1 d_1} = \frac{r_2}{f_2}$$

and consequently

$$\boxed{d_1 = f_1 - \frac{r_2 f_1}{f_2 \tan\theta_1}}. \tag{2.13}$$

The following steps summarize the procedure used to design the lens system:

1. Define the diameter D of the pinhole. The diameter has to be suitable with the laser wavelength to obtain a Fraunhofer diffraction image.

2. Select a divergent and a convergent lenses with the focal lengths $f_1(< 0)$ and $f_2(> 0)$ respectively.

3. Calculate the open angle of the Fraunhofer image through (2.3).

4. Define the desired magnification by fixing the radius spot r_2.

5. Calculate the distance d_1 by (2.13).

6. Calculate the seconddistance d_2 by (2.8).

In order to quantify the distances d_1 and d_2, two simulations are reported in Table 2.1 which consider the optical components available in our laboratory. In choosing the lenses, some mechanical constraints need to be taken into account, as the fact that the size should not be larger than avaiable mirrors and that there are some space limitations on the optical trench. A good compromise is adopting a beam diameter of 11 mm.

D = 150 µm f_1 = -50 mm f_2 = 150 mm			
spot (mm)	d_1 (mm)	d_2 (mm)	total (mm)
5,0	111,9	115,4	227,4
6,0	144,3	112,9	257,2
7,0	176,7	111,0	287,7
8,0	209,1	109,7	318,7
9,0	241,4	108,6	350,0
10,0	273,8	107,7	381,5
11,0	306,2	107,0	413,2
12,0	338,6	106,4	445,0
13,0	371,0	105,9	476,9
14,0	403,4	105,5	508,9
15,0	435,7	105,1	540,9
16,0	468,1	104,8	572,9
17,0	500,5	104,5	605,0
18,0	532,9	104,3	637,2
19,0	565,3	104,1	669,3
20,0	597,6	103,9	701,5
21,0	630,0	103,7	733,7
22,0	662,4	103,5	765,9

D = 200 µm f_1 = -50 mm f_2 = 150 mm			
spot (mm)	d_1 (mm)	d_2 (mm)	total (mm)
5,0	165,9	111,6	277,5
6,0	209,1	109,7	318,7
7,0	252,2	108,3	360,5
8,0	295,4	107,2	402,7
9,0	338,6	106,4	445,0
10,0	381,8	105,8	487,6
11,0	424,9	105,3	530,2
12,0	468,1	104,8	572,9
13,0	511,3	104,5	615,8
14,0	554,5	104,1	658,6
15,0	597,7	103,9	701,5
16,0	640,8	103,6	744,4
17,0	684,0	103,4	787,4
18,0	727,2	103,2	830,4
19,0	770,4	103,0	873,4
20,0	813,5	102,9	916,4
21,0	856,7	102,8	959,5
22,0	899,9	102,6	1002,5

Table 2.1: The tables describes different possible distances of the lenses in order to obtain a well collimated and magnified beam. D is the diameter of pinhole, f_1 is the focal length of the divergent lens, while f_2 is the focal length of the convergent lens. Different values of the diameter of the magnified beam *spot* are fixed and through the equation (2.3), (2.8) and (2.13) the distances d_1 and d_2 of the lenses are calculated. The *total* voice refers to the sum of d_1 and d_2.

2.2 Michelson Configuration

The easiest way to implement the variable polarization system is to add two polarizing elements in a Michelson interferometer (see Figure 2.7). Two polarizers are inserted in each line between the beam splitter and the mirror in such a way that they have the mean axis one perpendicular to each other (see Figure 2.7). One of the two mirrors is fixed on a nanometer translator, which controls the phase delay $\Delta\varphi$ of the system. This configuration is a base scheme of the system shown in Figure 2.2. The split system coincide with the recombination system in the unique beam splitter, while the two lines s and p are implemented by one polarizer and one retroreflection mirror. For convenience the s line has the main axes of the polarizer (P_1) set in a vertically position along the y direction, while the p line has the main axes of the polarizer (P_2) horizontally positioned along the x direction. In the following analysis it is supposed to work with linearly polarized input beams propagating along the z direction and having the electric vector lying on the xy plane with an orientation defined by a θ angle (see Fig 2.8).

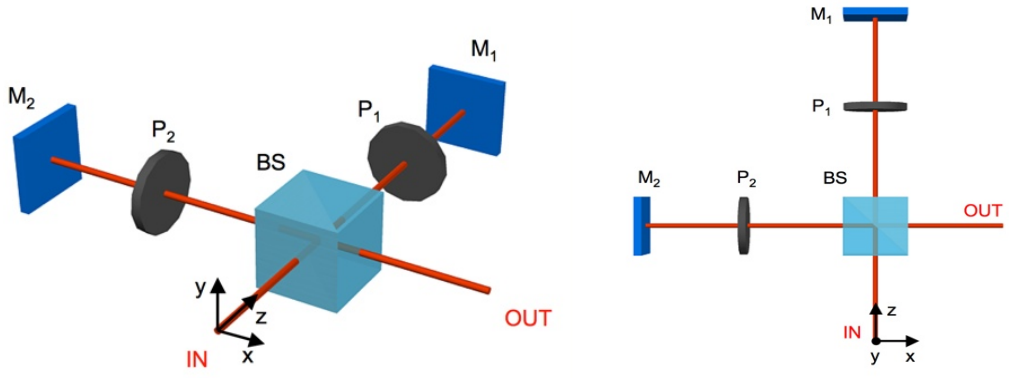

(a) (b)

Figure 2.7: The Michelson configuration is shown in a perspective view (a) and in a view from above (b). The (M) indicate the mirrors, (P) are the polarizers and (BS) is the beam splitter.

In this confiuration the optical path difference is given by

$$\Delta\varphi = \frac{2\pi\Delta l}{\lambda} \simeq \frac{4\pi d}{\lambda} \tag{2.14}$$

where Δl is the variation of the optical path, while d is the path difference introduced by the nanometric translator. As in real practice the mirrors work near to normal incidence, it is possible to make the approximation $\Delta l \simeq 2d$. The precision of the phase delay depends on the minimum variation step achievable in the optical path. Considering the relation

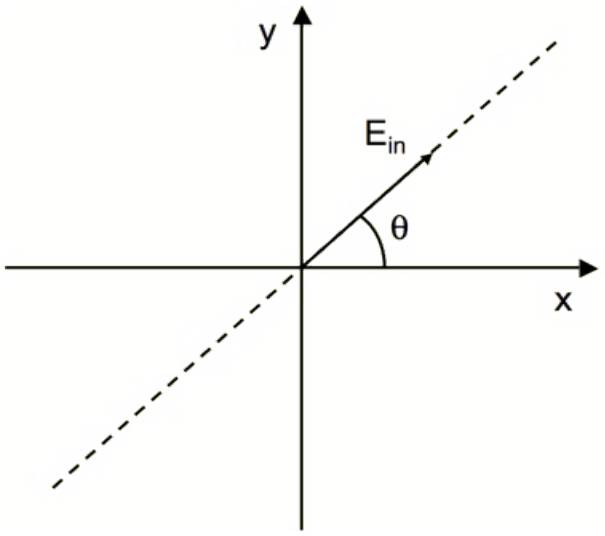

Figure 2.8: The input wave is linearly polarized and its electric vector lays on the xy plane and it is tilted of a θ angle with the respect to the x direction.

(2.14), a phase regulation with precision of $\frac{\pi}{N}$ requires an optical path variation step of

$$\Delta d = \frac{\lambda}{2N}.$$

A close loop piezoelectric translators is used to control the optical path with some nanometers of tolerance.

As discussed above (2.2), the entire system can be described by the Jones matrix of each singular component. Since (M_1) and (M_2) mirrors work in the geometry, hereafter the Jones matrices associated to both is indicated with (M). The same considerations are advanced for the polarizers. So a unique A_M and A_P matrix is defined for mirrors and polarizers

$$\boldsymbol{A}_M = |r_{Ms}|e^{j\varphi_{Ms}} \begin{pmatrix} 1 & 0 \\ 0 & P_M e^{j\Delta\varphi_M} \end{pmatrix}$$

$$\boldsymbol{A}_P = |t_{Ps}|e^{j\varphi_{Ps}} \begin{pmatrix} 1 & 0 \\ 0 & P_P e^{j\Delta\varphi_P} \end{pmatrix}.$$

As the beam splitter divides beam in two lines with different rejection coefficients, the A_{BSr} and A_{BSt} matrices are defined as the equivalent Jones matrix respectively for the reflected line and for the transmitted one

$$\boldsymbol{A}_{BSr} = |r_{BSs}|e^{j\varphi_{BSrs}} \begin{pmatrix} 1 & 0 \\ 0 & P_{BSr} e^{j\Delta\varphi_{BSr}} \end{pmatrix}$$

$$\boldsymbol{A}_{BSt} = |t_{BSs}|e^{j\varphi_{BSts}} \begin{pmatrix} 1 & 0 \\ 0 & P_{BSt} e^{j\Delta\varphi_{BSt}} \end{pmatrix}.$$

In both lines the beam is transmitted by the polarizer (P), then reflected on the mirror (M) and finally again transmitted by the polarizer (P). So the equivalent matrix for the s line is

$$\boldsymbol{A}_{SL} = \boldsymbol{A}_P \boldsymbol{A}_M \boldsymbol{A}_P = |r_{Ps}|^2 |r_{Ms}| e^{j(2\varphi_{Ps}+\varphi_{Ms})} \begin{pmatrix} 1 & 0 \\ 0 & P_P^2 P_M e^{j(2\Delta\varphi_P + \Delta\varphi_M)} \end{pmatrix} \tag{2.15}$$

and the matrix for the p line is calculated through the rotation transformation of the polarizer

$$\begin{aligned} \boldsymbol{A}_{PL} &= \boldsymbol{R}(90°)\boldsymbol{A}_P\boldsymbol{R}(-90°) \cdot \boldsymbol{A}_M \cdot \boldsymbol{R}(90°)\boldsymbol{A}_P\boldsymbol{R}(-90°) \\ &= |r_{Ps}|^2 |r_{Ms}| e^{j(2\varphi_{Ps}+\varphi_{Ms})} \begin{pmatrix} P_P^2 e^{j2\Delta\varphi} & 0 \\ 0 & P_M e^{j(\Delta\varphi_M)} \end{pmatrix} \end{aligned}$$

where $\boldsymbol{R}(90°)$ is the rotation matrix described in (1.19). Assuming that the nanometer translator is placed in the s line[2], its mechanical movement allows to introduce a d optical path difference between the two lines. The associated phase shift $\Delta\varphi$ can be mathematically taken into account by introducing the following matrix

$$\boldsymbol{A}_{shift} = e^{j\Delta\varphi}\boldsymbol{I} = \begin{pmatrix} e^{j\frac{2\pi d}{\lambda}} & 0 \\ 0 & e^{j\frac{2\pi d}{\lambda}} \end{pmatrix}.$$

When the outgoing beams from the two lines are recombined, the Jones vector of the emerging beam is

$$\vec{\boldsymbol{E}}_{out} = (\boldsymbol{A}_{BSr}\boldsymbol{A}_{PL}\boldsymbol{A}_{BSt} + \boldsymbol{A}_{BSt}\boldsymbol{A}_{shift}\boldsymbol{A}_{SL}\boldsymbol{A}_{BSr}) \cdot \vec{\boldsymbol{E}}_{in} = \boldsymbol{M}_{tot} \cdot \vec{\boldsymbol{E}}_{in}.$$

As all the matrices are diagonal ones, the commutation property is valid and the previous relation can be simplified in

$$\vec{\boldsymbol{E}}_{out} = \boldsymbol{A}_{BSr}\boldsymbol{A}_{BSt}(\boldsymbol{A}_{PL} + \boldsymbol{A}_{shift}\boldsymbol{A}_{SL}) \cdot \vec{\boldsymbol{E}}_{in}. \tag{2.16}$$

The term $\boldsymbol{A}_{BSr}\boldsymbol{A}_{BSt}$ is now calculated

$$\boldsymbol{A}_{BSr}\boldsymbol{A}_{BSt} = |r_{BSs}|t_{BSs}||e^{j(\varphi_{BSrs}+\varphi_{BSts})} \begin{pmatrix} 1 & 0 \\ 0 & P_{BSr}P_{BSt}e^{j(\Delta\varphi_{BSr}+\Delta\varphi_{BSt})} \end{pmatrix}$$

[2]For our purpose it is indifferent in which line the translator is positioned. However the analysis with the translator in the p line can be similarly conducted.

and for convenience it is summarized by the equivalent matrix A_{BS}

$$\boldsymbol{A}_{BS} = \boldsymbol{A}_{BSr}\boldsymbol{A}_{BSt} = |a_{BSs}|e^{j\varphi_{BS}} \begin{pmatrix} 1 & 0 \\ 0 & P_{BS}e^{j\Delta\varphi_{BS}} \end{pmatrix}. \tag{2.17}$$

The third term of (2.16) is indeed

$$\boldsymbol{A}_{PL} + \boldsymbol{A}_{shift}\boldsymbol{A}_{SL} = |r_{Ps}|^2|r_{Ms}|e^{j(2\varphi_{Ps}+\varphi_{Ms})} \ .$$

$$\cdot \begin{pmatrix} e^{j\frac{2\pi d}{\lambda}} + P_P^2 e^{j\Delta\varphi_P} & 0 \\ 0 & P_P^2 P_M e^{j(2\Delta\varphi_P+\Delta\varphi_M+\frac{2\pi d}{\lambda})} + P_M e^{j\Delta\varphi_M} \end{pmatrix}.$$

Now the total equivalent matrix M_{tot} is calculated as

$$\boldsymbol{M}_{tot} = \boldsymbol{A}_{BSr}\boldsymbol{A}_{BSt}(\boldsymbol{A}_{PL} + \boldsymbol{A}_{shift}\boldsymbol{A}_{SL}) = |a_{BSs}||r_{Ps}|^2|r_{Ms}|e^{j(\varphi_{BSs}+2\varphi_{Ps}+\varphi_{Ms})} \ .$$

$$\cdot \begin{pmatrix} e^{j\frac{2\pi d}{\lambda}} + P_P^2 e^{j2\Delta\varphi_P} & 0 \\ 0 & P_{BS}P_P^2 P_M e^{j(\Delta\varphi_{BS}+2\Delta\varphi_P+\Delta\varphi_M+\frac{2\pi d}{\lambda})} + P_{BS}P_M e^{j(\Delta\varphi_{BS}+\Delta\varphi_M)} \end{pmatrix}.$$

The scalar terms which multiply the matrix depend on the mirrors efficiency and phase and they are fixed once the optical components are determined. In the following it will be consider the M_{tot}^I matrix, which is the total system matrix normalized with the respect to this scalar term. The terms on the diagonal consist of two components, one dependent on the P rejection of the polarizers. As discussed in Chapter 1.2, the rejection coefficient for a real polarizer can be approximated to zero and its phase delay is assumed to be zero, since it works in transmission. On the base of these approximations, the equivalent Jones matrix of the system becames

$$\boldsymbol{M}_{tot}^I = \begin{pmatrix} e^{j\frac{2\pi d}{\lambda}} & 0 \\ 0 & P_{BS}P_M e^{j(\Delta\varphi_{BS}+\Delta\varphi_M)} \end{pmatrix}$$

which is equivalent to the matrix of a $\frac{2\pi d}{\lambda} - \Delta\varphi_{BS} - \Delta\varphi_M$ retarder. So in the case $P_P = 0$ the polarization state of the outgoing beam is elliptical with parameters dependent on θ and d. In order to investigate the emerging beam polarization state a modified sign function is defined asf equal to the standard sign function except in zero, where it assumes the value 1.

The Jones vector which describes the ingoing beam is

$$\boldsymbol{E}_{in} = |E_0| \begin{pmatrix} \cos\theta \\ \sin\theta \end{pmatrix} = |E_0| \begin{pmatrix} |\cos\theta| e^{j\left(\frac{\mathrm{sgn}\,(\theta+\frac{\pi}{2})+\mathrm{sgn}\,(\frac{\pi}{2}-\theta)-2}{2}\pi\right)} \\ |\sin\theta| e^{j\left(\frac{\mathrm{sgn}\,(\theta)-1}{2}\pi\right)} \end{pmatrix}$$

By applying (2.18) and (2.2), the Jones vector of the exiting beam is

$$\boldsymbol{E}_{out}^{I} = \boldsymbol{M}_{tot}^{I} \cdot \boldsymbol{E}_{in} = |E_0| \begin{pmatrix} |\cos\theta| e^{j\left(\frac{2\pi d}{\lambda} + \frac{\mathrm{sgn}\,(\theta+\frac{\pi}{2}) + \mathrm{sgn}\,(\frac{\pi}{2}-\theta) - 2}{2}\pi\right)} \\ |\sin\theta| P_{BS} P_M e^{j\left(\Delta\varphi_{BS} + \Delta\varphi_M + \frac{\mathrm{sgn}\,(\theta)-1}{2}\pi\right)} \end{pmatrix}, \tag{2.18}$$

where $-\pi < \theta \leq \pi$. With the notations of Chapter 1.1 and Figure 1.1, the $\vec{\boldsymbol{E}}_{out}^{I}$ is an elliptically polarized wave that is described by the equation of the ellipse (1.4)

$$\frac{E_x^2}{E_{0x}^2} + \frac{E_y^2}{E_{0y}^2} - 2\frac{E_x}{E_{0x}}\frac{E_y}{E_{0y}}\cos\delta = \sin\delta^2$$

where

$$\delta = \delta_y - \delta_x = \left(\Delta\varphi_{BS} + \Delta\varphi_M + \frac{\mathrm{sgn}\,(\theta) - 1}{2}\pi - \frac{2\pi d}{\lambda} - \frac{\mathrm{sgn}\,(\theta+\frac{\pi}{2}) + \mathrm{sgn}\,(\frac{\pi}{2}-\theta) - 2}{2}\pi\right)$$

is the total phase delay between the x and y axes induced by the system. The sign of δ defines the electric field rotation direction: for a positive phase delay the rotation is clockwise, for a negative phase delay is counterclockwise.

In order to determine the general conditions for obtaining a circular polarized light, the fallowing parameters need to be taken in account

$$\begin{cases} \tan\alpha = \frac{E_{0y}}{E_{0x}} = P_M P_{BS} |\tan\theta|, & 0 \leq \alpha \leq \frac{\pi}{2} \\ \tan\chi = \frac{|b|}{|a|}, & 0 \leq \chi \leq \frac{\pi}{4} \end{cases} \tag{2.19}$$

since they describe the circularity of a polarization ellipse. As shown in (1.10) and (1.11), it is proven the relationship

$$\sin 2\chi = \sin 2\alpha |\sin\delta| = \frac{2\tan\alpha}{1+\tan^2\alpha}|\sin\delta| = \frac{2P_M P_{BS}|\tan\theta|}{1 + P_M^2 P_{BS}^2 \tan^2\theta}|\sin\delta|.$$

The circular polarization is obtained for $\tan\chi = \tan\alpha = 1$. Accordingly it results that $\sin\chi = 1$ and, using the relations in (2.19) we retrieve the circular polarization conditions

$$\begin{cases} |\tan\theta| = \frac{1}{P_M P_{BS}} \\ \delta = (2m+1)\frac{\pi}{2} \end{cases}. \tag{2.20}$$

When the circular polarized light can be generated, the system is said to be equalized.

For the purpose it is not important to know the absolute phase delay of each optical component. Since the relative phase can be controlled and corrected by the translation stage. Suppose to fix a reference position of the transition stage, denoted with $d = 0$, where a linearly polarized light is obtained in output. In this case the χ coefficient of the

Element	Type	Working Angle	P	$\Delta\varphi = \varphi_p - \varphi_s$
M_x	Aluminum	0° in Reflection	1	0°
P_x	Polarizer	0° in Transmission	0	0°
BS	BK7	45° in Refl. and 0° in Tran.	0,85	0°

Table 2.2: Parameters adopted in the system simulation for the Michelson configuration.

output beam is 0, and consequently from the relation (1.10) the total phase delay results a multiple of 2π. All translations involve a total phase delay which depend only by the d parameter calculated from this reference

$$\delta = \frac{2\pi d}{\lambda} + 2\pi m \qquad\qquad m = 0, 1, 2...$$

2.2.1 Simulations

A numerical simulation has been performed, in order to determine the input θ angle on the basis of real values characterizing the rejection coefficients for an equalized system. As said a phase delays of each component can be neglected. We suppose to use a BK7 beam splitter the reflection and transmission coefficients of which have been directly obtained by the tests we have made in laboratory. The values of the coefficients are reported in Table 2.2.

By the circular polarization condition (2.19)

$$\theta = \arctan\frac{1}{P_{BS}} = \arctan\frac{1}{0,85} \backsimeq 50^\circ$$

2.3 Mach-Zehnder Configuration

The use of polarizers can be avoided in the Mach-Zehnder configuration (see Figure 2.10), where each line is polarized through a mirror (B) working at its Brewster angle. The beam is divided by the (BS_1) beam splitter in the two lines s and p. The mirror (B_1) and (B_2) polarize the beams on two different perpendicular planes. The s line is vertically polarized along the yz plane, while the p line is polarized on the horizontal xz plane. Finally the beams are superposed by the (BS_2) beam splitter in a unique interferometric beam. The (B_x) and (M_x) mirrors work at the same Brewster angle, while all the other mirrors (ML) are set to a incident angle of 45°. As for the Michelson configuration, we suppose to work with linearly polarized input beams as shown in Figure 2.8. The phase delay $\Delta\varphi$ is controlled by a piezo-electric translator, on which the (M_2) and (ML_5) mirror are mounted[3].

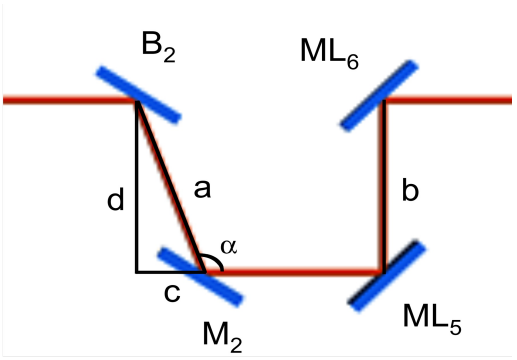

Figure 2.9: The path difference l is controlled by the s line. The (M_2) and (ML_5) mirrors are fixed on the nanometrical translator.

In order to analyze the optical path difference l, a schematic figure of the s line is shown in Figure 2.9. The total path difference is given by

$$l = \Delta a + \Delta b.$$

By the trigonometrical proprieties

$$\Delta a = \frac{\Delta d}{\sin(180° - \alpha)} = \frac{\Delta d}{\sin\alpha}$$

where Δd is the movement of the piezo-electric translator, while α is the Brewster angle of (B_2). For construction the term Δb is equal to Δd, so the total path difference becomes

$$l = \frac{\Delta d}{\sin\alpha} + \Delta d = \frac{\Delta d(1 + \sin\alpha)}{\sin\alpha}. \tag{2.21}$$

[3]The dual configuration can be obtained by fixing the nanometric translator on the p line.

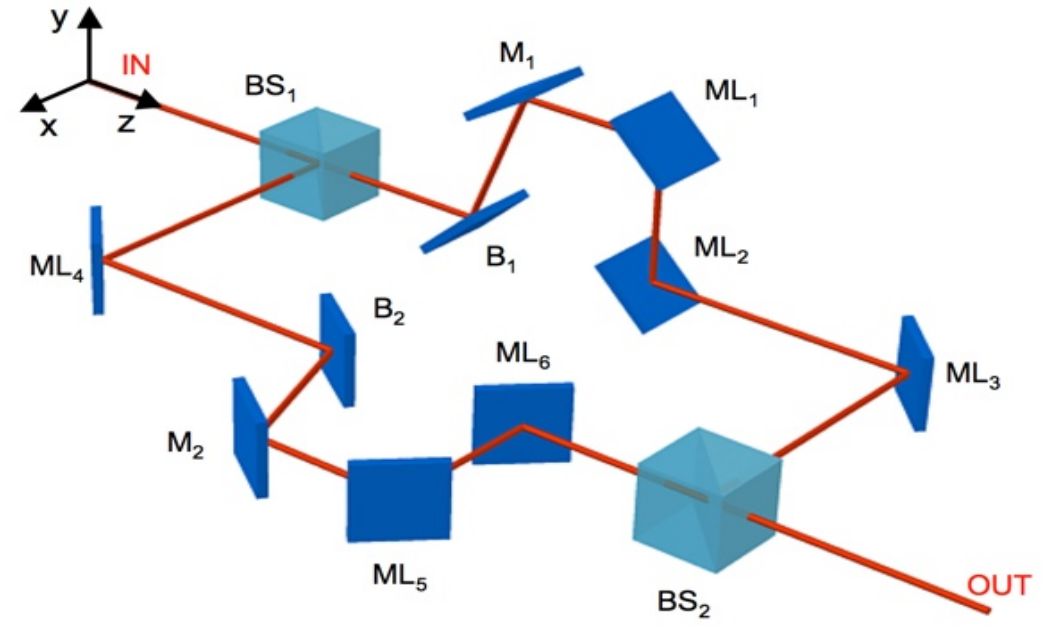

(a)

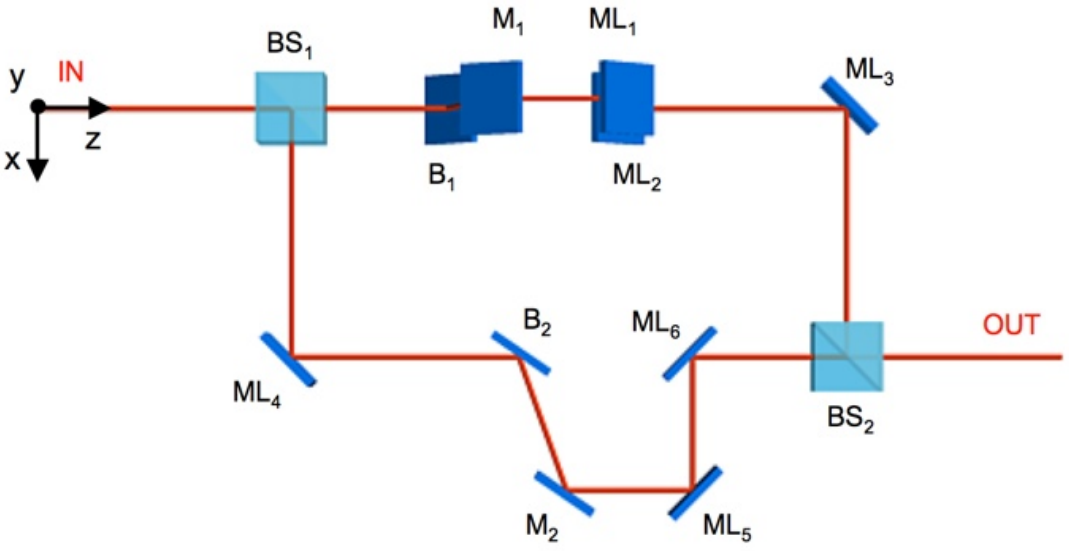

(b)

Figure 2.10: The Mach-Zehnder configuration is shown in a perspective view (a) and in a view from above (b). The ML indicate the mirrors at 45°, B are the mirrors working at their Brewster angle, M work at the same angle of (B) and BS are the beam splitters. Each line consists in one mirror (B) at Brewster angle and three sequential mirrors. The p line works with a perpendicular plane of incidence to the respect of the s line.

In order to characterize the Mach-Zehnder configuration, a similar analysis to the Michelson configuration by the Jones matrices is carried out. So the matrices of each optical component is defined as

$$\boldsymbol{A}_M = |r_{Ms}|e^{j\varphi_{Ms}} \begin{pmatrix} 1 & 0 \\ 0 & P_M e^{j\Delta\varphi_M} \end{pmatrix}$$

$$\boldsymbol{A}_{ML} = |r_{MLs}|e^{j\varphi_{MLs}} \begin{pmatrix} 1 & 0 \\ 0 & P_{ML} e^{j\Delta\varphi_{ML}} \end{pmatrix}$$

$$\boldsymbol{A}_B = |r_{Bs}|e^{j\varphi_{Ms}} \begin{pmatrix} 1 & 0 \\ 0 & P_B e^{j\Delta\varphi_B} \end{pmatrix}$$

$$\boldsymbol{A}_{BS} = \boldsymbol{A}_{BSr}\boldsymbol{A}_{BSt} = |a_{BS}|e^{j\varphi_{BSs}} \begin{pmatrix} 1 & 0 \\ 0 & P_{BS} e^{j\Delta\varphi_{BS}} \end{pmatrix}$$

where A_{BS} is the equivalent matrix for the beam splitter already defined in (2.17). So the s line is described by the matrix

$$\begin{aligned} \boldsymbol{A}_{SL} &= \boldsymbol{A}_{ML}^3 \boldsymbol{A}_B \boldsymbol{A}_M \\ &= |r_{MLs}|^3 |r_{Bs}||r_{Ms}| e^{j(3\varphi_{MLs}+\varphi_{Bs}+\varphi_{Ms})} \begin{pmatrix} 1 & 0 \\ 0 & P_{ML}^3 P_B P_M e^{j(3\Delta\varphi_{ML}+\Delta\varphi_B+\Delta\varphi_M)} \end{pmatrix} \\ &= r_L e^{j\varphi_{Ls}} \begin{pmatrix} 1 & 0 \\ 0 & P_{ML}^3 P_B P_M e^{j\Delta\varphi_{SL_p}} \end{pmatrix}. \end{aligned}$$

The presence of the translator in the s line is taken in account with the shift matrix

$$\boldsymbol{A}_{shift}\boldsymbol{A}_{SL} = r_L e^{j\varphi_{Ls}} \begin{pmatrix} e^{j\frac{2\pi l}{\lambda}} & 0 \\ 0 & P_{ML}^3 P_B P_M e^{j(\Delta\varphi_{SL_p}+\frac{2\pi l}{\lambda})} \end{pmatrix},$$

where the term l is the total path difference described in (2.21) introduced by the translator. Indeed the p line is characterized by the presence of rotational matrices, as some mirrors work perpendicularly on the yz plane

$$\begin{aligned} \boldsymbol{A}_{PL} &= \boldsymbol{A}_{ML}\boldsymbol{R}(90^\circ)\boldsymbol{A}_M\boldsymbol{A}_{ML}^2\boldsymbol{A}_B\boldsymbol{R}(-90^\circ) \\ &= |r_{MLs}|^3 |r_{Bs}||r_{Ms}| e^{j(3\varphi_{MLs}+\varphi_{Bs}+\varphi_{Ms})} \begin{pmatrix} P_M P_{ML}^2 P_B e^{j(2\Delta\varphi_{ML}+\Delta\varphi_B+\Delta\varphi_M)} & 0 \\ 0 & P_{ML} e^{j\Delta\varphi_{ML}} \end{pmatrix} \\ &= r_L e^{j\varphi_{Ls}} \begin{pmatrix} P_M P_{ML}^2 P_B e^{j\Delta\varphi_{PLs}} & 0 \\ 0 & P_{ML} e^{j\Delta\varphi_{PL_p}} \end{pmatrix}. \end{aligned}$$

The output electric $\boldsymbol{E}_{out}$ field can be found as

$$\begin{aligned}\boldsymbol{E}_{out} &= (\boldsymbol{A}_{BSt}\boldsymbol{A}_{shift}\boldsymbol{A}_{SL}\boldsymbol{A}_{BSr} + \boldsymbol{A}_{BSr}\boldsymbol{A}_{PL}\boldsymbol{A}_{BSt}) \cdot \boldsymbol{E}_{in} \\ &= \boldsymbol{A}_{BSt}\boldsymbol{A}_{BSr}(\boldsymbol{A}_{shift}\boldsymbol{A}_{SL} + \boldsymbol{A}_{PL}) \cdot \boldsymbol{E}_{in} \\ &= \boldsymbol{A}_{BS}(\boldsymbol{A}_{shift}\boldsymbol{A}_{SL} + \boldsymbol{A}_{PL}) \cdot \boldsymbol{E}_{in} \\ &= \boldsymbol{M}_{tot} \cdot \boldsymbol{E}_{in}\end{aligned} .$$

There the equivalent Jones matrix $\boldsymbol{M}_{tot}$ for the Mach-Zehnder configuration is now obtained

$$\boldsymbol{M}_{tot} = r_L e^{j\varphi_{Ls}} \cdot \begin{pmatrix} P_M P_{ML}^2 P_B e^{j\Delta\varphi_{PLs}} + e^{j\frac{2\pi l}{\lambda}} & 0 \\ 0 & P_{ML}^3 P_B P_M P_{BS} e^{j(\Delta\varphi_{SLp} + \frac{2\pi l}{\lambda})} + P_{ML} P_{BS} e^{j\Delta\varphi_{PLp}} \end{pmatrix}.$$

For convenience the total matrix $\boldsymbol{M}_{tot}$ is normalized to the constant term $r_L e^{j\varphi_{Ls}}$. In order to carry out a first approximation analysis, the rejection term of the mirrors (B_x) is neglected. On the basis of this approximation the normalized equivalent matrix M_{tot}^I

$$\boldsymbol{M}_{tot}^I = \begin{pmatrix} e^{j(\frac{2\pi l}{\lambda})} & 0 \\ 0 & P_{ML} P_{BS} e^{j(\Delta\varphi_{ML} + \Delta\varphi_{BS}} \end{pmatrix}.$$

Maintaining the notation for the input beam described in (2.2) and Figure 2.8, the Jones vector of the exiting beam is

$$\boldsymbol{E}_{out}^I = \boldsymbol{M}_{tot}^I \boldsymbol{E}_{in} = |E_0| \begin{pmatrix} |\cos\theta| e^{j\left(\frac{\operatorname{sgn}(\theta+\frac{\pi}{2}) + \operatorname{sgn}(\frac{\pi}{2}-\theta) - 2}{2}\pi + \frac{2\pi l}{\lambda}\right)} \\ |\sin\theta| P_{ML} P_{BS} e^{j\left(\Delta\varphi_M + \Delta\varphi_{BS} + \frac{\operatorname{sgn}\theta - 1}{2}\pi\right)} \end{pmatrix}.$$

The degree of ellipticity χ is derived by the relations (1.10) and (1.11),

$$\sin 2\chi = \sin 2\alpha |\sin\delta| = \frac{2\tan\alpha}{1+\tan^2\alpha} |\sin\delta| = \frac{2P_{ML}P_{BS}|\tan\theta|}{1 + P_{ML}^2 P_{BS}^2 \tan^2\theta} |\sin\delta|, \tag{2.22}$$

where δ is the phase delay between the vertical and horizontal components of the outgoing beam

$$\delta = \delta_y - \delta_x = \Delta\varphi_{ML} + \Delta\varphi_{BS} + \frac{\operatorname{sgn}\theta - 1}{2}\pi - \frac{\operatorname{sgn}(\theta+\frac{\pi}{2}) + \operatorname{sgn}(\frac{\pi}{2}-\theta) - 2}{2}\pi - \frac{2\pi l}{\lambda}.$$

As in the previous section, the state of polarization of the output electric field is described by the parameters

$$\begin{cases} \tan\alpha = \frac{E_{0y}}{E_{0x}} = P_{ML}P_{BS}|\tan\theta|, & 0 \le \alpha \le \frac{\pi}{2} \\ \tan\chi = \frac{|b|}{|a|}, & 0 \le \chi \le \frac{\pi}{4} \end{cases}.$$

Element	Type	Working Angle	P	$\Delta\varphi = \varphi_p - \varphi_s$
ML_x	Aluminum	45° in Reflection	0,94	12°
M_x	Aluminum	56,6° in Reflection	0,89	20°
B_x	BK7	56,6° in Reflection	varied	-180°
BS	BK7	45° in Refl. and 0° in Tran.	0,85	0°

Table 2.3: Parameters adopted in the system simulation for the Mach-Zehnder configuration.

The circular polarization is obtained for $\tan\chi = \tan\alpha = 1$. Consequently by relation (2.22), the $\sin\chi = 1$, which leads to the equalizing condition for the Mach-Zehnder configuration

$$\begin{cases} |\tan\theta| = \frac{1}{P_{ML}P_{BS}} \\ \delta = (2m+1)\frac{\pi}{2} \end{cases} . \tag{2.23}$$

2.3.1 Simulations

In real practice it is impossible to perfectly align the mirror at its Brewster angle and, consequently, the rejection coefficient of (B_x) mirrors should be taken in account and such analysis become more complex. In order to understand the degradation of the outgoing beam polarization due to the noise component, a numerical simulation of the system has been performed for different values of the P_B. The mirrors parameters have been computed by IMD program [19], while the parameters for the beam splitter have been obtained by measuraments in our laboratory. The values used for the rejection coefficients and phase delays are reported in Table 2.3.

The ingoing polarization plane inclination θ and the phase delay have been adjusted to obtain an output circular polarization when $P_B \to 0$. By the circular polarization condition (2.23) it follows

$$\theta = \arctan\frac{1}{P_{BS}P_{ML}} = \arctan\frac{1}{0.89 \cdot 0.85} \backsimeq 52°.$$

A noise component has been added using the equivalent matrix M_{tot} to this theoretical signal and the principal parameters of the polarization ellipse have been computed. Figure 2.11a reports the parameters that describe the ellipticity of the outgoing beam, while Figure 2.11b shows the degradation of the circular polarization for different values of P_B. From the simulations it is evident that the P_B parameter should not be neglected, as the ellipticity of the outgoing beam has a high sensitivity to the spurious component.

However a lower sensitivity can be achieved by substituting the (M_x) aluminum mirrors with a BK7 ones working at the Brewster angle as (B_x). In this way each line is polarized by two sequential mirrors at the Brewster angle. The quality of polarization of the lines improves proportionally to the second power of P_B and consequently the effects of the

spurious components decrease (see Figure 2.12). In this last configuration the ellipticity of the outgoing beam has a lower sensitivity to the noise so that the polarization properties can be considered ideal up to a rejection parameter P_B of 0.1.

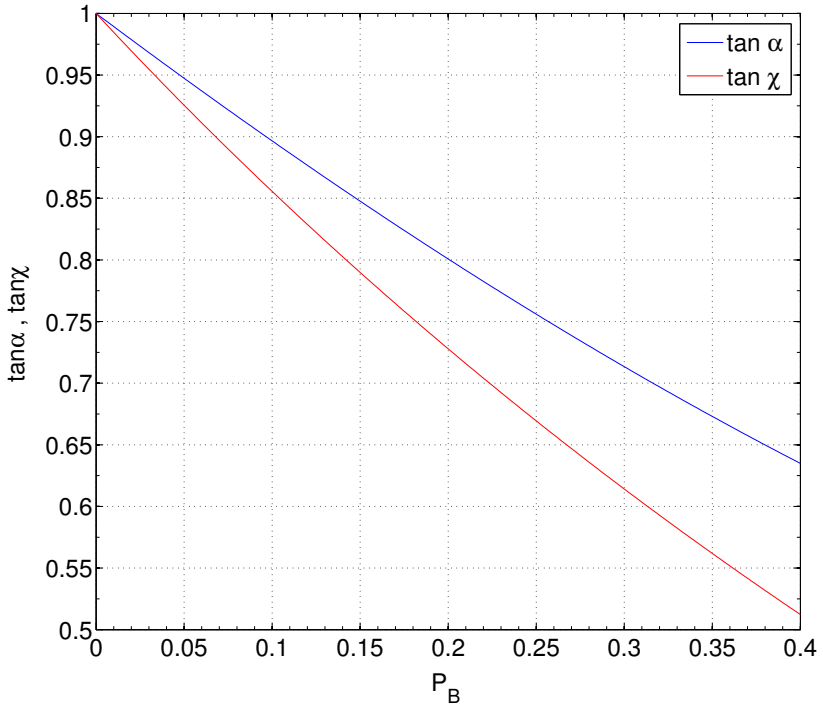

(a)

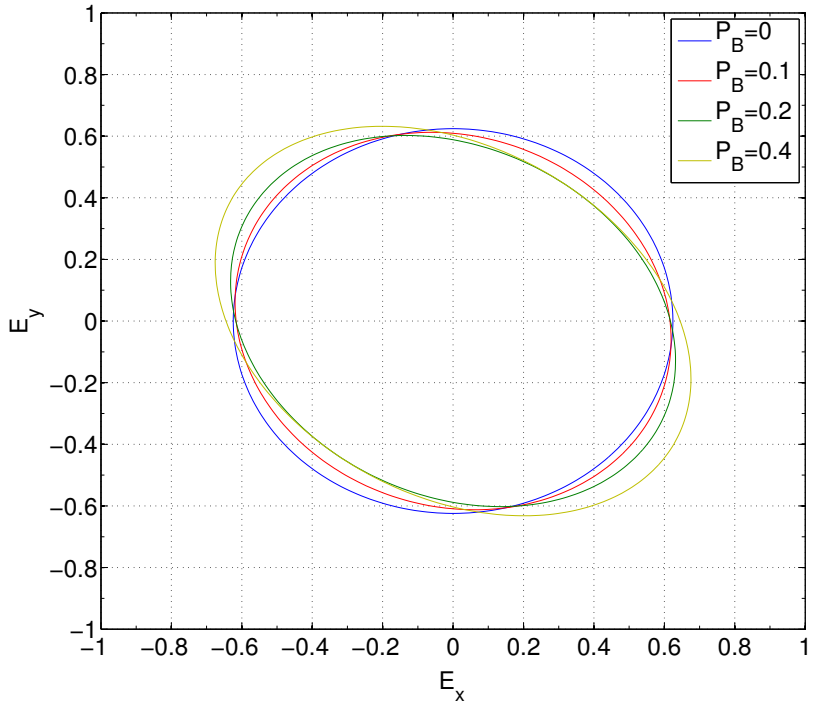

(b)

Figure 2.11: (a) A simulation of the $\tan\alpha$ and $\tan\chi$ parameters of the outgoing beam versus P_{ML}. (b) A simulation of the degradation of the ellipses for different values of P_{ML}.

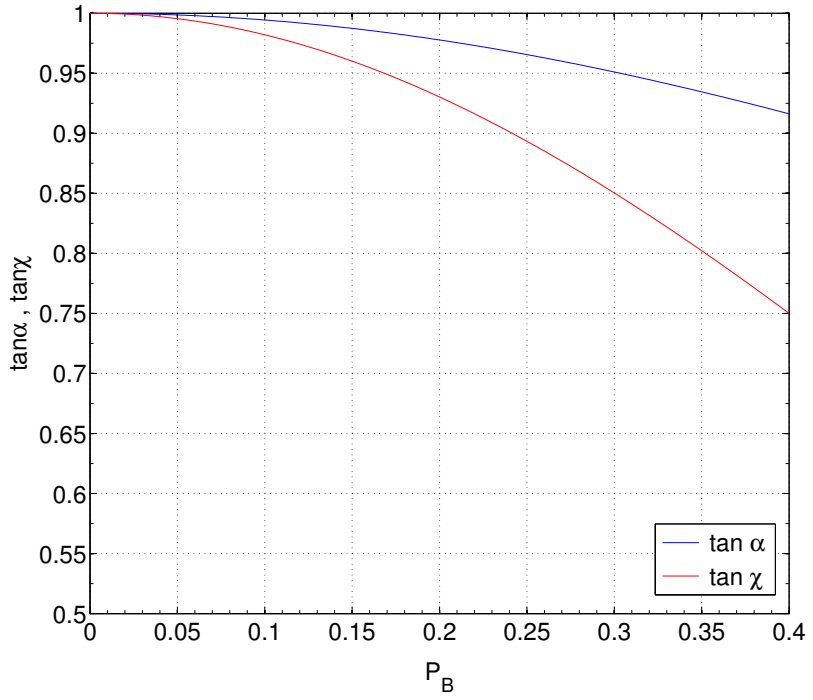

(a)

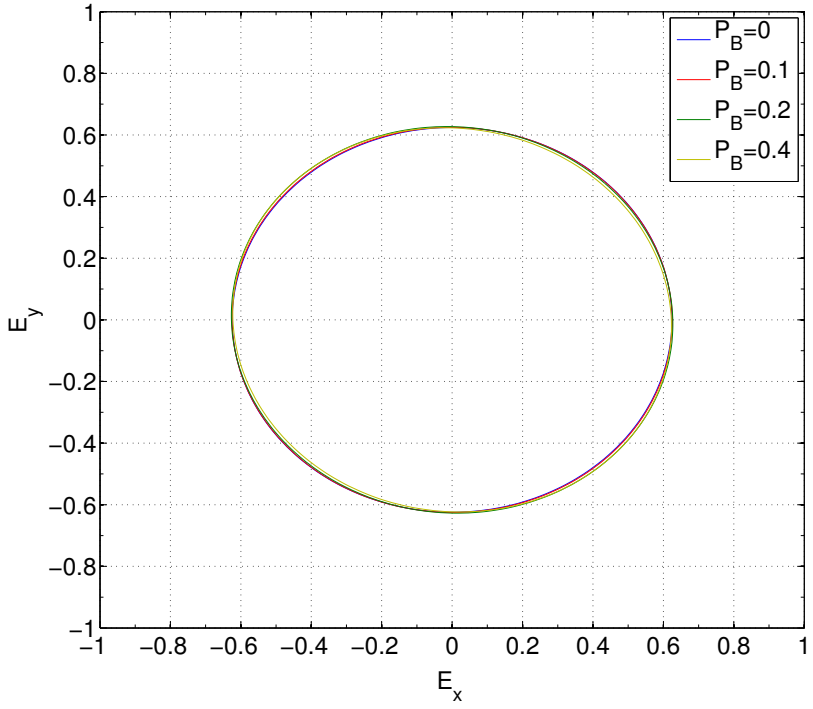

(b)

Figure 2.12: (a) A simulation of the $\tan\alpha$ and $\tan\chi$ parameters of the outgoing beam versus P_{ML}. The system is set to have two mirrors working at the Brewster angle. (b) A simulation of the degradation of the ellipses for different values of P_{ML}. The system is set to have two mirrors working at the Brewster angle.

2.4 Analysis System

The analysis system should be able to identify the polarization status of the outgoing beam. It consists of an optical system based on the series of two lenses, a polarizer and two possible detectors: a CCD camera or a photometer. In Figure 2.13 it is shown a scheme of the disposition of the optical components. In order to magnify the beam,

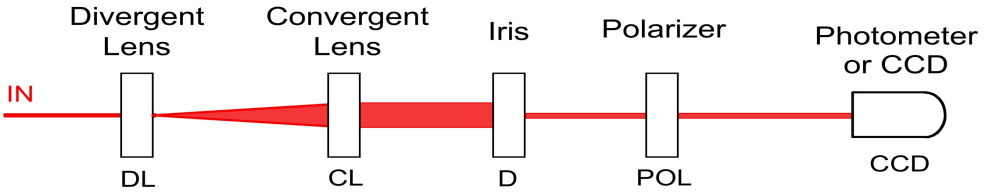

Figure 2.13: The analysis system is composed by a magnification system of one divergent lens (DL) and one convergent lens (CL). A iris (D) select a part of the beam to be tested. Finally the polarization status of the beam is analyzed by a polarizer (POL), followed by a photometer or CCD (CCD).

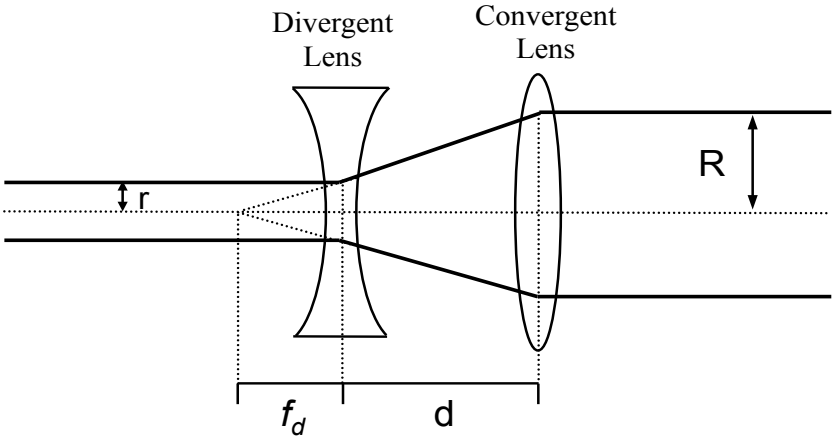

Figure 2.14: The magnification system is realized by one divergent lens (DL) followed by one convergent lens (CL). The lenses are placed at the distance d.

a convergent (CL) and a divergent (DL) lenses are placed in front of the detector (see Figure 2.14). By the lens equation (2.4) we obtain the collimation condition

$$d = |f_c| - |f_d| \tag{2.24}$$

where d is the distance between the two lenses, while f_c and f_d are the focal length respectively for the convergent lens and the divergent lens. For construction, the magnification expression is given by

$$M = \left| \frac{f_c}{f_d} \right|. \tag{2.25}$$

The magnification system is composed by a divergent lens of $f_d = -50$ mm and a convergent lens of $f_c = +100$ mm. Consequently, by (2.24) and (2.25) the distance between the lenses is $d = 50$ mm, while the magnification results $M = 2$x.

A iris (D) allows to select a part of the magnified beam, which pass through the polarizer (POL). Then the beam image is acquired by a CCD or its intensity is measured by a photometer. A picture of the real analysis system is shown in Figure 2.15.

The intensity of a wave which results from a polarizer follows the Malus law. Supposing to have a wave E propagating along the z direction through a polarizer from (1.3) and (1.13) it results that the total intensity can be written as

$$I = E_{0x}^2 \cos^2 \alpha + E_{0y}^2 \sin^2 \alpha$$

where α is the angle between the polarizer axis and the x direction. In first approximation it is easy to identify a circular polarized wave as its intensity doesn't change for any rotation of the polarizer. On the contrary a linear polarized wave has a maximum and a minimum intensity on two different angles α of the polarizer. The intensity is maximum, when the axis of the polarizer is parallel to the oscillating plane and it has a minimum, when they are perpendicular to each other. Some simulations are made in order to understand how the intensity varies according to the rotation of the analysis polarizer and to the phase delay δ. For convenience the simulations have been conducted using cartesian coordinates instead of polar ones. Fixing the maximum amplitude E_{0x} and E_{0y} of the electric field respectively of the p and s lines, and by rotating the polarizer of 360° the trend of the intensities are found for different values of the phase delay δ. As underlined in Figure 2.16a each point of the graphic is identified by the angle α and by an intensity I. Figure 2.16 shows the intensities for balanced systems, while Figure 2.17 refers to unequalized systems.

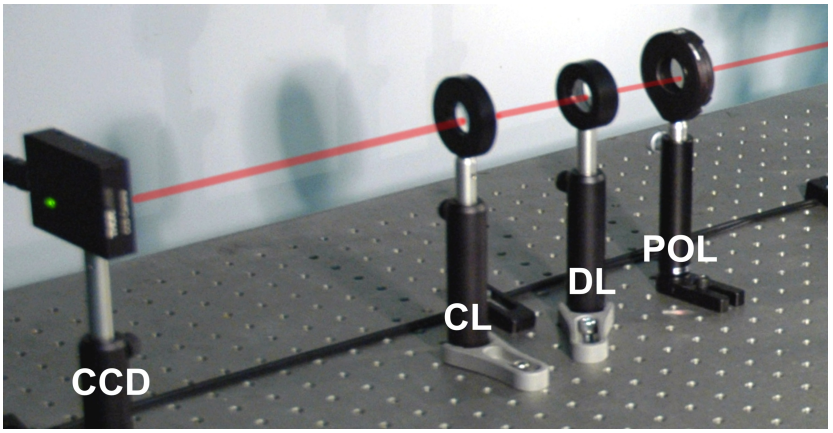

Figure 2.15: Our analysis system in laboratory. The iris is not present because the interested part of the spot is selected through the software of the CCD. However when the photometer is used, the iris was essential in order to select only a limited part of the interferometric figure.

The quadratic terms of cosine and sine determine the trend of the intensity values. For example for a balanced system all graphics intersect each other in four different points, which are at the same distance from the origin (see Figure 2.16). Even modifying the polarization status, their distance should be always equal and whenever it changes, it reveals that the system is not longer balanced, as, for example, it is in Figure 2.17.

The final goal is to find the polarization ellipse. A set of measurements to different α angles are obtained and they are reported in a I_x and I_y graph. At this point, simulations similar to those shown in Figure 2.16 and 2.17 are carried out changing the δ, in order to fit the experimental data. In this way the polarization ellipse for each different position of the piezoelectric translator is obtained.

In real experiment the superposition of the two beams is not ideal and they recombine having a hit angles, which causes the appearance of interferometric fringes. For this reason, during the test the alignment is optimized to enlarge the central fringe, which is selected by the iris. However as in the system the s line and p lines are linearly polarized on two perpendicular direction, the interferometric image is not directly seen. The fringes appears only if the analysis polarizer is inserted with the angle α at $\pm 45°$. To understand this phenomenon suppose to deal with a Michelson interferometer, which creates an interferometric image shown in Figure 2.18. The wedge effect of the retro reflection mirrors causes the formation of a interferometric image that shows the sequence of clear and dark fringes. The maximum peaks denote that the lines are in phase $\delta = 0$, while the dark sides of the image indicate that the lines s and p are in opposite phase $\delta = \pi$. Suppose now to insert the two polarizers in each line to obtain the variable polarization control system in the Michelson configuration explained in Section 2.2. Obviously the interferometric image disappears as the lines are polarized in two perpendicular directions, but no spatial changes are involved in the distribution of phase delay in different areas of the spot (see Figure 2.18). The phase dalays are so related with the polarization status of beam:

- $\delta = 0$: the s and p components are superposed in phase, and consequently $+45°$ linearly polarized waves are obtained.
- $\delta = \pi/2$: counterclockwise circular polarized waves are obtained.
- $\delta = \pi$: the lines are in opposite phase and -45° linearly polarized waves are obtained.
- $\delta = 3\pi/2$: clockwise circular polarized waves are obtained.

In order to characterize the distribution we insert an analysis polarizer (POL). The new interferometric image is shown in Figure 2.19 for different angle α of the polarizer. When the axis of polarizer is positioned with a α angle of $+45°$, we can see a new interferometric image. The clear areas indicates the presence of a +45 linear polarization, while the dark areas is characteristic of a -45° linear polarization. By rotating slowly the polarizer, the

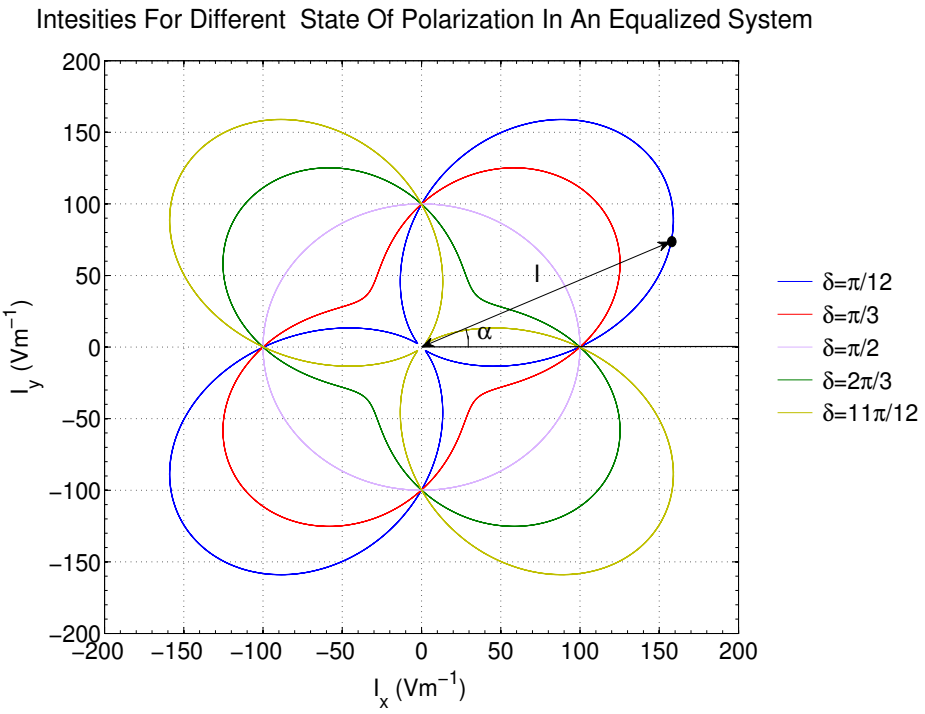

(a)

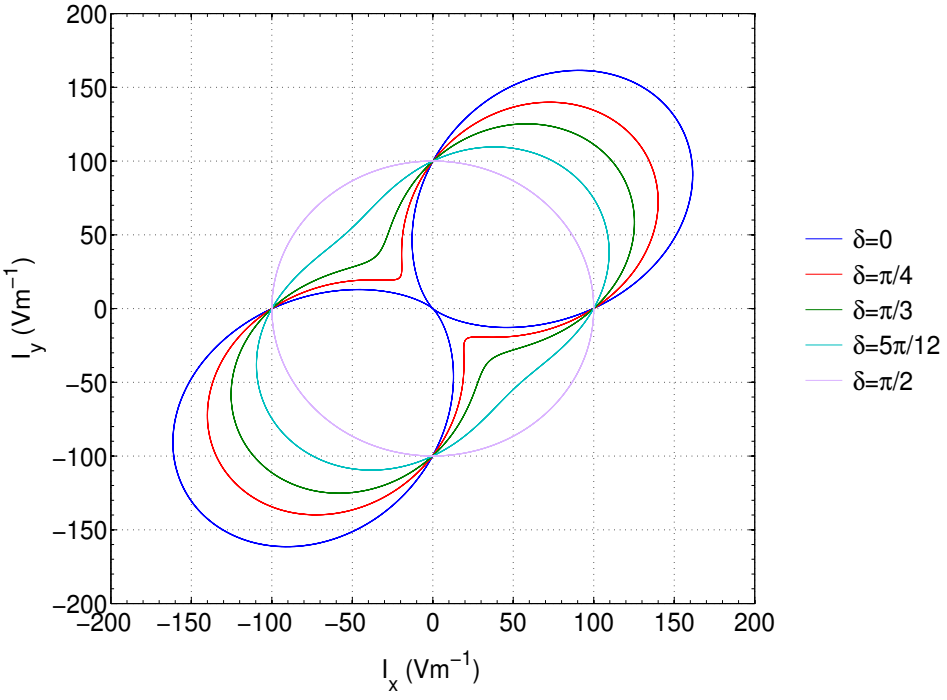

(b)

Figure 2.16: Simulations of the intensities obtained by the analysis of a polarizer for different value of phase delay δ. The system is balanced and circular polarization is obtained. The inclination α coincides to the rotation of the axis of polarizer with the respect of the x direction, while I is the intensity detected by the photometer.

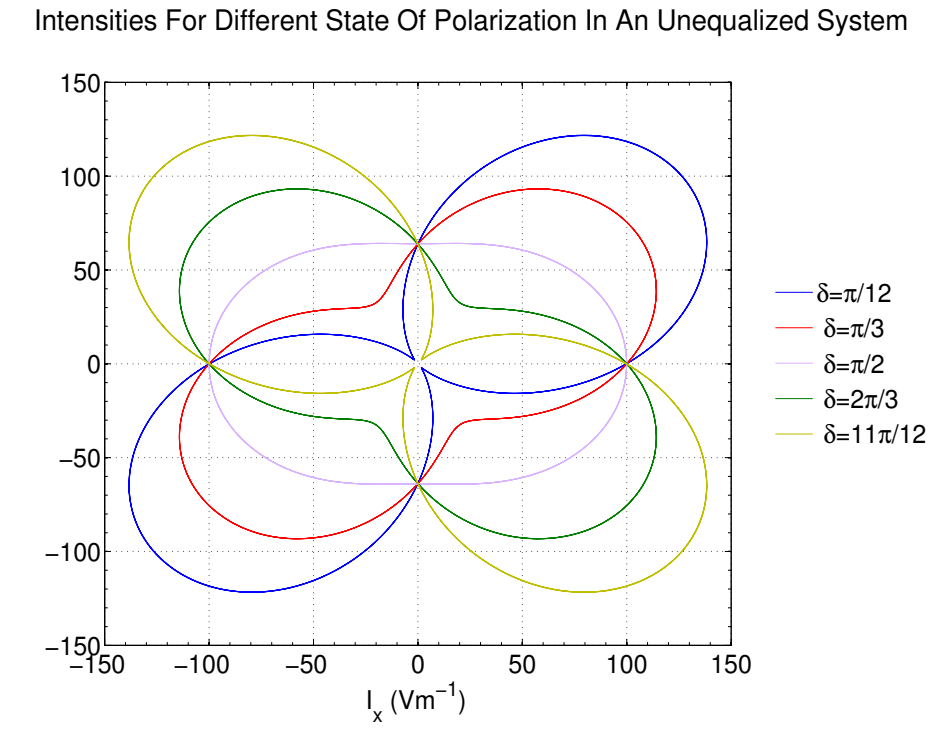

(a)

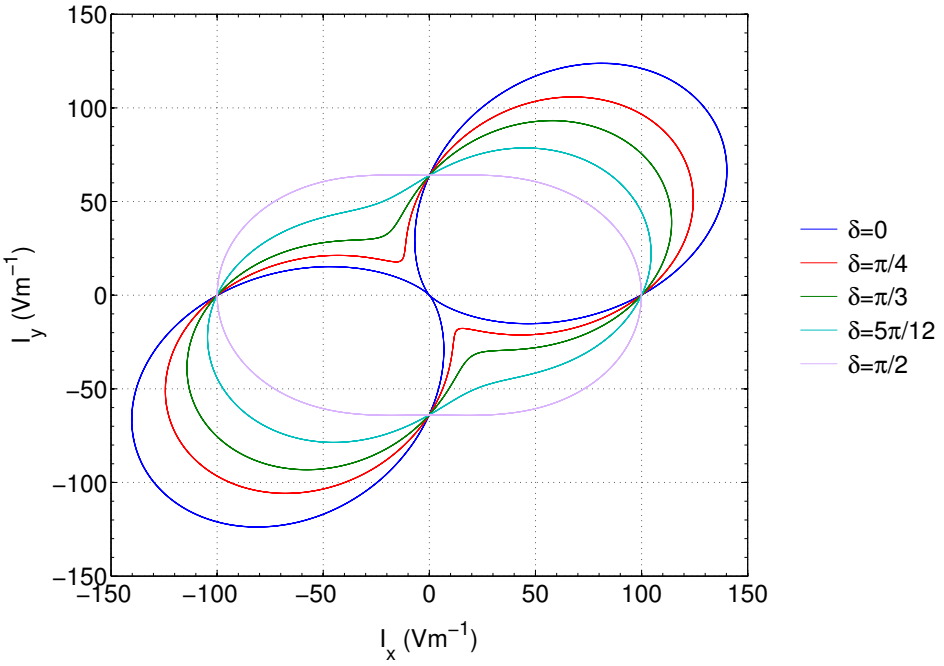

(b)

Figure 2.17: Simulations of the intensities obtained by the analysis of a polarizer for different value of phase delay δ. The system is unequalized and only elliptical and linear polarization is obtained.

fringes start disappearing until a uniform spot is viewed. In this condition the polarizer is set with the main axis parallel to the x direction. As the s line is completely killed, there is no interference between the beams. Keeping rotating the polarizer until $\alpha = -45°$, the fringes reappear, but with an opposite disposition: the minimum peaks are replaced by maximum ones (see Figure 2.19). However there are some fringes, which remain clear for each rotation of the polarizer. These areas are positioned between dark and clear fringes and they are coincident with a circular polarization status. Their intensity is approximately half of the clear fringes for $\alpha = \pm 45°$ and they are expected to remain constant for any rotation of the polarizer.

The entire analysis can be similarly performed for an angular range $45° < \alpha < +135°$, or generally for each angle α of the analysis polarizer.

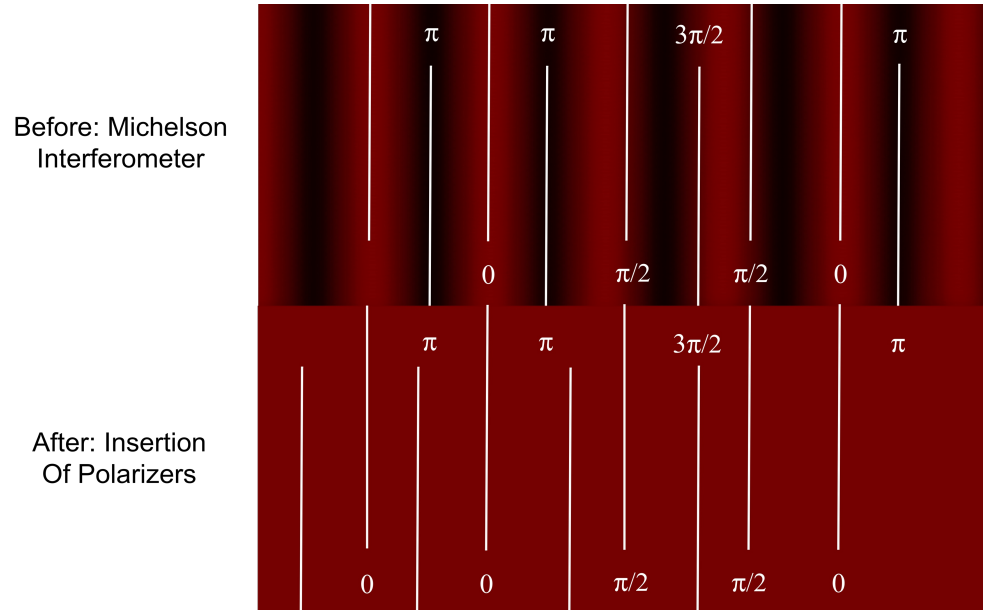

Figure 2.18: Simulation of a interferometric image created by the wedge effect in a Michelson interferometer. We indicate the phase delay δ for some areas. When the polarizers are inserted in the lines, the fringes disappear, but spatially the phase delay δ doesn't change.

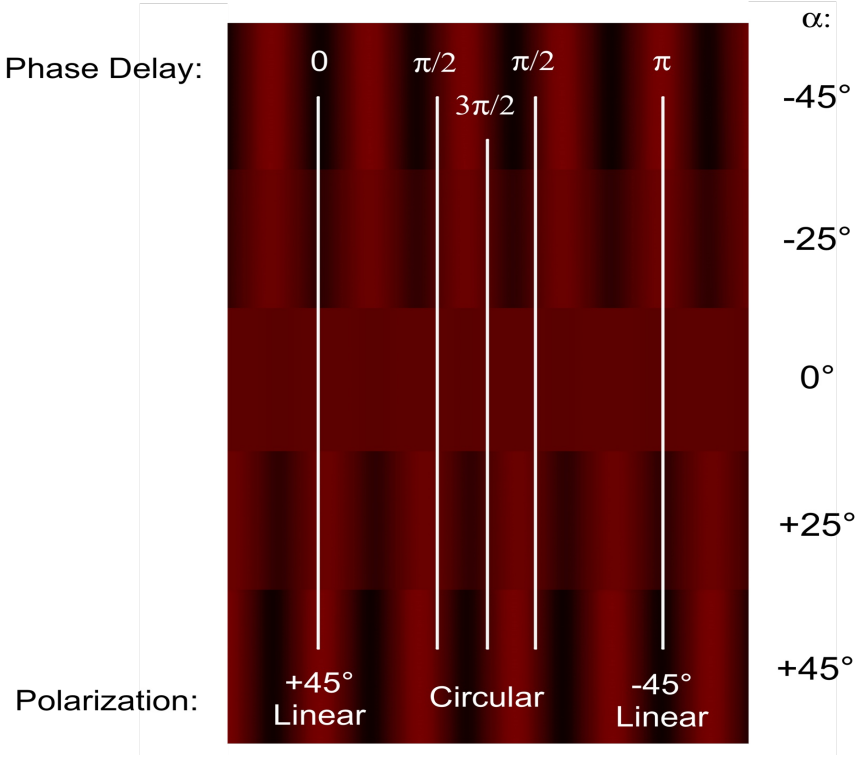

Figure 2.19: A simulation of the interferometric image for different rotation α of the polarizer. We aspect to find a sequence of fringes differently polarized. We observe that for $\delta = \frac{\pi}{2}, \frac{3\pi}{2}$ the borders of the fringe are composed of circular polarized waves, which don't disappear for any rotation of the polarizer. On the contrary, for $\delta = 0, \pi$ the fringes alternate each other for $\alpha = \pm 45°$, as they result linearly polarized in two perpendicular directions (+45° and -45°).

Chapter 3

The Alignment Procedure and Tests

In Chapter 2 the system has been analyzed from a theoretical point of view. At CNR-IFN of Padova two working prototypes of the system have been realized adopting a Michelson and Mach-Zehnder configuration scheme respectively. This chapter describes the alignment procedures and the tests carried out on both configuration.

For convenience the Michelson and Mach-Zehnder configurations are tested on a unique optical bench, since the piezoelectric translator stage was shared between the two. Each interferometer is provided with a He-Ne 632,8 nm laser source. In Figure 3.1 the laser traces on the optic table are shown: the Michelson one is in blue trace, while the Mach-Zehnder one is in red trace. With (IN) is indicated the polarizer placed just in front of the beam-splitting system. Th function of the polarized was explained in section 2.2 and shown in Figure 2.8. Experimentally it is needed to generate a input beam with different polarization characteristic necessary to test the system; it is fundamental in the case that the s and p component are needed equalized.

Mirrors not labelled are those used in the set up to change the direction of the beam for convenience. In the Mach-Zehnder configuration the beam-splitters are replaced by two grazing mirrors (SM), which are able to spatially divide and recombine the beam in the respective s and p lines. This configuration is the last improvement of the Mach-Zehnder configuration and it is called the *all-reflective Mach-Zehnder configuration*, which is introduced in the next chapter.

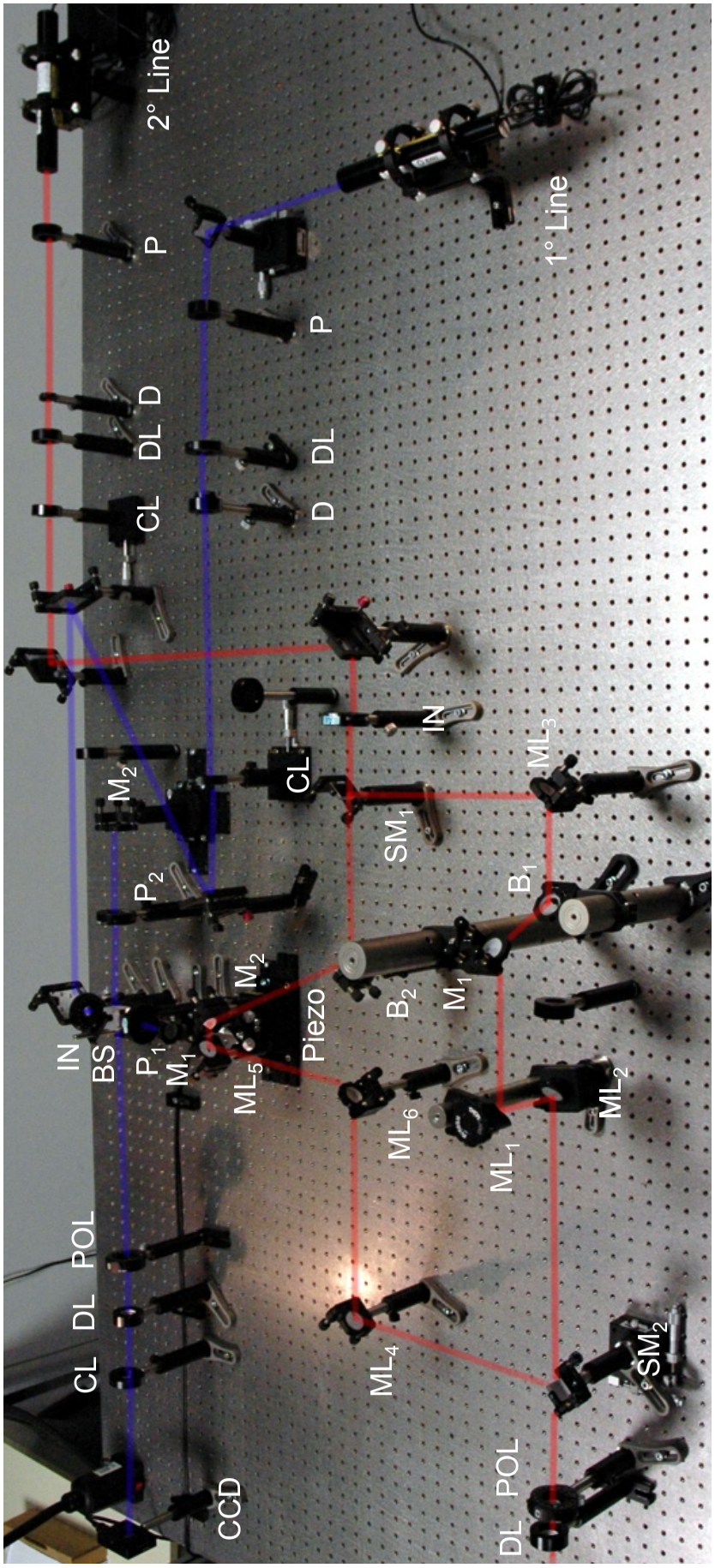

Figure 3.1: A general view of the optical bench. The blue line tests the Michelson configuration, while the red one tests the Mach-Zehnder configuration.

3.0.1 The Isolation Of The Ambience Noise

As both systems requires precision of nanometers, it is essential to isolate the system from noise vibrations of the ambiance and to use stable supports for the optical elements. After the alignment procedure, all support were strongly fixed on table through threaded screws. The system is very sensible to the mechanical vibration. The most unstable optical elements were the highest, such as the high supports on the p line in the Mach-Zenhnder configuration. For this reason the beam is set to propagate more closer as possible to the plane table. During the measurements the optical table should not be minimally touched. So the analysis system was dislocated on a different optical table, as the manual rotation of the analysis polarizer would have compromised the measures. Moreover any vibrating or movable object should not be placed on the optical table. The ground vibration can be absorbed by pumping the air bearing of the optical table. However this solution should be adopted only if the analysis system is mounted on the same table of the main system. Otherwise it can be counterproductive due to the continuos misalignment between the main system and the analysis one.

Other noise factors were the vibrations of the ambiance air, which can nanometrically misaligned the optical elements. It was convenient to switch off the air ventilation to remove eventual air turbulence in the room. Speaking close to a mirror changed the interferometric figure, too. In conclusion it is essential to isolate the entire system by the ambience, which can produce unwanted mechanical vibrations of the optical elements.

3.0.2 The Coherence Test Of The Source Device

Before proceeding on the alignment of the final configuration the coherence degree of the laser devices have been tested through the Michelson interferometer. The used laser devices have a coherent length greater then 2 meters and present clear interferometric fringes. The stability of fringes over the time is essential during the test of Michelson and Mach-Zehnder configurations. The analysis of the state of polarization of the beam requires the manual rotation of the analysis polarizer, which took about 4-5 minutes. In this period of time the selected interferometric image should not shift or change, otherwise measures result to be affected by an error due to the change of the state of polarization.

3.1 First Step: Collimator

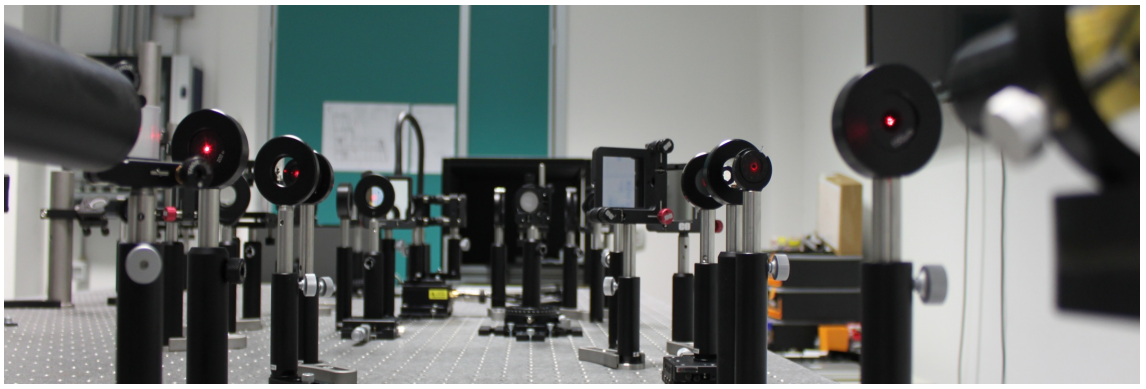

Figure 3.2: A central view of the disposition of the beam lines on the optical table. For practice two source systems are used (one on the left and one on the right) to test the two configurations of the final system.

As described above, on the optical bench there are two different lasers (see Figure 3.2 and Figure 3.3). Both lasers devices emit a red beam at the wavelength of 632,8 nm, which is then magnified to a beam diameter of 11 mm. The magnification system is realized by selecting two different solutions presented in Section 2.1 in Table 2.1. For the Michelson configuration

$$\text{conf. 1)} \quad D = 200\ \mu\text{m} \quad f_1 = -50\ \text{mm} \quad f_2 = 150\ \text{mm} \quad d_1 \simeq 425\ \text{mm} \quad d_2 \simeq 105\ \text{mm},$$

while for the Mach-Zehnder configuration

$$\text{conf. 2)} \quad D = 150\ \mu\text{m} \quad f_1 = -50\ \text{mm} \quad f_2 = 150\ \text{mm} \quad d_1 \simeq 306\ \text{mm} \quad d_2 \simeq 107\ \text{mm}.$$

A picture of the configuration 2) is shown in Figure 3.4.

The effects of the source system are shown in Figure 3.5, which reports two intensity snapshots of the spot of 1° line. The Figure 3.5a shows the initial distribution of the intensity of the spot just at the exit of the laser device; the intensity distribution is clearly not uniform. In Figure 3.5b the beam is filtered by the source system; the spot presents a uniform and circular intensity distribution.

Both collimation system has been aligned in the following steps:

1. The laser device is fixed on the optical bench and it is vertically and horizontally aligned.

2. The pinhole (P) is fixed on a horizontal micrometrical translation stage and it positioned in such a way that the laser beam impinges in the center of the hole. The micrometer translator is useful to the fine alignment of the pinhole. The diffraction

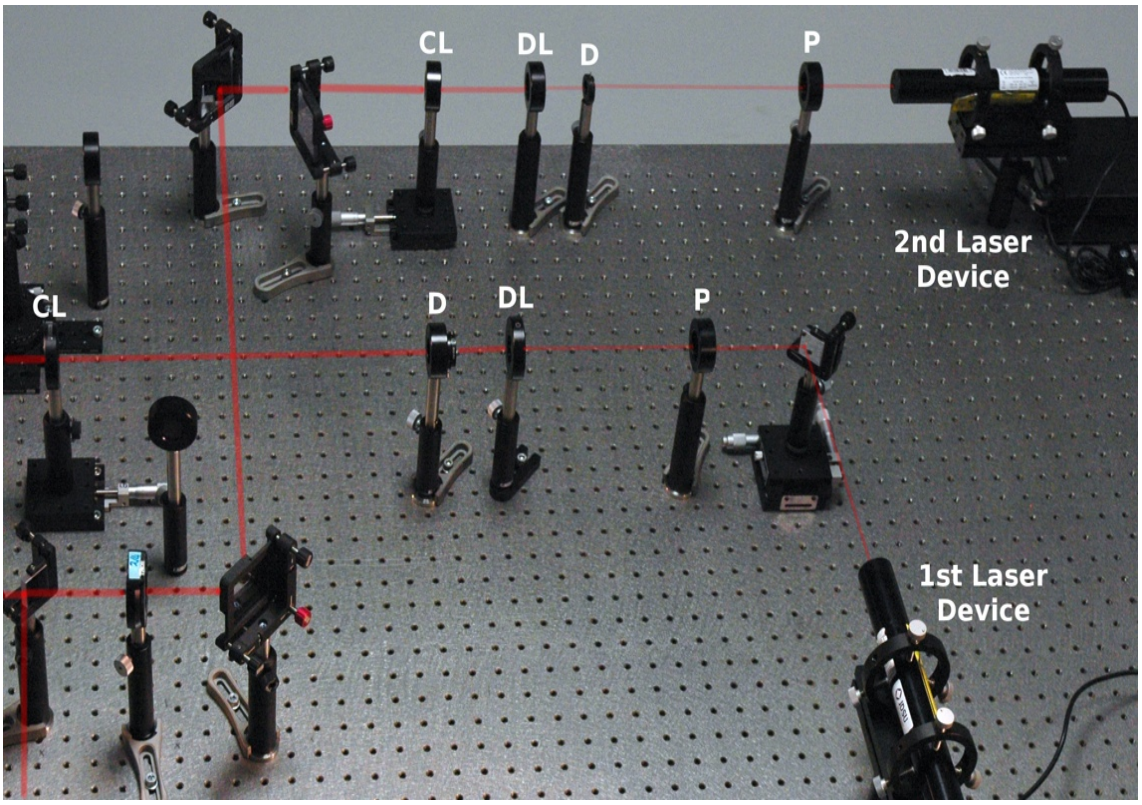

Figure 3.3: The two different source lines, created by independent source systems, aligned in order to test the Michelson and the Mach-zehnder configurations. The presence of the micrometrical translator under the convergent lenses (CL) permits a fine adjustment of the collimation.

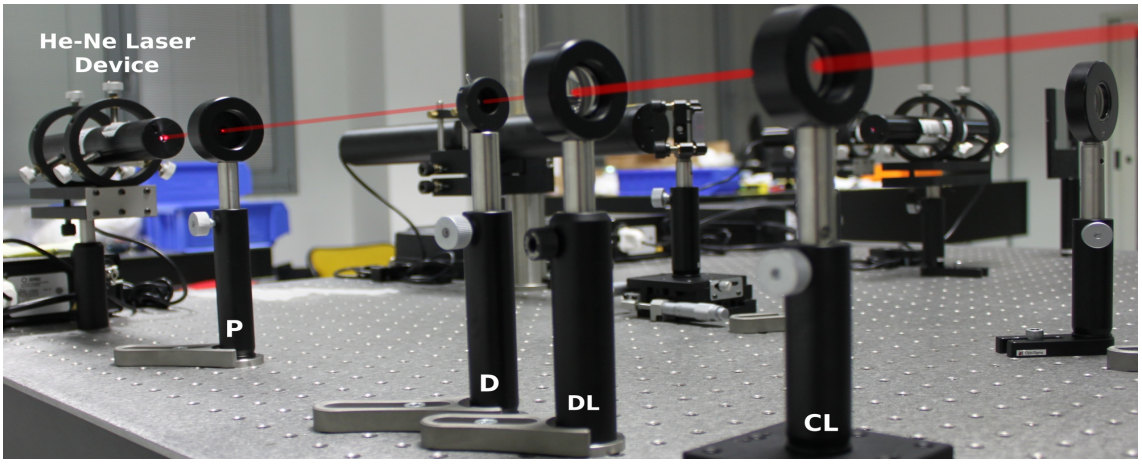

Figure 3.4: A He-Ne device creates the laser beam. A pinhole (P) creates the diffraction image, but only the central peak is selected by the iris (D). Finally the beam is collimated by a diverging lens (DL) followed by a converging one (CL).

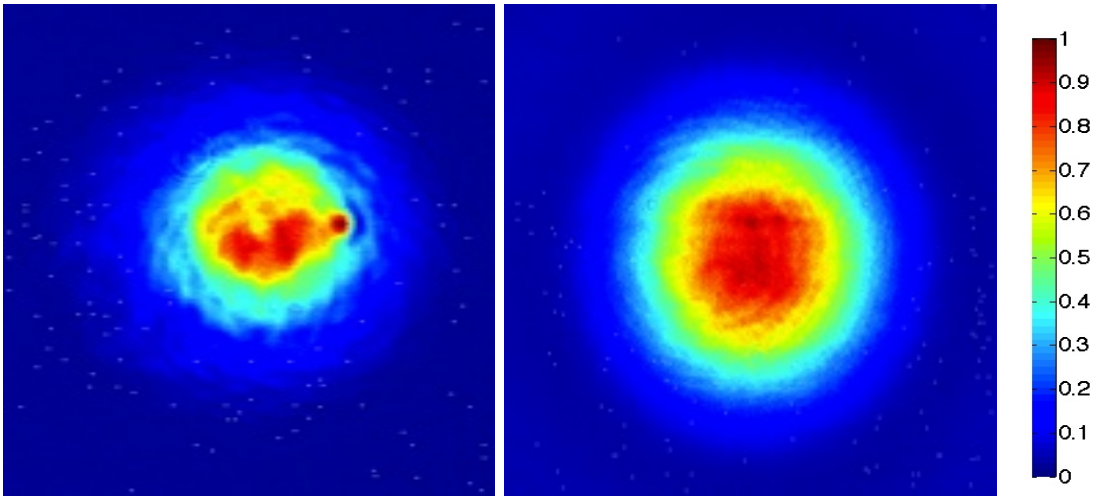

(a) (b)

Figure 3.5: The effects of the source system in the first line. Both snapshots are made using the same laser device. In (a) is shown the laser beam directly created by the laser device. The spot presents one spurious mode on the right side. In (b) the laser beam is purified by the source system. The spot is uniform and it presents a unique central mode.

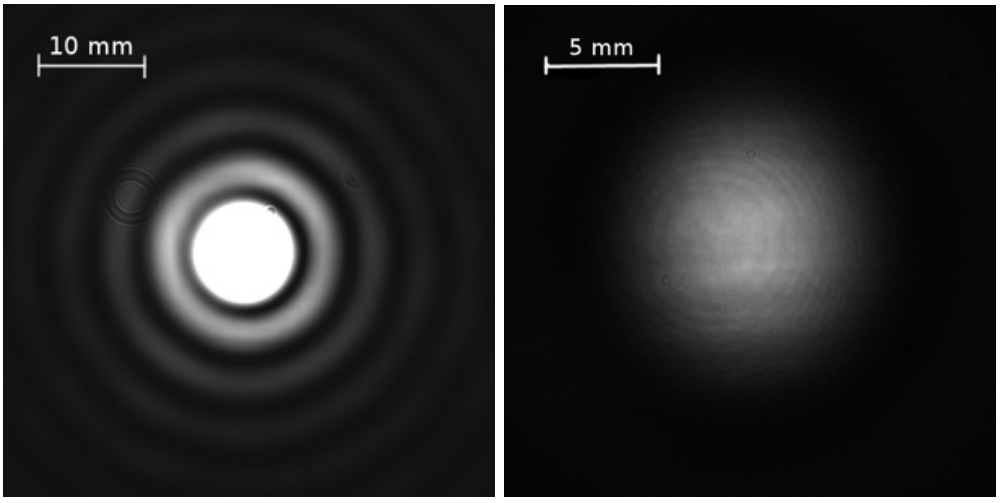

(a) (b)

Figure 3.6: (a) The diffraction image created by the pinhole $D = 200$ μm in the 1° line. The snapshot is saturated in order to show higher peaks around the main one. (b) The central peak of the diffraction image is selected by the iris (D) and a new filtered beam is created.

image is shown in Figure 3.6a.

3. The iris (D) is centered and sufficiently closed in order to select the central part of the diffraction image. If circular diffraction fringes appear close to the border of the spot, it means that the alignment of the iris is not precise, as that part of the central spot is cutted. The alignment needs to be redone.

4. The divergent lens (DL) is placed at the distance d_1 from the pinhole (P). As the distance d_1 control the magnification, it can be coarsely measured with a millimeter ruler.

5. The convergent lens (CL) is positioned at the distance d_2 on a micrometrical translation stage, which allows to adjust finely the collimation of the beam (see Figure 3.3). In order to verify the collimation condition, the diameter of the spot is measured for different distances from the (CL). If all measures are equal, then the beam is well collimated. On the contrary a better collimation should be achieved by controlling the micrometer translation stage.

6. A magnified and collimated beam is obtained (see Figure 3.6b). Some mirrors are placed in order to freely control and transfer the beam lines in different positions of the optical bench.

3.2 Second Step: The Polarization System with Michelson Configuration

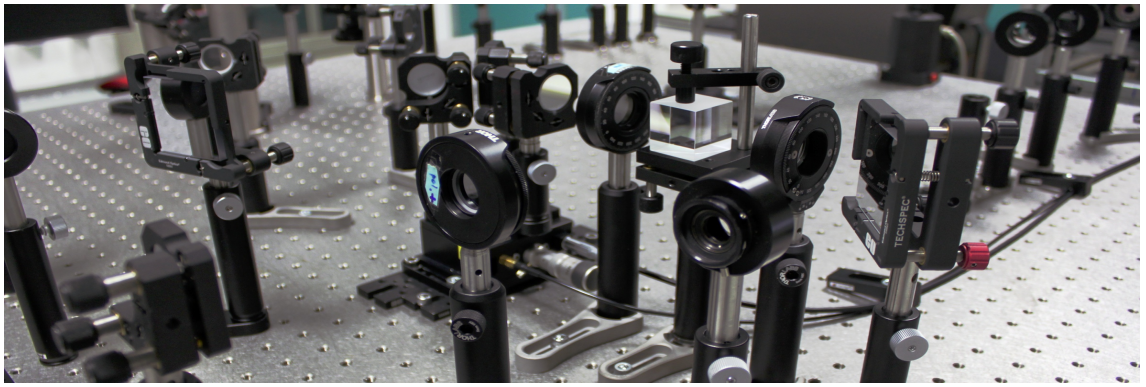

Figure 3.7: The real Michelson configuration characterized by the central positioned beam splitter and the two polarized lines.

After aligning the source system as described in the previous section, the Michelson configuration has been realized. A general view of the Michelson system is shown in Figure 3.7, which faithfully reproduces the design illustrated in Figure 2.7. The main used components are:

- 1x BEAM SPLITTER: the beam splitter is a BK7 one with intensity division of 50/50.
- 2x MIRRORs: plane aluminum mirrors. Each mirror is fixed on its proper tip-tilt support.
- 2x POLARIZERs: common linear polarizers with parallel surface. Each polarizer is mounted on its proper support, which allows the rotation of the main axis with a precision of 2°.
- 1x PIEZOELECTRIC STAGE: the piezoelectric stage is configured in close loop mode with a declared fine control of 10 nm.

The realization is very simple: after the alignment of a Michelson interferometer, two polarizers are added in the two lines (see Figure 3.8). The alignment procedure consists in the following steps:

1. Firstly the retro reflection mirror (M_1) is mounted on the piezo-electric stage. As it works at normal incidence, the alignment of (M_1) is led looking at direction of the reflected beam on the (D) iris surface of the source system. A perfect alignment is reached when the beam passes through the center of (D). The beam splitter is slightly tilted in order to avoid multiple reflection and propagation of spurious beam. The s line is now aligned.

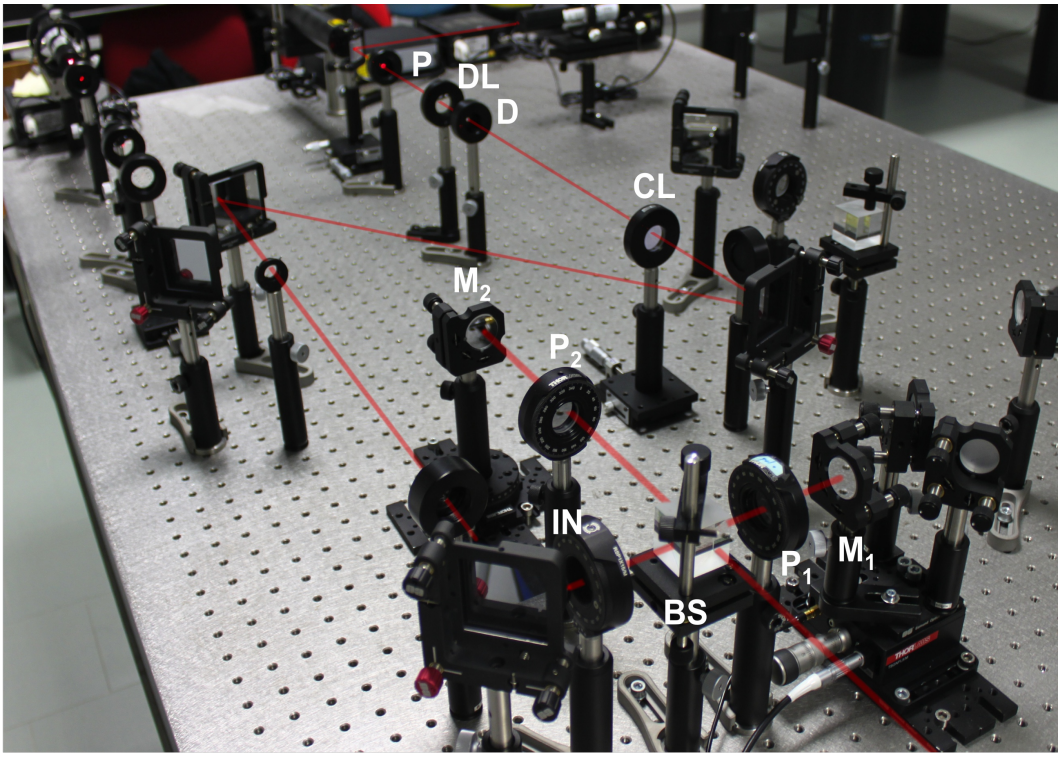

(a)

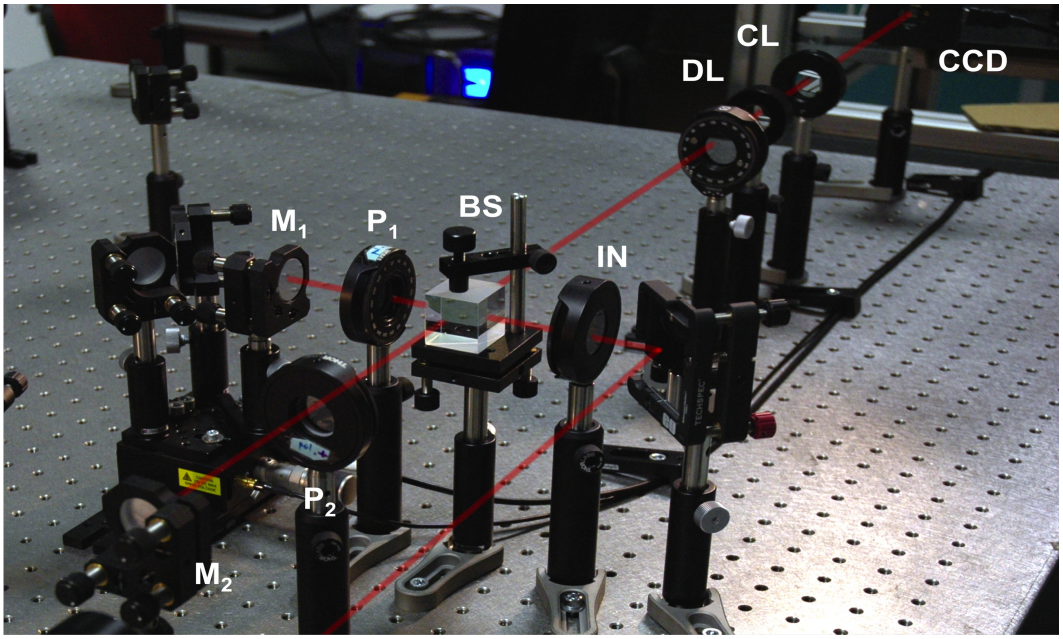

(b)

Figure 3.8: (a) The view of Michelson configuration at the source system side. The (IN) element is the input polarizer, which is essential in order to equalize the system. The series of (P_1) and (M_1) identify the s line, while (P_2) and (M_2) are characteristic of the p line. (b) The view of Michelson configuration at the analysis system side.

2. The beam splitter (BM) is mounted and aligned in such a way that the direction of the second line results perpendicular to the first one. The vertically alignment can be led by the help of two irises regulated at the same height.

3. The mirror (M_2) is then aligned. This mirror is fixed on a micrometer rotation stage, in order to correct precisely the angle of incidence. By controlling the micrometer rotation stage is possible to change the fringe frequency. The p line is now aligned.

4. The width of fringes is finely controlled by the micrometer rotator of (M_2) which can eliminate the wedge effect until obtaining a unique interference fringe (see Figure 3.9a). If the interference image appears as a uniform spot, probably the fringes are too much closer to each other to be seen by human eye. This situation is derived by a bad alignment procedure. However the absence of the fringes can be caused by other factor, such as the loss of temporal coherence along the beam trace. To test the functionality and the sensibility of the piezoelectric translator is by observing the fringes system. When the piezo-electric stage is moved by steps of $\Delta l = \lambda/4 \simeq 158$ nm, the passage from a constructive and destructive interference on the same spatial position must be evident and clear as shown in Figure 3.9b.

5. The last step to the Michelson configuration is inserting the two polarizers in the lines of interferometer. As described in Section 2.2, the s line is characterized by the (P_1) polarizer, which has the main axis parallel to the vertical y direction, while the (P_2) polarizer has the main axis parallel to the horizontal x direction. As the lines are polarizing along two perpendicular directions, the interferometric image disappears and a uniform spot is seen.

The final Michelson configuration is now aligned, but it needs to be equalized. The equalization procedure consists on positioning the main axis of the input (IN) polarizer to the correct inclination θ, in order to have the same final intensity in both p and s lines. The intensity is measured by aligning the analysis system with the photodiode, as described in Section 2.4, with the difference that the analysis polarizer (POL) is removed. As the two output beams are superposed, the intensities of one line is measured by stopping the propagation of the opposite line, for example by covering one optical element. The equalization is finely adjusted by manually rotating the (IN) polarizer. The two intensity values are measured and compared until they are equal. At the end the system is equalized for $\theta = +49°$,

$$P_s = 85,5 \text{ nA} \qquad P_p = 85,4 \text{ nA}$$

where P_s is the power of the s line, while P_p is the power of the p line[1]

[1]For convenience the power measured by the photodiode can be normalized to its supply voltage, and consequently it assumes the expression in Ampere.

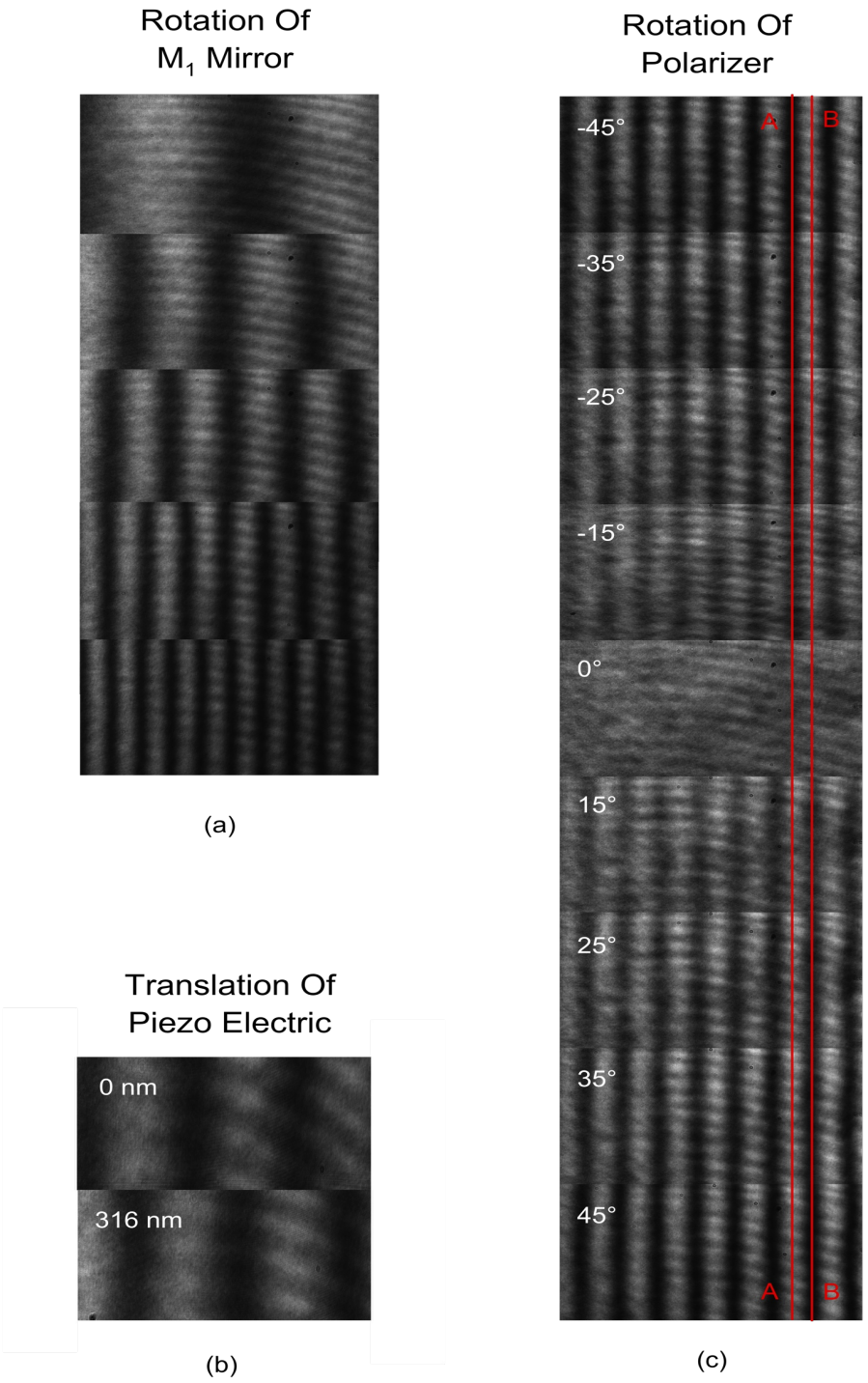

Figure 3.9: (a) The image shows the effects of the rotation of M_1 mirror placed on the rotator in the Michelson interferometer. The sequence is made for rotations of a constant angle at the order of some μrad. (b) The piezoelectric translator was firstly tested by making a translation of $\lambda/2 \simeq 316$ nm. An inversion of the fringe position was aspected, and so it was in real practice, too. (c) The real interferometer image in Michelson configuration for different rotations of the polarizer. The angle indicates the position of the main axis of polarizer with the respect to the vertical direction y. The red traced lines A and B shows the expected effect of the appearing and disappearing fringes described in Section 2.4. The linearly $\pm 45°$ polarized areas are clearly visible, as they are denoted by maximum and minimum peak.

3.2.1 The Tests

Different experimental tests have been carried out to verify the proper functioning of the system.

The first test is carried to verify the polarization states in the fringes system, as described in Section 2.4. For this purpose the photodiode is replaced by a CCD and the (POL) analysis polarizer is slowly rotated. The phenomenon of the appearing and disappearing of polarized fringes is clearly seen and it is shown in Figure 3.9c. The positions of the maximum and minimum peaks correspond to the linearly polarized areas. While the central part of transition regions indicates the circularly polarized areas, whose intensity never changes for any rotation of (POL). Moreover it is possible to see the inversion of the fringes, when the (POL) analysis polarizer rotates from -45° position to +45° position. For example in reference to Figure 3.9c, the area crossed by the red line A has a minimum peak (of intensity close to 3 nA) when the (POL) is rotated of -45°, while it has a maximum peak (of intensity close to 130 nA) when the (POL) is rotated of +45°. This means that the area is characterized by a linearly +45° polarized waves. On the contrary, the inversion of fringes on the red line B indicates that the area is linearly -45° polarized.

The second test is aimed to verify the controllability of the polarization through the piezoelectric. The polarization state of the output beam is measured for different position of the piezoelectric. As the interferometric image is structured in fringes, it doesn't present a uniform polarized spot. So the fringes are enlarged by acting the rotator of (M_2) mirror, until obtaining only a unique fringe. A small central area of the unique fringe is selected by aligning the iris (D) of the analysis system, which permits a fine selection. Figure 3.10 and Figure 3.16 show some of the possible polarization state of the output beam for different positions of the piezoelectric. The measures and fits are obtained by fixing the piezoelectric in a position and by measuring the intensities for a complete 360° rotation of the analysis polarizer (POL) in steps of 10°. The measured values are graphically fitted by using the phase delay δ as variable parameter; then the ellipses are recovered (see Figure 3.11). Table 3.1 describes the datas and fits reported in Figure 3.10.

Translator (nm)	**Polarization**	**Angle Of Ellipticity χ**	**Phase Delay (rad)**	**Figure Color**
N/D	Linear	0.18°	0.0	Red
20	Elliptical	20.05°	0.7	Blue
60	Almost Circular	38.43°	1.8	Green
120	Almost Linear	12.65°	2.7	Orange
150	Elliptical	18.86°	3.8	Brown
388	Circular	44.64°	4.7	Purple

Table 3.1: The Polarization states obtained by the Michelson configuration in reference to Figure 3.10. The angle of ellipticity χ is obtained by the original relation described in equation (1.9).

In order to test the sensibility of the system to the movement of the piezoelectric stage, three consecutive measures are shown in Figure 3.14. The measured intensities refer to three different position of the piezoelectric, which is moved by steps of $\Delta l = 20$ nm. Again after performing the graphical fits, the polarization ellipses are recovered and shown in Figure 3.15.

An example of data referring to a measure with an output beam in linear polarization state is shown in Figure 3.12. The maximum intensity value is 126 nA, while the minimum intensity is 6 nA, measured respectively when the main axis of the analysis polarizer (POL) is set at +45° and -45°. Its angle of ellipticity results to be 0.18°. By moving the piezoelectric of a step $\Delta l = 40$ nm, the angle of ellipticity χ changes to 20.05°, as shown in the Figure 3.12.

The final consists in measuring the path difference Δl of the piezoelectric between a -45° linear polarization and a +45° linear polarization state. This corresponds to the translation from a minimum peak to a maximum peak, when the analysis polarizer (POL) is set to have the main axis at +45° with the respect to the vertical direction. Theoretically the translation between the two linear polarized states occurs when the total phase displacement is π, and consequently the path difference Δl is $\lambda/4 \simeq 159$ nm. As shown in Figure 3.17, the real results are in agreement with the theoretical expectation as clearly graphically demonstrated. The quantification of the error requires the definition of a method and procedure, which is part of a future work.

In conclusion, the tests confirm a fine controllability of the polarization state,as the results faithfully follow the theoretical simulations.

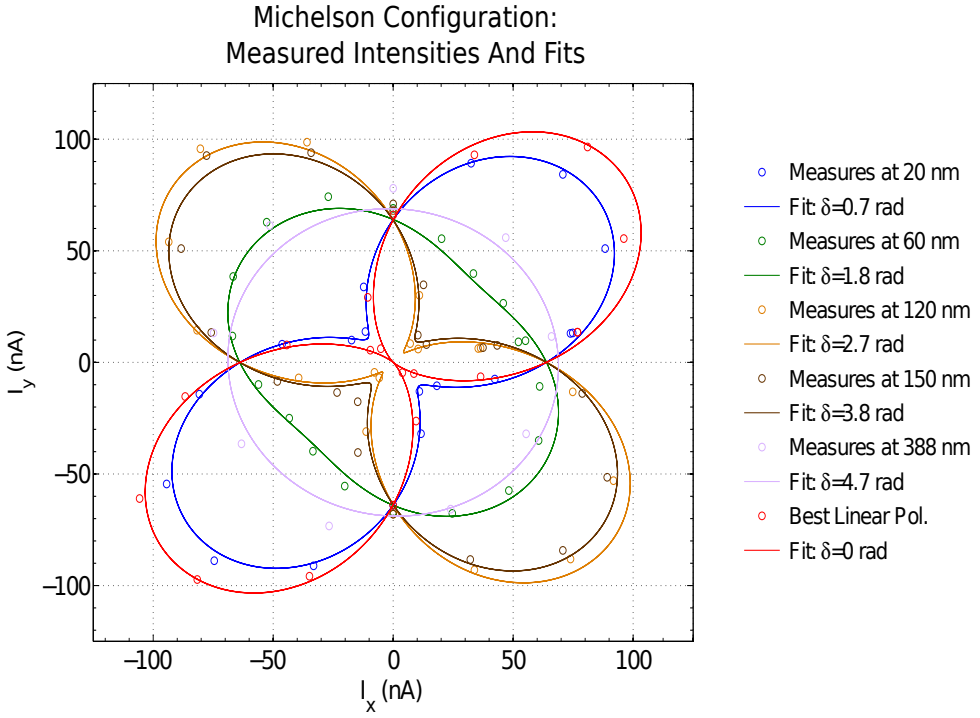

Figure 3.10: The figure shows the intensity distribution, obtained for different translations of the piezoelectric in the Michelson configuration. For each translation of the piezoelectric, the intensities are measured for a complete rotation of 360° of the analysis polarizer (POL). The (POL) polarizer is manually rotated with step of 10°. The measured intensities are indicated with circles, while the lines indicates the graphical fits of the measures.

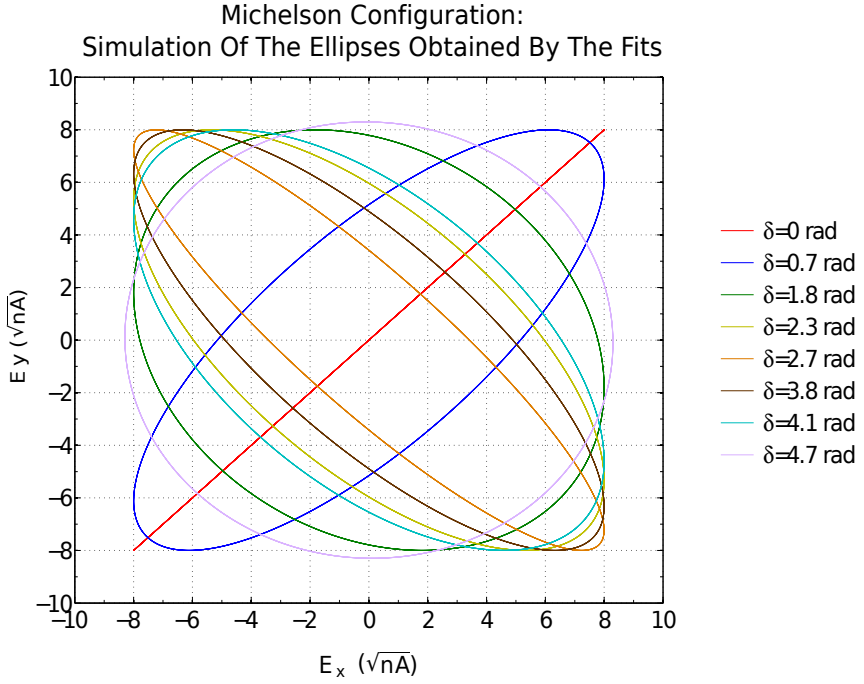

Figure 3.11: The graphical fits of the intensity distribution of Figure 3.10 provide the phase delaies δ, which permits the reconstruction of the polarization ellipse.

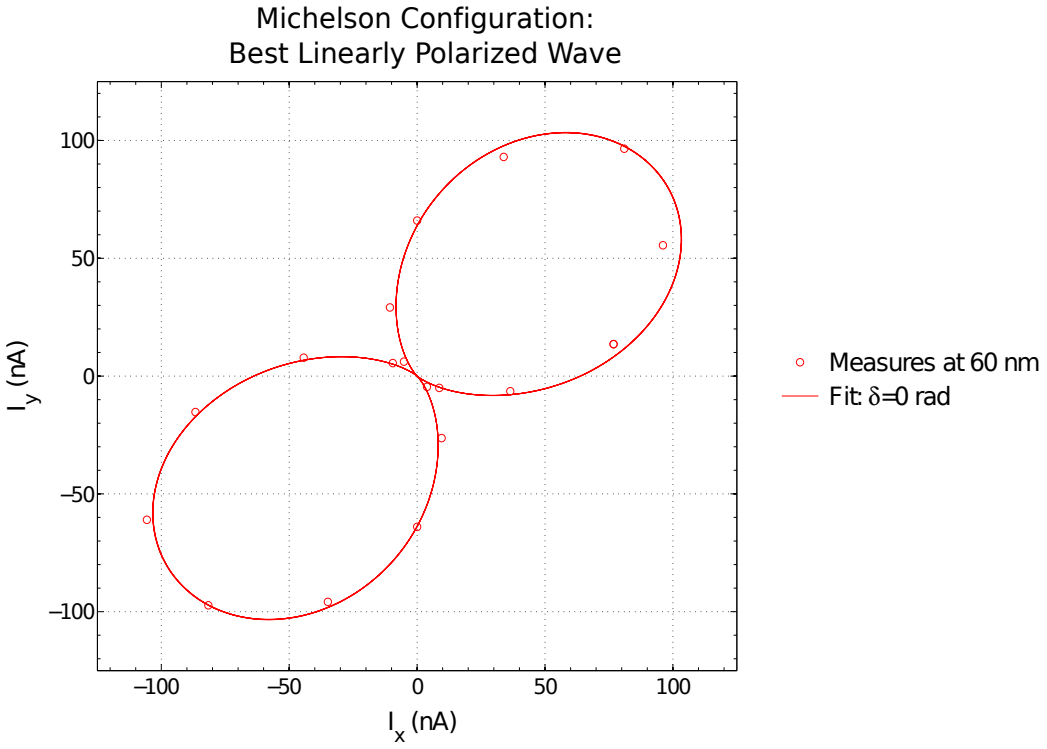

Figure 3.12: The best linearly polarized state obtained in the Michelson configuration. Its real angle of ellipticity is 0.18°.

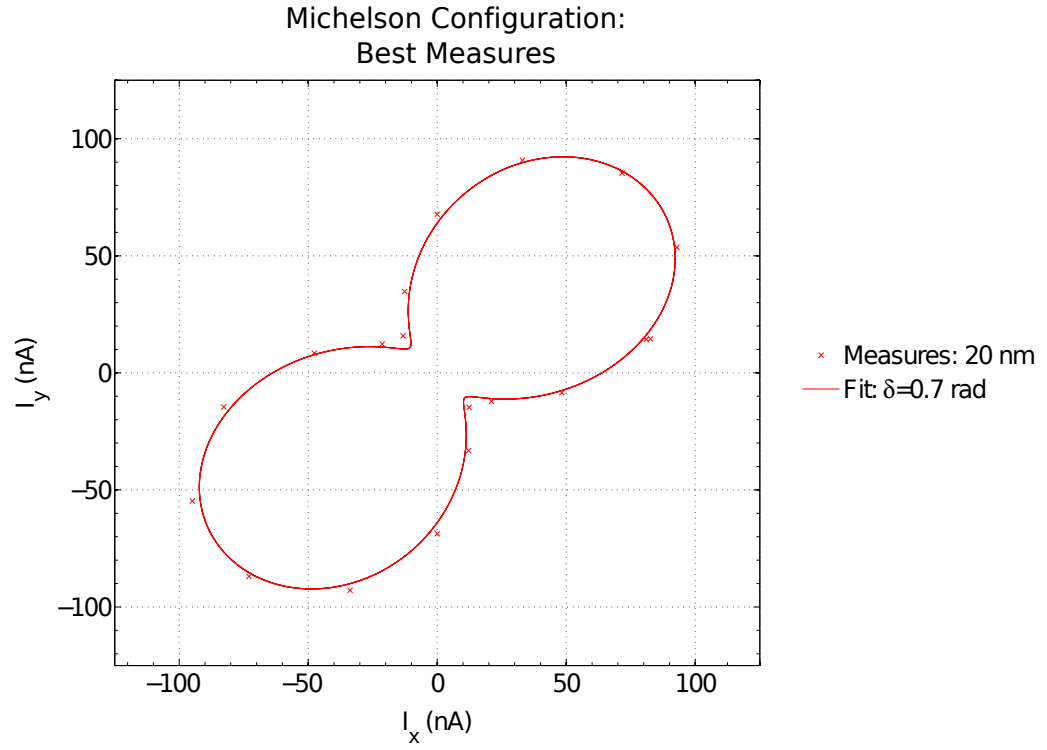

Figure 3.13: In reference to Figure 3.12, by translating the piezoelectric of 40 nm from the linearly polarized position, an elliptical polarization beam of phase delay $\delta = 0.7$ rad is obtained. Its real angle of ellipticity is 20.05°.

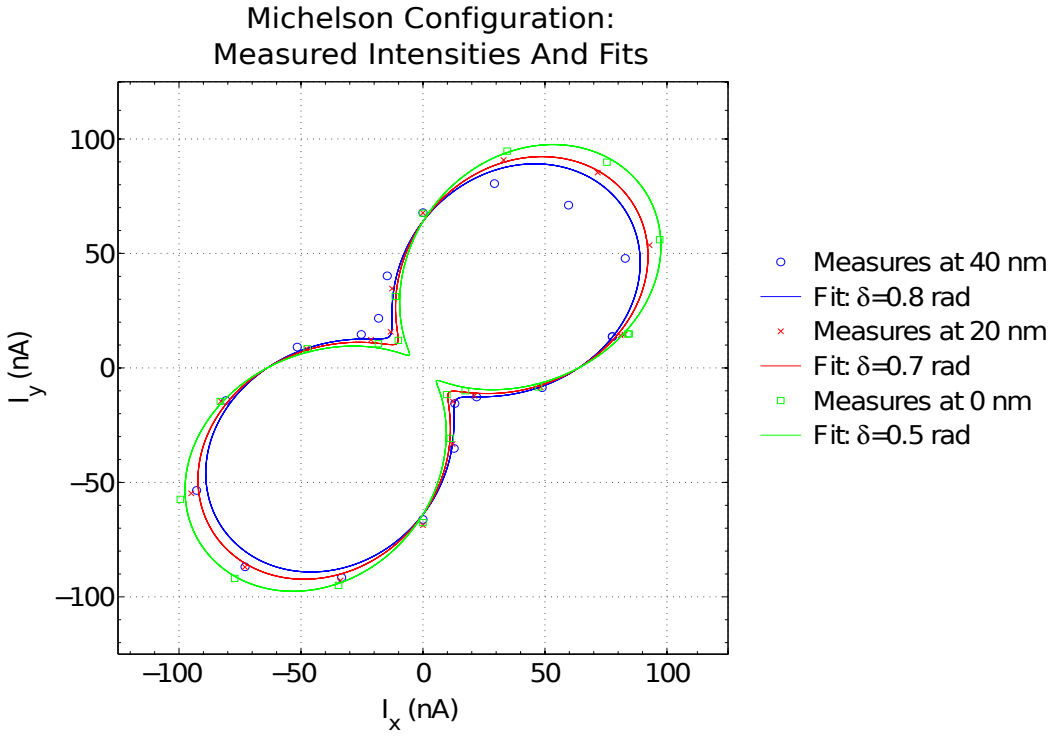

Figure 3.14: The system is very sensible to the movements of the piezoelectric. The figure show three consecutive measures obtained by moving the piezoelectric of a step of 20 nm.

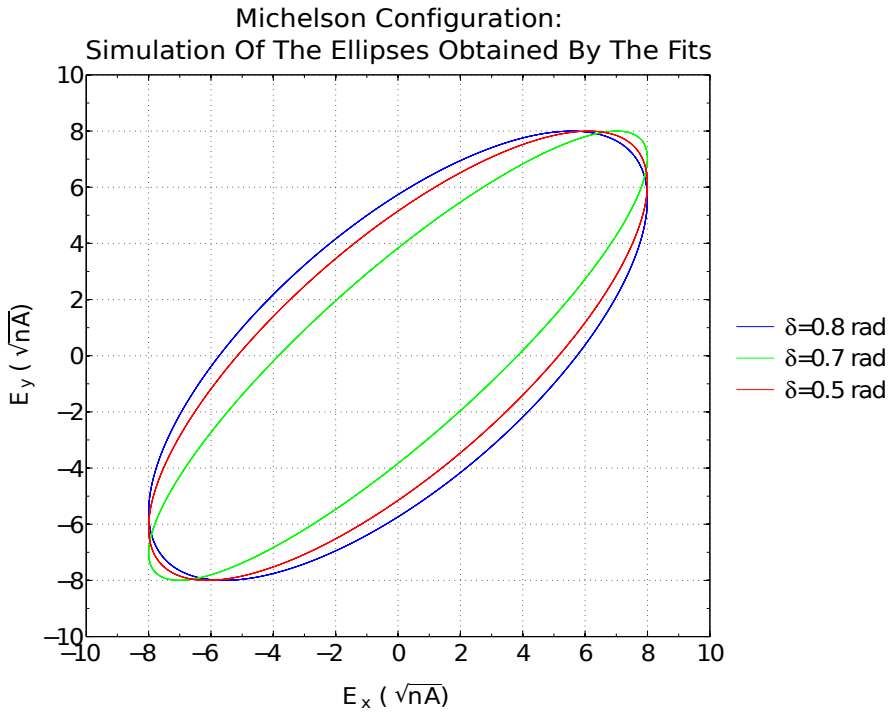

Figure 3.15: The ellipses in reference to Figure 3.14.

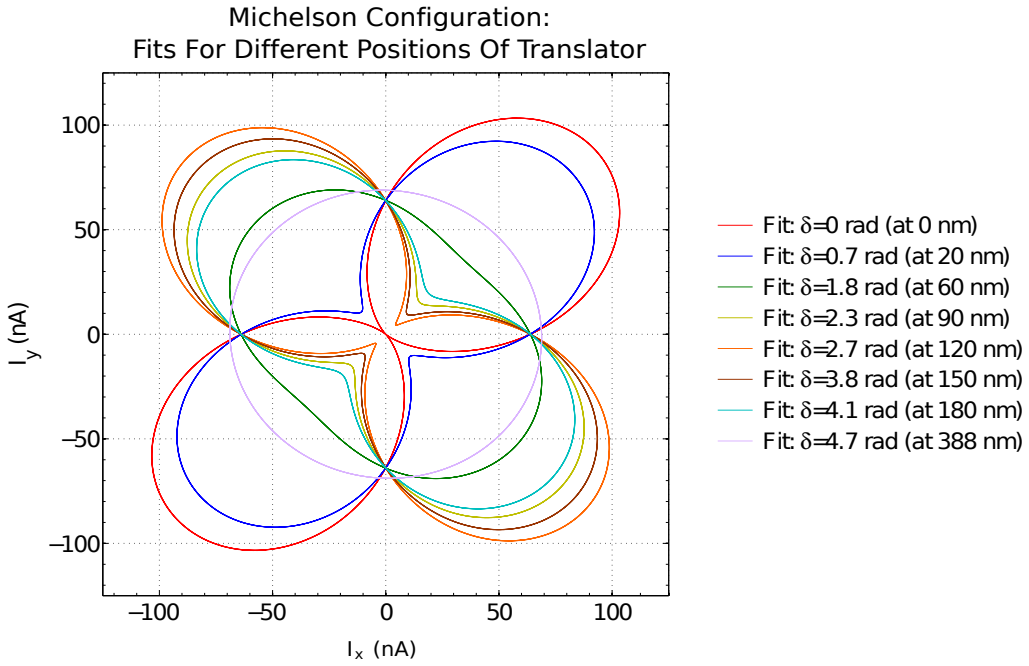

Figure 3.16: All possible states of polarization obtained by the Michielson configuration: from ±45 linearly polarized waves to circularly polarized. For clearness the measured datas are not reported.

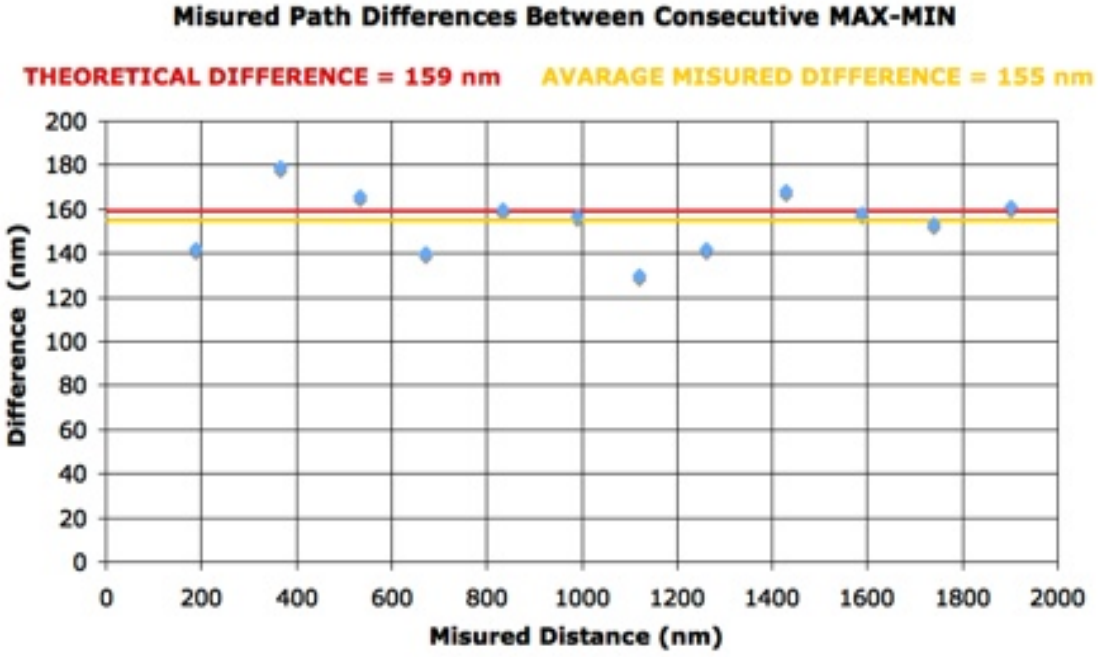

Figure 3.17: The analysis polarizer is set along the +45° direction, coincident to the inclination of the oscillating plane of linearly polarized waves. The test consists in measuring the difference path of the piezoelectric between the series of consecutive max-min or min-max peaks. The x axis refers to the position of the piezoelectric, while the y axis refers to the difference path between two consecutive measurements of max-min or min-max peaks. The red line indicates the theoretical path difference for two consecutive measurements, which is $\Delta l = \lambda/4 \simeq 159$ nm. The yellow line is the arithmetic mean of the measures, which is 155 nm.

3.3 Third Step: The Polarization System with Mach-Zehnder Configuration

The Mach-Zehnder configuration described in section 2.3 has been realized on an optical bench: a view of the final system is shown in Figure 3.18 and Figure 3.19. The main elements used are:

- 2x BEAM SPLITTER: the beam splitters are BK7 ones with intensity division of 50/50.
- 8x MIRRORs: plane aluminum mirrors. Each mirror is fixed on its proper tip-tilt support, which permits a fine regulation along the 3 axis.
- 2x BREWSTER WINDOW: the Brewster windows are BK7 ones working at 56° of incident angle.
- 1x PIEZOELECTRIC STAGE: it is the same used in Michelson configuration. It is configured in close loop mode with a declared fine control of 10 nm.

The alignment procedure is mainly organized in the following steps:

1. The first beam splitter (BM_1) is placed and aligned.
2. The mirror (ML_3) is aligned, in order to obtain a parallel propagation of the s and p lines beams.
3. The Brewster window (B_1) is placed to polarize the beam along the horizontal direction. For this purpose the input polarizer (IN) is set with the main axis perpendicular to the horizontal direction x and (B_1) is finely tilted until the reflected beam completely disappear. In this position (B_1) works at its Brewster angle.
4. The (M_1), (ML_1) and (ML_2) mirrors are sequentially aligned.
5. The Brewster window (B_2) is aligned in order to polarize the beam along the vertical direction. The alignment procedure of (B_2) is similar to (B_1): the (IN) polarizer is set with the main axis perpendicular to the vertical direction y.
6. The (M_2), (ML_5) and (ML_6) mirrors are sequentially aligned. The (M_2) and (ML_5) are placed on the piezoelectric stage.
7. The (ML_4) is fixed on a rotator stage, and aligned in order to achieve a perpendicular intersection between the s and p beam.
8. The beam splitter (BM_2) is placed and aligned in order to recombine the beams coming from the s and p lines. However, the interferential effects obtained from this

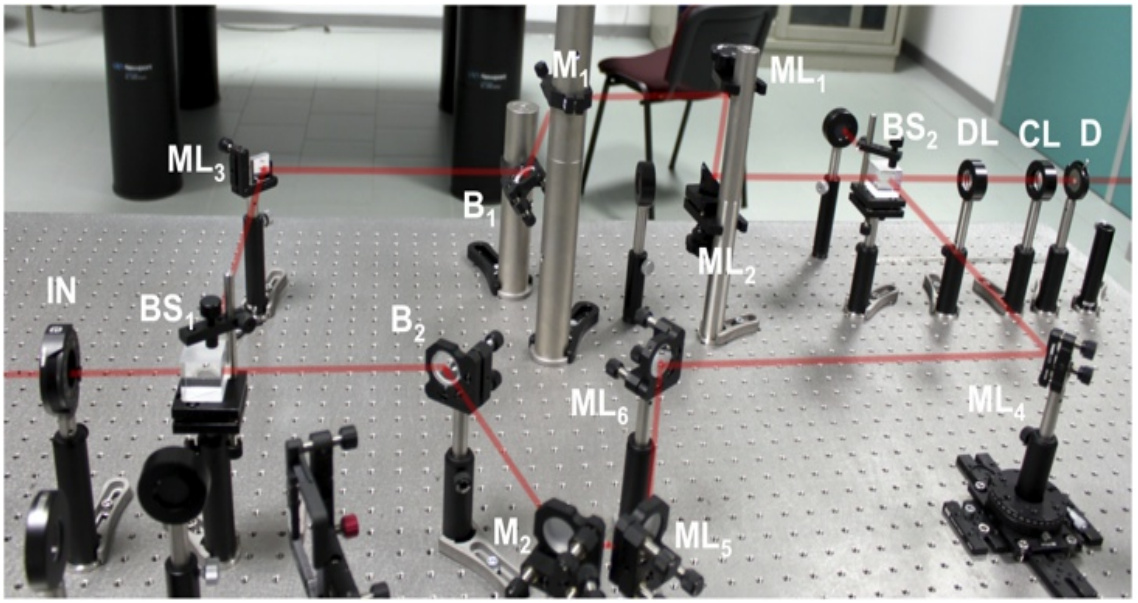

Figure 3.18: A general view of the Mach-Zehnder configuration. The input polarizer (IN) is used to balance the system. The optical elements (DL), (CL) and (D) belong to the analysis system. The mirror (ML_4) is mounted on a micrometer rotator bench, in order to controll the width of interferometric fringes.

superposition doesn't create a fringes pattern because the beams are perpendicularly polarized to each other. On the other hand, by inserting an analysis polarizer (POL) with the main axis at $\pm 45°$, the fringes pattern appears and their distribution can be finely controlled by the micrometer rotator of (ML_4).

The final Mach-Zehnder configuration is now aligned, but it has to be equalized. The equalization procedure is the same adopted for the Michelson system: the input polarizer (IN) is finely rotated until the two lines have the same beam intensity value. At the end of the equalization process the input rotation was $\theta = 50°$, with

$$P_s = 26,1 \text{ nA} \qquad P_p = 26,2 \text{ nA}$$

where P_s is the power of the s line, while P_p is the power of the p line.

3.3.1 Tests

Different experimental tests have been carried out to verify the proper functioning of the system.

The first test is aimed to verify the polarization states in the fringes system. The test is led similarly to the Michelson one: the photodiode of the analysis system is replaced by a CCD and the analysis polarizer (POL) is slowly rotated. The appearance and disappearance of the fringes is shown in Figure 3.20.

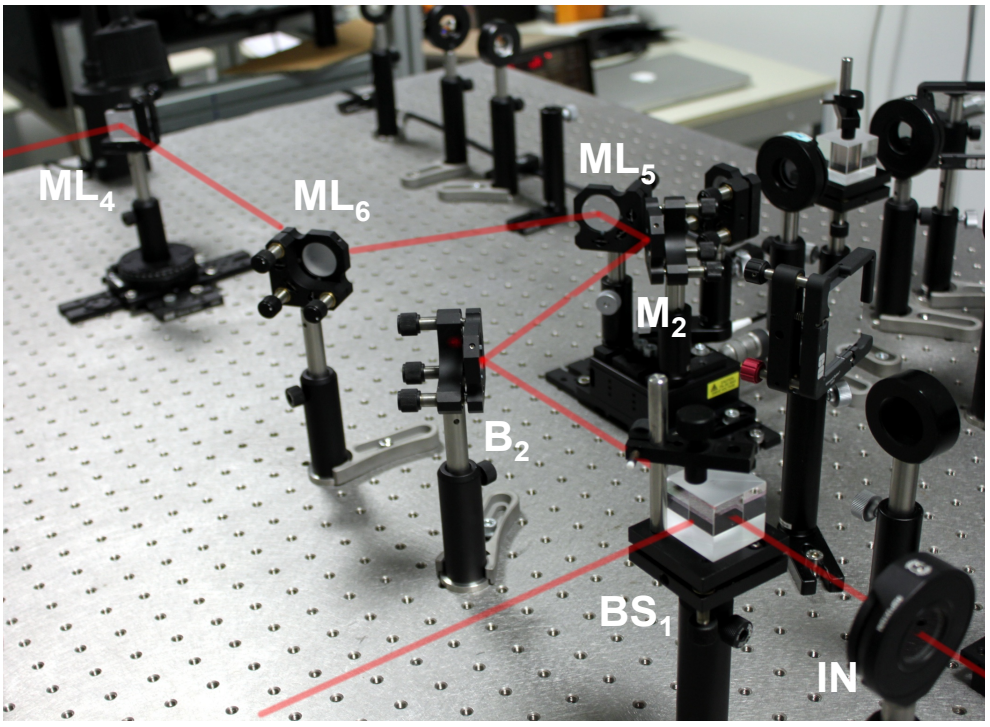

(a)

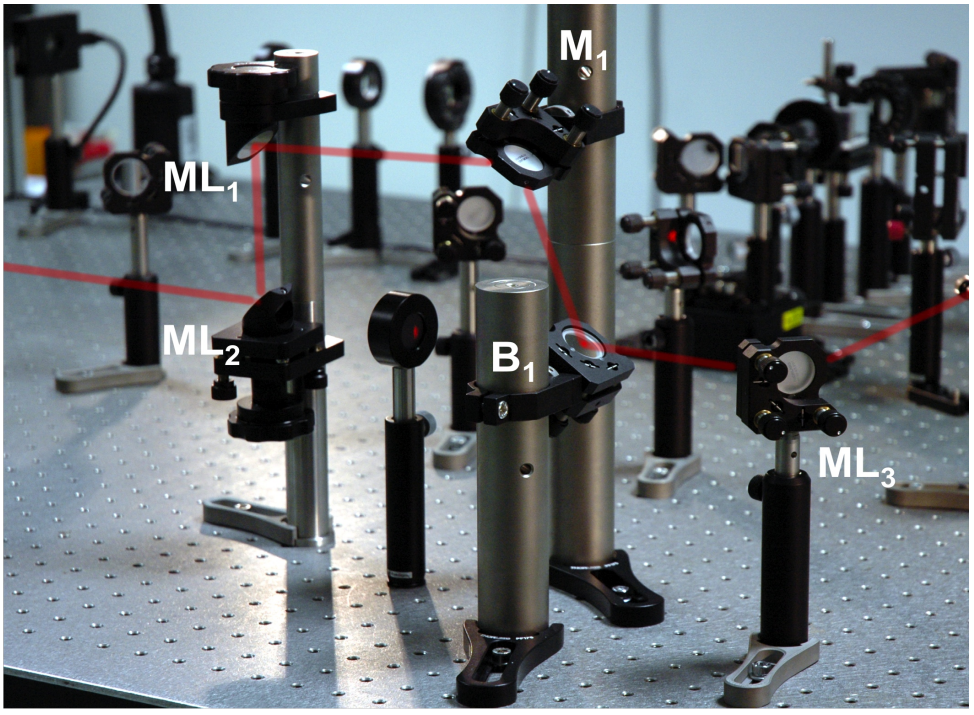

(b)

Figure 3.19: (a) In the s line the (ML_5) and (M_2) mirrors are fixed on the piezoelectric bench, which is able to control the optical path difference between the lines. (b) In the p line the optical elements works rotated of 90° with the respect to the s line, as the Brewster window has to polarize the beam along the p horizontal direction.

Polarization	**Angle Of Ellipticity χ**	**Phase Delay (rad)**	**Figure Color**
Almost Linear	9.61°	0.0	Red
Almost Linear	10.87°	0.7	Blue
Circular	43.60°	1.8	Green

Table 3.2: The Polarization states obtained by the Mach-Zehnder configuration in reference to Figure 3.21. The angle of ellipticity χ is obtained by the original relation described in equation (1.9).

Polarization	**Angle Of Ellipticity χ**	**Phase Delay (rad)**	**Figure Color**
Almost Linear	32.17°	1.0	Blue
Almost Linear	27.38°	0.9	Red

Table 3.3: The Polarization states obtained by the Mach-Zehnder configuration in reference to Figure 3.23. The angle of ellipticity χ is obtained by the original relation described in equation (1.9).

The second test is carried out to verify the controllability of the polarization through the piezoelectric actuator. As for the Michelson test, the fringes are enlarged by acting the rotator of (ML_4) mirror, until obtaining only a unique fringe. A small central area of the unique fringe is selected by a iris (D) of the analysis system. Figure 3.21 shows some of the possible polarization state of the output beam for different positions of the piezoelectric actuator. The piezoelectric is fixed at different positions and the intensities are measured for a complete 360° rotation of the analysis polarizer (POL) in steps of 10°. The measured values are graphically fitted by using the phase delay δ as variable parameter; then the ellipses are recovered (see Figure 3.22). Table 3.2 summarizes the datas and fits reported in Figure 3.21.

The last test was devoted to determine the sensibility of the system to the piezoelectric stage movement. Two consecutive measures are shown in Figure 3.23, by steps of $\Delta l = 20$ nm. Their polarization states are reported in Table 3.3. Again after the graphical fits, the polarization ellipses are recovered and shown in Figure 3.24.

In conclusion, as for the Michelson configuration, the quantification of the error requires the definition of a method and procedure, which will be investigated in a future work. But the results faithfully reproduce the theoretical simulations and they confirm the fine controllability of the polarization state of the outcoming beam.

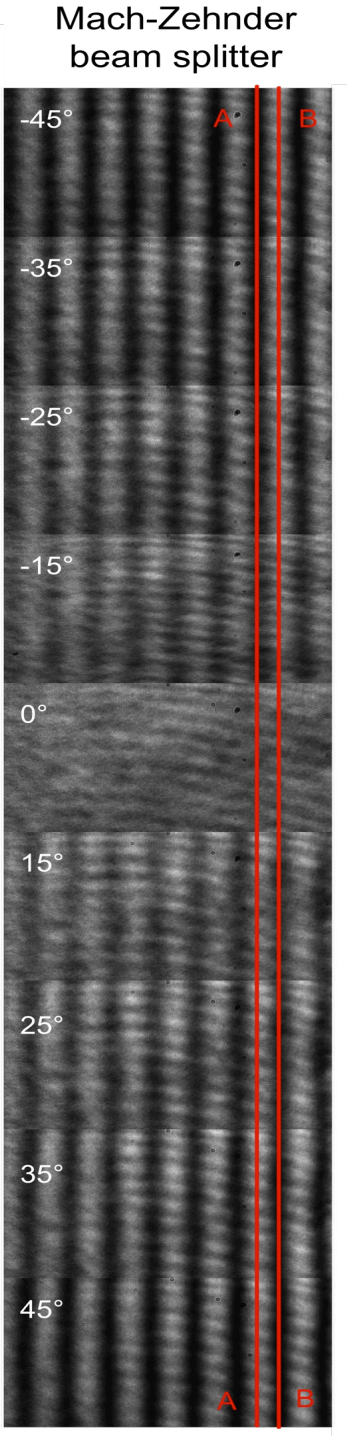

Figure 3.20: The effect of the appearing and disappearing fringes in the Mach-Zehnder configuration for different angle of the analysis polarizer (POL). The angle values refer to the position of the main axis of (POL) with the respect of the y vertical direction. The red line A indicates a +45° linearly polarized area, while the line B indicates a -45° linearly polarized area.

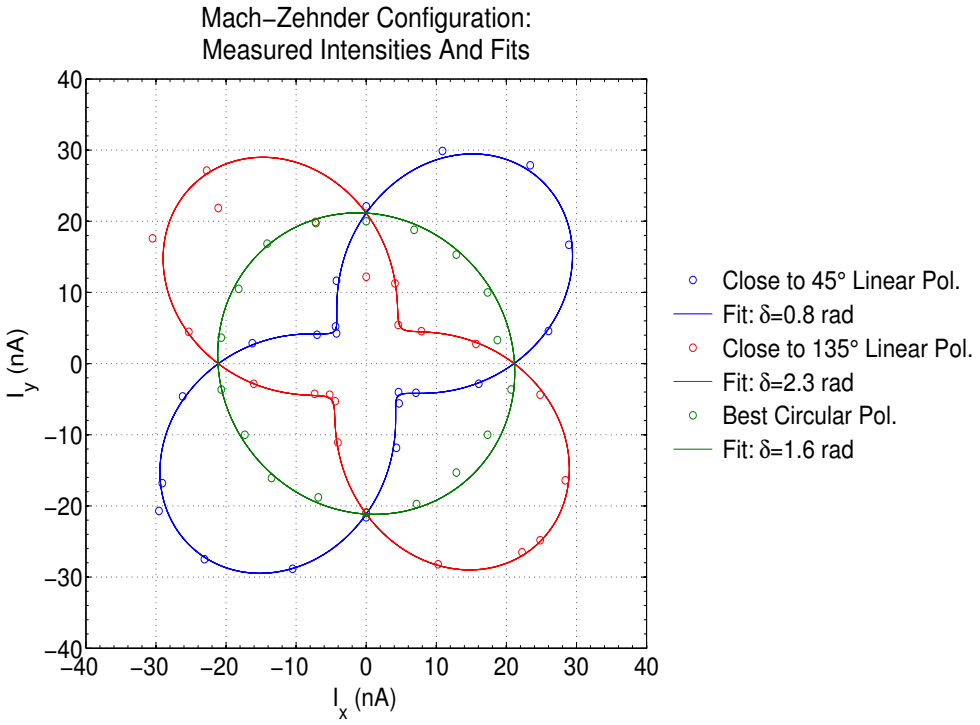

Figure 3.21: The best linear polarized and circular polarization state in Mach-Zehnder configuration. The system should be optimized with higher performance elements to obtain a better linear polarization state.

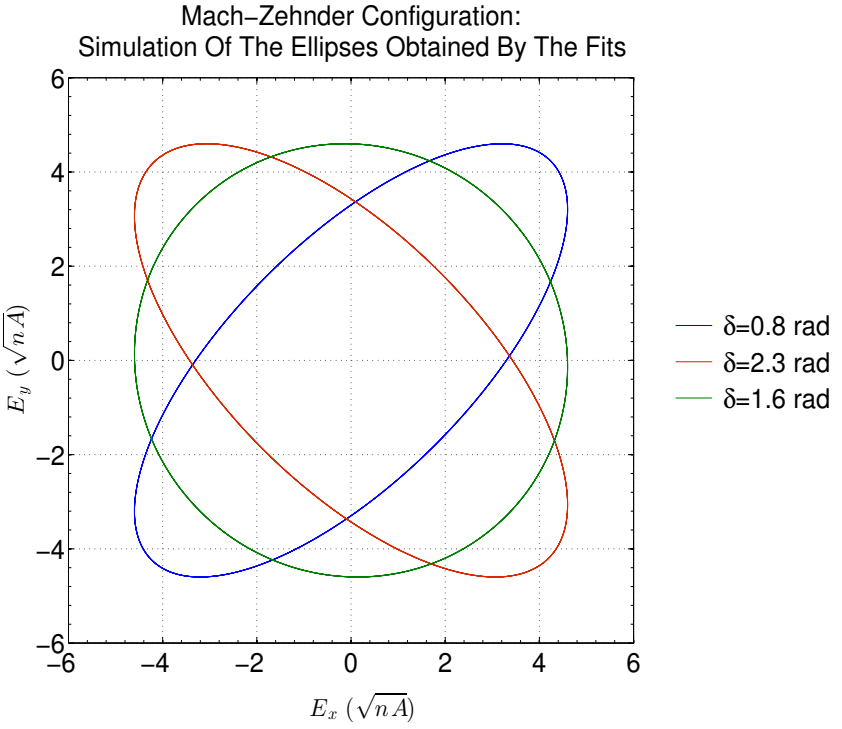

Figure 3.22: By the fits of Figure 3.21 the polarization ellipse are obtained.

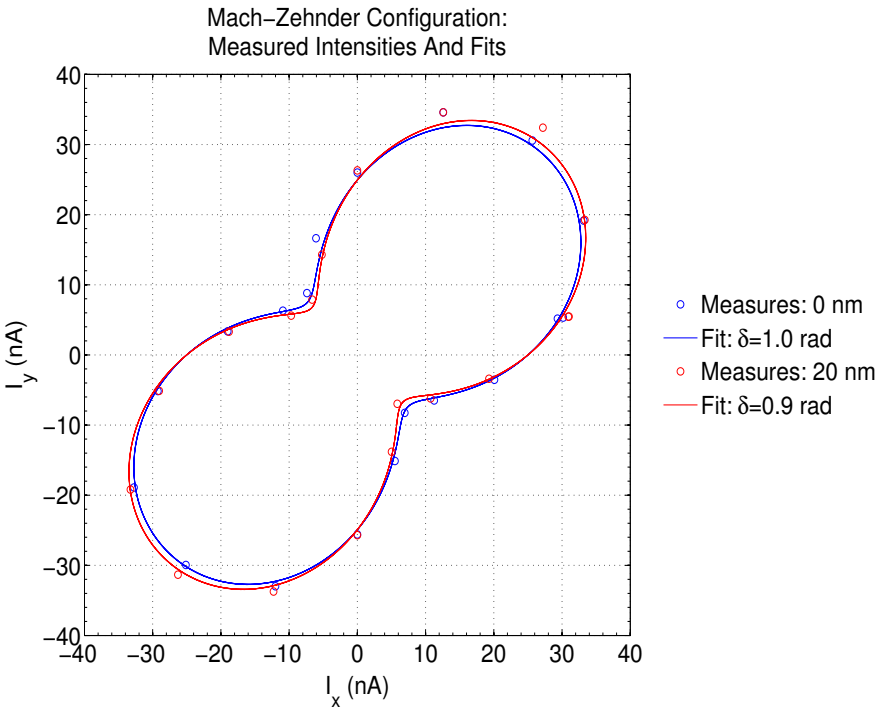

Figure 3.23: The figure shows the intensity distribution, obtained for different translations of the piezoelectric in the Mach-Zehnder configuration. For each translation of the piezoelectric, the intensities are measured for a complete rotation of 360° of the analysis polarizer (POL). The (POL) polarizer is manually rotated with step of 10°. The graph shows as the Mach-Zehnder configuration can finely control the polarization status of the beam by a translation $\Delta l = 20$ nm.

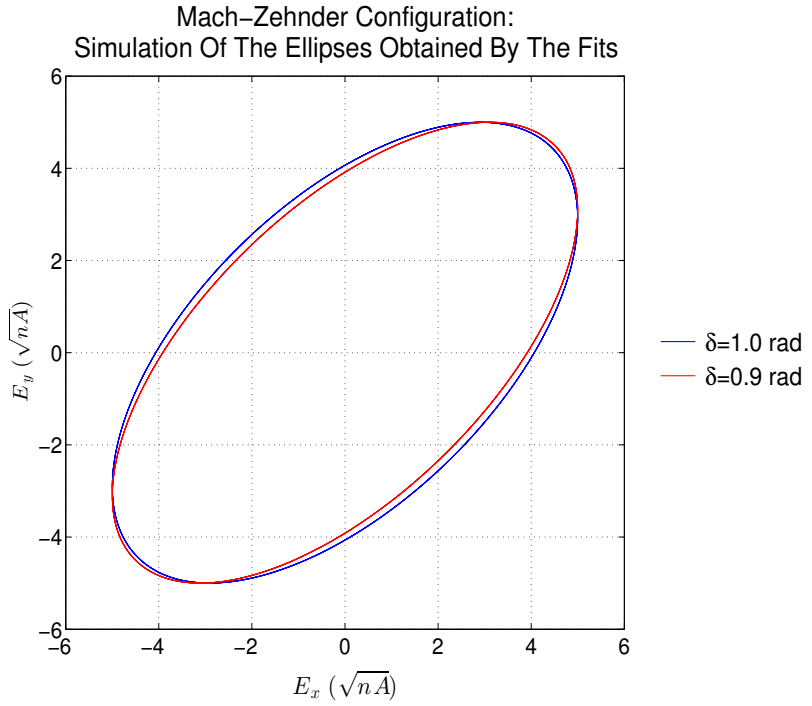

Figure 3.24: By the fits of Figure 3.23 the polarization ellipse are obtained.

Chapter 4

Future Perspectives

Michelson and Mach-Zehnder configurations have been developed in the VIS range. The next step is to verify the functionality of the systems for wavelengths in the UV (200 − 400 nm). Theoretically both systems should work in the UV band, since there are no substantial differences than the VIS range, beside optimization of the efficiency of the optical elements. On the contrary at shorter wavelengths in the extreme ultraviolet EUV band (<200 nm), the materials become opaque, and it is necessary to use optical systems which work completely in reflection. For this reason, an all-reflective Mach-Zehnder has been realized on the optical bench (see Figure 4.1). Beam splitter elements working in transmission have been replaced with mirrors working in grazing incidence and in Iloyd configuration. The beam impinges the edge of the mirror (SM_1), which divides it into two spots with the shape of a half moon. The recombination of the s and p lines is done by

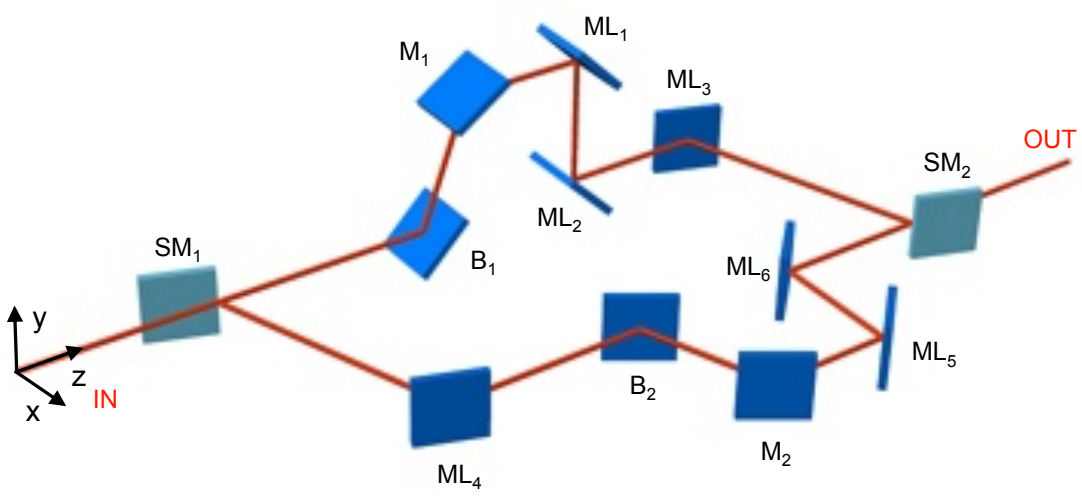

Figure 4.1: A schematic view of the Mach-Zehnder configuration with only mirrors: the beam is split and superposed by two grazing mirrors (SM).

superposing the small central area of each half moon through the grazing mirror (SM_2).

As a first experiment, the all-reflective Mach-Zehnder configuration has been built and tested at CNR - IFN in Padova (see Figure 4.2); but nevertheless, to complete the experimental analysis, some optical elements must be replaced with some higher performancing ones. The alignment of this system is particularly critical for different reason. First of all the grazing incidence mirror needs to be positioned with special care. Than the recombination of the beam presents some intrinsic limitation, for example due to the fact that the Iloyd configuration determines a tilt between the two s and p wavefronts that determine the appearance of a fringes system; selection of the central fringe with desired width is no longer possible, and the uniform area of the central portion of the beam is very limited. However, some interesting and promising results have been obtained. Figure 4.3 shows the effect of the fringes that appear and disappear depending on the position of the axis of the analysis polarizer (POL). Such a result confirms the controllability of the polarization status for the all-reflective Mach-Zehnder. Actually this configuration requires further studies and tests, but it opens new fronts to the control of the state of polarization for wavelengths in the EUV band.

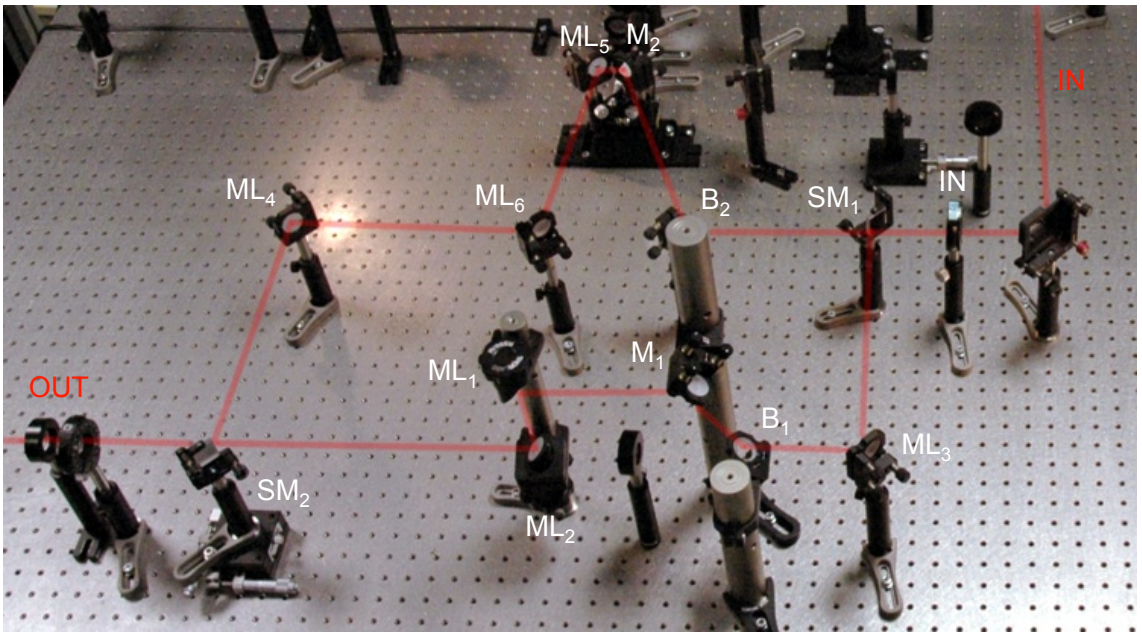

Figure 4.2: The Mach-Zehnder with only mirrors: the (SM_1) mirror spatially divides the beam in the the s and p line, while the (SM_2) recombine the lines in a unique interferometric beam. The (SM) mirrors theoretically work at the grazing incidence, however for convenience in this first test the working angle is set to 45°.

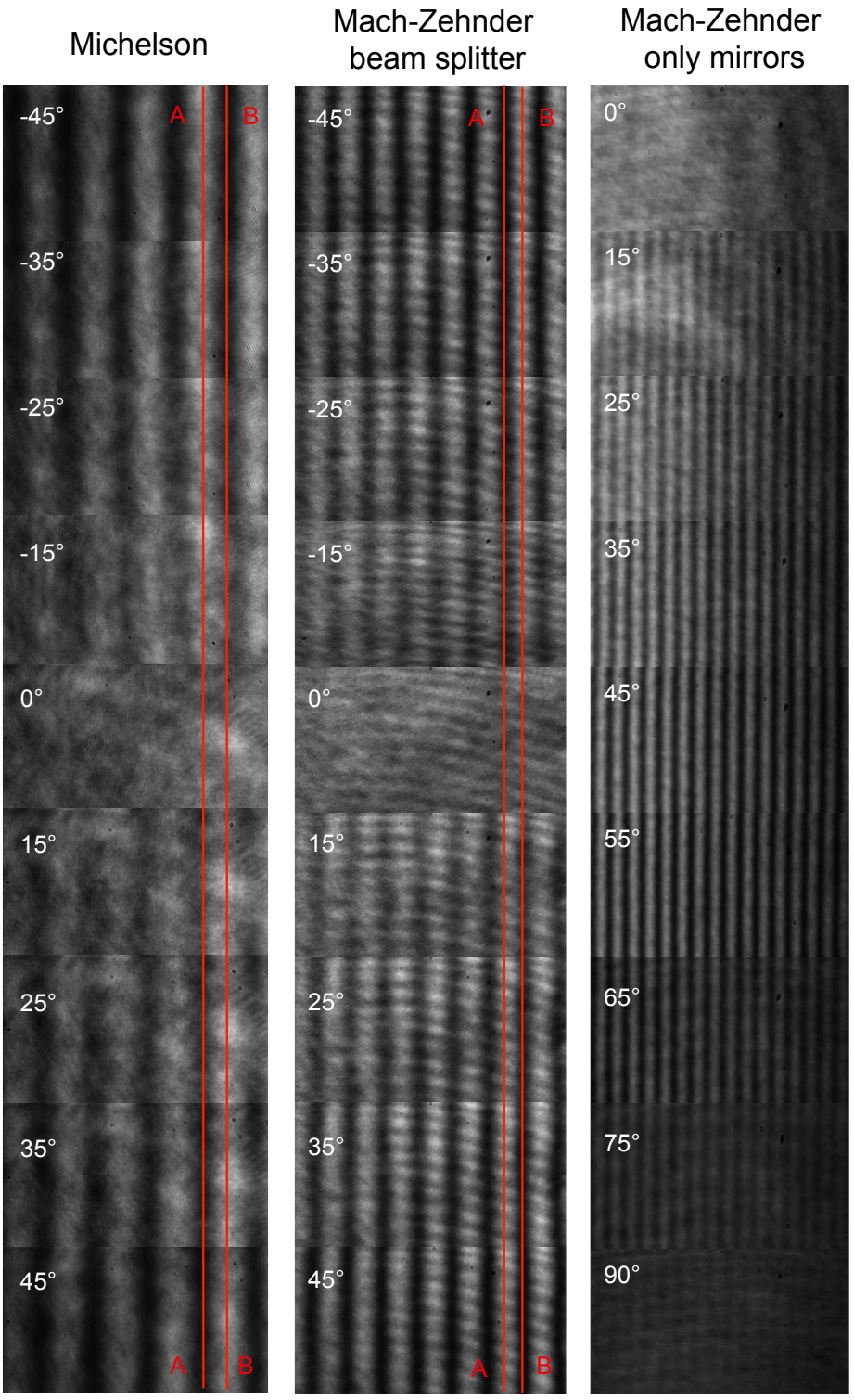

Figure 4.3: The appearing and disappearing phenomena is shown for the three configuration of the system for different angle of the analysis polarizer (POL).

Acknowledgements

Desidero ringraziare tutti coloro che mi hanno aiutato ad affrontare il peso dello studio. In particolare un sentito ringraziamento ai miei genitori, che, con il loro incrollabile sostegno morale ed economico, mi hanno permesso di raggiungere questo traguardo, incoraggiandomi durante il corso degli studi e sostenendomi in ogni mia scelta. Un Grazie a mia sorella Cinzia, che ha sempre saputo regalarmi un sorriso nei momenti più difficili.

Un Grazie alla Prof.ssa Maria Guglielmina Pelizzo per la grande disponibilità e cortesia dimostratemi, e per avermi offerto questa preziosa esperienza universitaria. Un Grandissimo Grazie al mio correlatore Dott. Alain Corso, per i suoi innumerevoli consigli durante la stesura della tesi, e per i preziosi aiuti tecnici durante il lavoro di laboratorio presso il CNR - IFN di Padova. Un Grazie alla Dott.ssa Paola Zuppella per avermi incoraggiato nel proseguire le analisi di laboratorio, ogniqualvolta che mi imbattevo in esiti negativi.

Un ultimo ringraziamento ai miei amici e ai compagni di studi per avermi rallegrato le giornate e per essere stati sempre vicini nei momenti di studio, ma anche in quelli felici.

Ricordo infine che questo lavoro è stato realizzato con il supporto finanziario della Cassa di Risparmio di Padova e Rovigo (CARIPARO), Fondazione nel quadro di Bandi di Eccellenza 2009/2010 nell'ambito del progetto ADORA.

References

[1] W. A. Shurcliff, *Polarized Light Production and Use*. Cambridge, Mass, Harvard University Press, 1962.

[2] W. L. Pritchard and J. A. Sciulli, *Satellite Communication Systems Engineering*. Prentice-Hall, Inc., New Jersey, Chap. 10, p. 333 1986.

[3] A. Yariv and P. Yeh, *Photonics: Optical Electronics in Modern Communications*. 6th ed., Oxford University Press Oxford, Chap. 16, p. 719, 2007.

[4] J. Louis, Jr. Ippolito, *Satellite Communications System Engineering ‚Äì Atmospheric Effects*. Satellite Link Design and System Performance ITT Advanced Engineering And Sciences, USA, and the George Washington University, Washington, DC, USA, A John Wiley and Sons.

[5] H. K. Lo, S. Popescu, and T. Spiller, *Introduction to Quantum Computation and Information*. World Scientific, Singapore, p. 120,1998.

[6] H. C. Liu and F. Capasso, *Intersubband Transitions in Quantum Wells: Physics and Device Applications I*. Academic San Diego, Chap. 1, p. 8, 2000.

[7] N. Berova, K. Nakanishi, and R. W. Woody, *Circular Dichroism: Principles and Applications*. 2nd ed., Wiley-VCH, New York, Chap. 1, p. 28, 2000.

[8] Eli Peli, M.SC., O.D., *Ophthalmic applications of circular polarizers*. Journal of the American Optometric Association 57, 4, p. 299, 1986.

[9] *Eye examination apparatus employing polarized light probe*. United States Patent – Patent Number: 5 787 890 – Date of Patent: Aug. 4, 1998.

[10] L. M. Azzam, *Polarization Michelson inetrferometer : principles and applications*. Proceed. SPIE vol. 3754, 0277, July 1999.

[11] N. Yu, Q. J. Wang, C. Pflugl, L. Diehl, F. Capasso, T. Edamura, S. Furuta, M. Yamanishi, and H. Kan, *Semiconductor lasers with integrated plasmonic polarizers*. Appl. Phys. Lett. 94, 151101, 2009.

[12] R. Gordon, A. G. Brolo, A. McKinnon, A. Rajora, B. Leathem, and K. L. Kavanagh, *Physical Reiew Letters*. 92, 037401, 2004.

[13] P. Fischer, *Exploring nanoscale magnetism in advanced materials with polarized X-rays*. LBNL Paper LBNL-5104E, 2012.

[14] E. Allaria, C. Callegari, D. Cocco, W. M. Fawley, M. Kiskinova, C. Masciovecchio, F. Parmigiani. *The FERMI@Elettra free-electron-laser source for coherent x-ray physics: photon properties, beam transport system and applications*. New Journal Of Physics 12, 075002, 2010.

[15] Dennis Goldstein. *Polarized Light*. Marcel Dekker AG, 2nd Edition, 2003.

[16] H. Mueller. *Fundamental Of Optics*. Journal of the Optical Society of America 38, 661, 1948.

[17] Jones, R. Clark. *A new calculus for the treatment of optical systems*. Journal of the Optical Society of America 31, Issue 7, pp. 488,Äì493, 1941.

[18] Frank L. Pedrotti, Leno M. Pedrotti, Leno S. Pedrotti. *Introduction To Optics*. 3rd Edition, 2006.

[19] D. L. Windt. *IMD - Software for modeling the optical properties of multilayer films*. Computers in Physics, 12, 360, 1998.